T H E U N I V E R S I T Y O F T U L S A

THE GRADUATE SCHOOL

INJECTION/FALLOFF TESTING IN RADIALLY HETEROGENEOUS RESERVOIRS

by

Rajarshi Banerjee

A thesis submitted in partial fulfillment of

the requirements for the degree of Master of Science

in the Discipline of Petroleum Engineering

The Graduate School

The University of Tulsa

1997

T H E U N I V E R S I T Y O F T U L S A

THE GRADUATE SCHOOL

INJECTION/FALLOFF TESTING IN RADIALLY HETEROGENEOUS RESERVOIRS

by

Rajarshi Banerjee

A THESIS

APPROVED FOR THE DISCIPLINE OF

PETROLEUM ENGINEERING

By Thesis Committee

_____, Co-Chairperson

_____, Co-Chairperson

_____

ABSTRACT

Banerjee, Rajarshi. (Master of Science in Petroleum Engineering)

Injection/Falloff Testing in Radially Heterogeneous Reservoirs (132 pp. - Chapter IV)

Directed by Dr. Leslie G. Thompson and Dr. Albert C. Reynolds.

(150 words)

This work presents procedures for analyzing water injection and falloff welltest data for radially heterogeneous reservoirs. The work is based on multiphase flow welltest theory.

We present a new method for obtaining radial permeability distribution from injection tests. It is shown that the pressure derivative response from such a test reflects permeability of the reservoir at the flood front as well as that of the uninvaded zone. We also present a new method for calculation of mechanical skin for injection tests.

We show that for water falloff tests, unlike injection tests, single-phase analysis techniques may be applied successfully. Specifically, we demonstrate that the Inverse

Solution Algorithm[12] can be applied to obtain permeability-mobility profile. Furthermore, we present a new method for calculation of mechanical skin. We also show that mutirate injection tests can be analyzed in a manner similar to falloff tests.

Throughout the work we support our derivations by analyzing a number of synthetic data sets.

ACKNOWLEDGEMENT

I would like to express my gratitude to Dr. Albert C. Reynolds and Dr. Leslie G. Thompson for their invaluable assistance and guidance, both personal and academic, throughout my stay at the University of Tulsa. This work also reflects their endurance and patience.

I would also like to thank K.V.K. Prasad of Amoco Production Co. for serving on my thesis committee and for his comments and suggestions. I am grateful to the faculty members and to my graduate student colleagues, who contributed to my education.

The financial support received throughout my MS studies from the Tulsa University Petroleum Reservoir Exploitation Projects (TUPREP) and the Petroleum Engineering Department is acknowledged. I am grateful to Ms. Judy Teal, Administrative Assistant, TUPREP, for making my tenure a smooth one.

I am thankful to my parents Satya and Gouri Banerjee and my son Srinjoy for their encouragement, love and support. I dedicate this work to my wife Nandita for her unfailing devotion in making this work my highest academic achievement.

CONTENTS

LIST OF FIGURES

LIST OF TABLES

CHAPTER I

INTRODUCTION

Classical well test analysis procedures are based on the assumption of flow of a slightly compressible, constant viscosity fluid in a homogeneous reservoir. In practice, most reservoirs flow multiple phases and all reservoirs are heterogeneous. Therefore, there is reason for concern about the applicability of classical well test analysis procedures to commonly encountered multiphase flow field data. In this work, we focus on injection/falloff testing and provide a simple theory that explains the pressure transient behavior of these tests. Based on our theory, we suggest possible methods of data analysis which are applicable to radially heterogeneous reservoirs.

Injection testing is pressure transient testing during injection of a fluid into a well. It is analogous to drawdown testing for both constant and variable rates. Shutting in an injection well results in a pressure falloff which is similar to pressure buildup in a production well. However, the distinction between injection/falloff and conventional drawdown/buildup testing is that the flow characteristics of the injected fluid are different from those of the original reservoir fluid.

Analysis of pressure falloff tests with multiphase flow effects was first presented by Hazebroek, Rainbow and Matthew [1]. The authors assumed a single-layer, three-zone model consisting of a water bank, an oil bank and an unflooded region. They explained

that when water is injected into the reservoir through a well at a constant rate, an oil bank is built up and gas is expelled from the space as shown in Fig. 1.1. They considered that the saturation in each zone changes abruptly at the boundaries of the zone and that the diffusivity equation is valid for each zone. Their model did not consider the effect of an oil/water transition region or heterogeneity.

The problems of interpreting falloff tests were discussed by Kazemi, Merrill and Jargon[2]. These authors formulated a numerical simulation model for a pressure fall-off test. Their model was similar to the model use by Hazebroek, et al[1]. A series of falloff tests were simulated assuming a constant pressure at the outer radius of the oil bank. They concluded that the first straight line of a falloff curve gives the true mobility of the invaded zone for negligible afterflow effects. Further, they deduced that the second straight line approximates the true mobility of the oil bank only if the storage capacity (ϕc_t) of the two zones are equal and the radius of the oil bank is greater than 10 times the radius of the invaded zone. They also remarked that a falloff test cannot be interpreted if the wellbore storage constant, as calculated from field data, exceeds the physical value for the system.

The work of Ref. 2 was further extended by Merrill, Kazemi and Gogarty[3] . Assuming different specific storage capacity ratios, they presented a procedure for estimating mobilities and saturation on both sides of the front, and distance to the front.

Weinstein[4] examined pressure falloff data using a numerical model which included relative permeability and viscosity as a function of temperature. Since all his cases had favorable mobility ratios, they represented piston-like displacement. Therefore, the effect of a transition zone was not apparent.

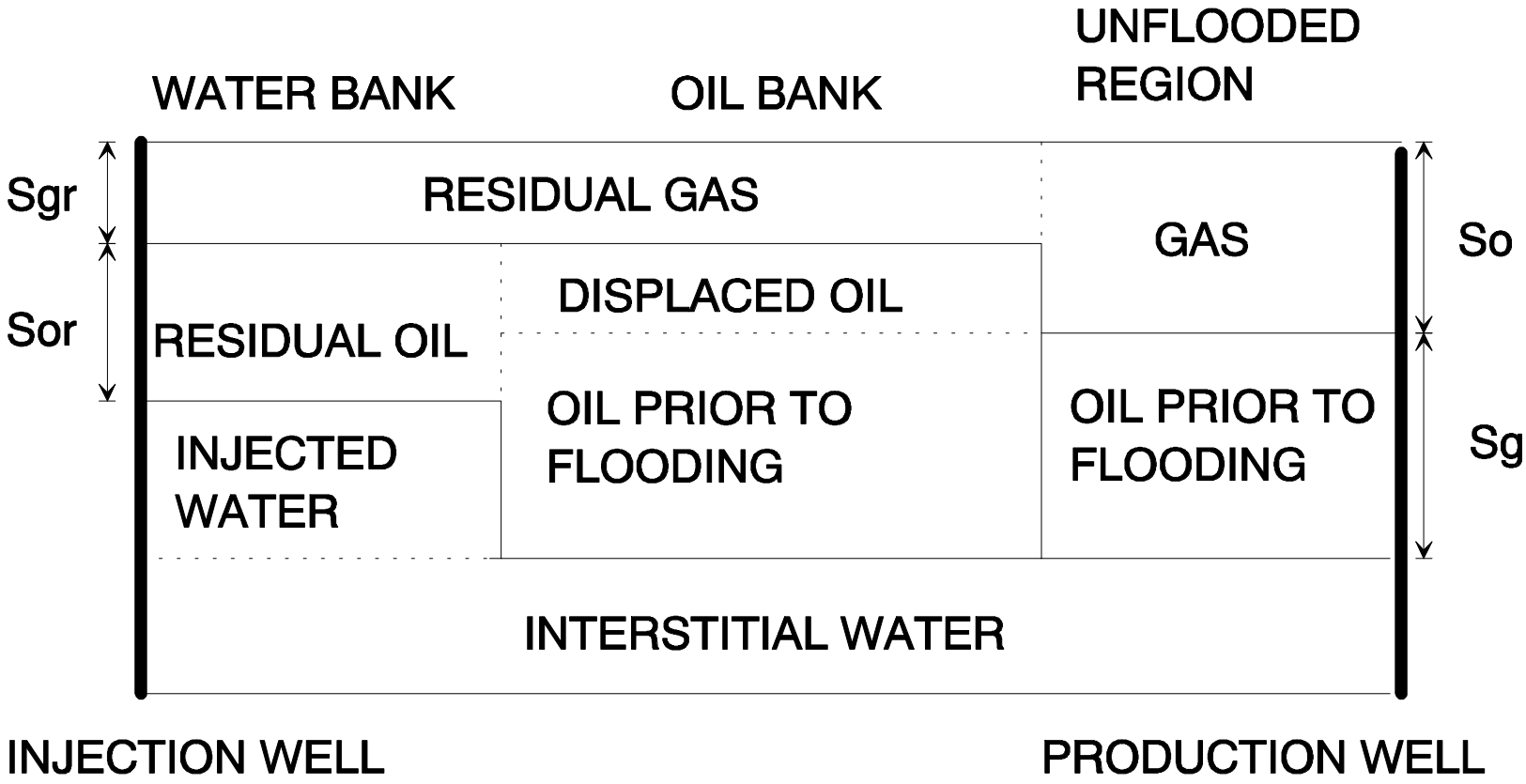
UNFLOODED
REGION
WATER BANK
OIL BANK
Sgr
Sor
RESIDUAL GAS
GAS
So
DISPLACED OIL
RESIDUAL OIL
OIL PRIOR TO
FLOODING
OIL PRIOR TO
FLOODING
Sg
INJECTED
WATER
INTERSTITIAL WATER
INJECTION WELL
PRODUCTION WELL

15

While the above mentioned studies assumed constant saturations in each zone and abrupt changes in saturation at the boundaries, Sosa, Raghavan and Limon[5] avoided such assumptions. They used a reservoir simulator to study liquid-liquid displacement considering different relative permeability curves. They concluded that the distance to the flood front cannot be determined from a falloff test; the best approximation is given by Buckley-Leverett theory. They found that while the slope of the first straight line on a Horner plot is proportional to the transmissibility of the water zone, interpretation of the second or the third straight lines, if any, depends on the mobility ratio and the shut in time. However, their study did not provide any analysis procedure for the interpretation of injection/falloff data.

In 1989 Abbaszadeh and Kamal[6] presented a method to interpret injectivity and falloff tests in a single-layer reservoir under waterflooding. First they considered a reservoir consisting of two zones having different fluid properties. Then they expanded their solution to a multizone system in which the saturation in each zone is constant but different from that of the neighboring zones. Thus in their model, they argued, the transition zone could be approximated by several zones of constant but different saturation.

They presented analytical solutions for pressure and saturation distribution in Laplace space. While they did suggest a numerical solution for the moving interface problem, their analytical solution assumed a static interface between the zones. Using this solution and relative permeability curves, they generated customized type curves for falloff tests. Matching the appropriate type curve yields total fluid mobilities in the water

and oil banks, the saturation or mobility distribution in the transition bank, the flood front location, average reservoir pressure and the formation skin factor.

Yeh and Agarwal[7] took a different approach to analysis of injection/falloff tests. While the researchers discussed earlier relied on analytical or numerical solutions to the problem, Yeh and Agarwal developed a methodology based on simulation of a large number of injection and falloff tests.

In order to facilitate discussion of the results of Ref. 7, we introduce the following definitions:

- injection pressure change, $\Delta p_{wf} = p_{wf} - p_i$;
- injection pressure change derivative, $\Delta p'_{wf}(t) = \dfrac{d\Delta p_{wf}(t)}{d \ln t}$, where t is the injection time;
- falloff pressure change, $\Delta p_{ws} = p_{wf}\big|_{\Delta t=0} - p_{ws}$;
- and falloff pressure drop derivative, $\Delta p'_{ws} = \dfrac{d\Delta p_{ws}}{d \ln \Delta t_e}$, where Δt_e denotes the Agarwal equivalent time[7] ($\Delta t_e = \dfrac{t \times \Delta t}{t + \Delta t}$) where Δt represents the shut-in time and t is the total time of injection.

For injection testing, Yeh and Agarwal showed that, except at early times, the pressure derivative is constant and the associated semi-log straight line reflects the mobility in the flooded zone. For one example, they showed that the skin factor computed based on this semi-log straight line overestimates the true skin factor. Later in this work, we derive a method for generating an accurate estimate of the true mechanical skin factor using pressure data obtained during water injection.

For falloff pressure data, Yeh and Agarwal presented a procedure to estimate the mobility profile in the reservoir. They recognized that in general, the mobility calculated from

$$\overline{\lambda_t} = \frac{70.6 q_{inj} B_w}{h \Delta p'_{wf}}, \tag{1.1}$$

reflects an average value in some region of the reservoir. Their interpretation of $\overline{\lambda_t}$ in Eq. 1.1 was

$$\begin{aligned} \overline{\lambda_t} &= \frac{1}{V}\int_V \lambda_t dV \\ &= \frac{2}{\left(r^2 - r_w^2\right)}\int_{r_w}^{r} \lambda_t r dr \ . \end{aligned} \tag{1.2}$$

Differentiating Eq. 1.2 and rearranging we get

$$\lambda_t = \frac{r^2 - r_w^2}{2r}\frac{d\overline{\lambda}_t}{dr} + \overline{\lambda_t}. \tag{1.3}$$

They assumed that the total mobility , λ_t, is related to the radius of investigation by the following formula

$$r = 0.024\left[\frac{\lambda_t \Delta t_e}{\phi c_t}\right]^{0.5}. \tag{1.3b}$$

In their calculations, they neglected r_w^2 term in Eq. 1.3 and were able to generate good approximations to the true mobility profile at the instant of shut-in. They also presented a procedure for approximating the pressure profile at the instant of shut-in.

The method suggested by Yeh and Agarwal does not require prior knowledge of relative permeability curves and their study provided valuable insight into the mechanics of injection well testing. However, their interpretation method was presented only for homogeneous reservoirs.

Ramakrishna and Kuchuk[8] presented analytical solutions for the pressure response under various assumptions for injection and falloff tests. For a constant down hole injection rate, they obtained exact solutions for an infinite reservoir during both the injection and the falloff periods. However, due to the inherent nonlinearity of the problem they employed an approximate method for varying flow rate problems. Their technique can be used with an altered form of convolution and permits calculation of the pressure response for arbitrary rate data. In a later work[9] they presented a perturbation theory for mutiphase testing involving slightly compressible fluids and examined variable rate test procedures in the light of the theory.

Oliver[10] investigated the averaging process in permeability estimation for single phase flow and presented an approximate perturbation solution for the pressure response in radially heterogeneous reservoirs where permeability varies slightly about some average value. He found that permeability estimates obtained from semi-log analysis represent a weighted average of the permeabilities within an annular region whose

position and areal extent varies with time; he found that the annular region within which permeability was averaged extended from $r_D = 0.12\sqrt{t_D}$ to $r_D = 2.34\sqrt{t_D}$.

Feitosa, Chu, Thompson and Reynolds[11] modified Oliver's solution and applied it successfully to multicomposite reservoirs with a large variation in permeability. Their equation for the pressure derivative in terms of an analytical weighting function is

$$\frac{d\Delta p_{wf}(t)}{d\ln t} = \frac{q_{sf}\mu}{C_1 r_w}\int_{rw}^{\infty} K_o\left(r', \hat{k}, t\right)\frac{1}{k(r')}dr' . \qquad (1.4)$$

In Eq. 1.4, q_{sf} is the constant sandface production rate, K_o is an analytical kernel function and $\hat{k}$ is the instantaneous value of permeability computed from pressure derivative at time t. Based on Eq. 1.4 the authors presented a means by which an inverse solution algorithm[12] could be applied to pressure buildup data to obtain the permeability distribution in a radially heterogeneous reservoir.

A novel insight into the mechanics of multiphase flow pressure transient testing was presented by Thompson and Reynolds[13,14]. They presented a theory that describes the averaging process that occurs during multiphase flow drawdown and buildup tests. Their theory explained pressure transient behavior of both single and multiphase flow in radially heterogeneous reservoirs. Although the focus was on gas condensate reservoirs, their studies included a variety of systems including black oil reservoirs, retrograde gas condensate reservoirs and injection/falloff testing. In summary, the theory stated that well test mobilities reflect weighted average mobilities in those regions of the reservoir where rate is changing with time and where mobility is changing with time.

They concluded that for drawdown in gas condensate reservoirs, changing mobility is the dominant phenomenon, so the pressure derivative in this case reflects mobility in the reservoir region where mobility changes most rapidly; i.e., the region neighboring the radius to the critical oil saturation. They added that in the case of buildup the effect of rapidly changing mobility in the region close to the wellbore is nullified by a propagating zero flow rate zone so, the behavior is similar to single-phase buildup and could be successfully analyzed using single-phase analysis techniques.

They extended the argument to pressure transient data observed during injection/falloff tests, and argued that if changing mobility were the dominant factor occurring during the injection phase, the theory could explain the common belief that it is impossible to see beyond the "flood front" during injection. However, they presented a set of water injection data from a heterogeneous reservoir that seemed to indicate that the pressure derivative was being influenced by heterogeneities beyond the position of the saturation flood front. They offered no explanation as to the cause of this apparent anomaly.

In this work, we investigate this apparently anomalous behavior carefully, and show that pressure transient data from injection tests are indeed influenced by heterogeneties beyond the flooded zone. Even though the observation made by Thompson and Reynolds that drawdown gas condensate pressure derivative data reflect properties close to the critical oil saturation front is perfectly valid for condensate systems, in general, the multiphase flow pressure derivative data contains information both about the moving flood front and the unflooded zone ahead of the front.

CHAPTER II

INJECTION TESTING IN HETEROGENEOUS RESERVOIRS

We begin this chapter by briefly summarizing the general multiphase flow well test theory of Thompson and Reynolds, which serves as a basis for our understanding, and analyzing pressure transient data from injection and falloff tests. We then proceed to derive an approximate analytical solution for water injection in radially heterogeneous reservoirs. We also investigate the relationship between the apparent skin factor obtained by classical analysis of injection test pressure data from a homogeneous reservoir with skin damage and the true mechanical skin factor. Finally, we validate our theory by analyzing synthetic well test data generated using a two-phase simulator.

2.1 General Theory of Multiphase Flow Well Testing.

Isothermal multiphase flow in radially heterogeneous reservoirs is described by a system of partial differential equations that satisfies conservation of oil, gas and water components in black oil systems and conservation of individual chemical components in compositional systems. More specifically, the flow equations are derived from the continuity equation (conservation of mass) and Darcy's law. In particular, for a black oil

system at any radial location, the total reservoir flow rate is the sum of the rates of each individual phase, i.e.,

$$\begin{aligned} q_t(r,t) &= q_o(r,t) + q_g(r,t) + q_w(r,t) \\ &= C_1 r k(r) \lambda_t \frac{\partial p(r,t)}{\partial r} \quad , \end{aligned} \tag{2.1.1}$$

where

$$\lambda_t(r,t) = \frac{k_{ro}}{\mu_o} + \frac{k_{rg}}{\mu_g} + \frac{k_{rw}}{\mu_w} \ . \tag{2.1.2}$$

In writing Eq. 2.1.1, capillary pressure effects and gravity effects have been neglected. If we consider phase rates in RB/day, the constant C_1 in Eq. 2.1.1 is given by

$$C_1 = 2\pi\left(1.127 \times 10^{-3}\right)h \ . \tag{2.1.3}$$

It should be noted that Eq. 2.1.1 applies to both bounded or infinite acting reservoirs. In the case of an infinite acting reservoir we can separate the variables in Eq. 2.1.1 and integrate over radius to obtain

$$\int_{r_w}^{\infty} \frac{\partial p}{\partial r} \partial r = \frac{1}{C_1} \int_{r_w}^{\infty} \frac{q_t(r',t)}{r' k(r') \lambda_t(r',t)} dr' \quad , \tag{2.1.4}$$

with the boundary condition

$$\lim_{r\to\infty} p(r,t) = p_i \ . \qquad (2.1.5)$$

Integrating Eq. 2.1.4, we obtain an expression for the pressure drop at the wellbore under multiphase flow as:

$$\Delta p_{wf}(t) = p_i - p_{wf}(t) = \frac{1}{C_1}\int_{r_w}^{\infty} \frac{q_t(r',t)}{r' k(r') \lambda_t(r',t)} dr' \ . \qquad (2.1.6)$$

The corresponding pressure derivative observed at the wellbore can be obtained by differentiating Eq. 2.1.6 with respect to the natural log of time. Performing the indicated differentiation, we have

$$\frac{d\Delta p_{wf}(t)}{d\ln t} = \frac{1}{C_1}\int_{r_w}^{\infty} \frac{1}{k(r')}\frac{1}{r'}\left[\frac{1}{\lambda_t(r',t)}\frac{\partial q_t(r',t)}{\partial \ln t} - \frac{q_t(r',t)}{\lambda_t^2(r',t)}\frac{\partial \lambda_t(r',t)}{\partial \ln t}\right] dr' \ . \qquad (2.1.7)$$

Eq. 2.1.7 applies to any radial flow system producing at an arbitrary constant or variable rate; it indicates that the pressure derivative observed at the wellbore reflects a weighted harmonic average permeability. The maximum weights in the averaging process are given to those regions where rate and mobility are changing most rapidly with time. The kernel that is applied to the reciprocal of permeability in the averaging process is given by

$$K(r',t) = \frac{1}{r'}\left[\frac{1}{\lambda_t(r',t)}\frac{\partial q_t(r',t)}{\partial \ln t} - \frac{q_t(r',t)}{\lambda_t^2(r',t)}\frac{\partial \lambda_t(r',t)}{\partial \ln t}\right]. \qquad (2.1.8)$$

Similarly, the kernel that is applied to the reciprocal of the permeability-mobility product in the averaging process is given by

$$K_M(r',t) = \frac{1}{r'}\left[\frac{\partial q_t(r',t)}{\partial \ln t} - \frac{q_t(r',t)}{\lambda_t(r',t)}\frac{\partial \lambda_t(r',t)}{\partial \ln t}\right]. \qquad (2.1.9)$$

Eq. 2.1.9 has two components, a rate kernel, K_R defined as

$$K_R(r',t) = \frac{1}{r'}\left[\frac{\partial q_t(r',t)}{\partial \ln t}\right], \qquad (2.1.10)$$

which incorporates the contribution of those reservoir regions where rate is changing rapidly to the well test mobility, and a mobility kernel defined by

$$K_\lambda(r',t) = \frac{1}{r'}\left[\frac{q_t(r',t)}{\lambda_t(r',t)}\frac{\partial \lambda_t(r',t)}{\partial \ln t}\right], \qquad (2.1.11)$$

which provides weighting for those reservoir regions where saturation (or mobility) is changing.

For single-phase, slightly-compressible, liquid systems where viscosity is constant, λ_t does not vary with time, and the mobility kernel, K_λ, vanishes. Thus, Eq. 2.1.7 can be simplified to yield

$$\frac{d\Delta p_{wf}(t)}{d\ln t} = \frac{\mu}{C_1}\int_{r_w}^{\infty}\frac{1}{k(r')}\frac{1}{r'}\left[\frac{\partial q_t(r',t)}{\partial \ln t}\right]dr'. \qquad (2.1.12)$$

Eq. 2.1.12 suggests that the pressure derivative observed at the wellbore for single phase liquid flow in a heterogeneous reservoir is a weighted harmonic average of the absolute permeability in that region of the reservoir where rate is changing as a function of time. For production at a constant rate, Ref 11 showed that the rate changes in an annular reservoir region (concentric with the wellbore) that expands in area and moves away from the wellbore with time. This behavior is qualitatively similar to the averaging theory presented by Oliver[10] for radially heterogeneous reservoirs.

For multiphase flow in radially heterogeneous reservoirs, Eq. 2.1.7 cannot be simplified. The pressure derivative observed at the wellbore is influenced by mobility both in regions where rate is changing as a function of time and where mobility is changing as a function of time. Further, for multiphase flow it is not necessary that regions where rate is changing most rapidly are coincident with regions where mobility is changing most rapidly.

In the case of production from retrograde gas condensate reservoirs where the wellbore pressure is below the dewpoint, there exists an annular region around the wellbore where we have two phase flow. During production, as liquid drops out of the gas phase and exceeds critical oil saturation, the mobility of each phase, hence the total mobility, changes rapidly in this region, resulting in large value of K_λ. On the other hand, the total rate changes most rapidly far away from the wellbore resulting in a high value of K_R in the single phase region. Thompson and Reynolds have shown that in the case of gas condensate drawdown testing, K_λ is many orders larger than K_R. Therefore, the

drawdown pressure derivative data reflect near wellbore properties, or more specifically, properties in the region where the total mobility is changing most rapidly, i.e., the region near where the critical oil saturation is located. However, in the case of buildup, K_λ tends to zero as rate tends to zero (see Eq. 2.1.11), therefore, buildup data are most influenced by the rate kernel and behave in a manner similar to single phase buildup. Buildup data can be analyzed using single phase techniques.

In the case of water injection testing, K_λ is a maximum at the flood front where mobility is changing most rapidly. In this work, we establish that, unlike the gas condensate drawdown case, the rate kernel, K_R always plays an important part in the mobility averaging process, and cannot be ignored. As a result injection pressure derivative data reflect properties both at the flood front and in the unflooded region. Therefore, for a radially heterogeneous reservoir it is possible to detect the permeability changes ahead of the flood front. In the following section we present an analytical model to analyze injection pressure transient data from a multicomposite reservoir.

As in the retrograde condensate gas reservoir case, the falloff derivative is not affected by K_λ, since the near-wellbore rate rapidly approaches zero. Thus falloff tests conform well with single phase theory and can be analyzed using conventional techniques. This point is illustrated in the next chapter.

2.2 Approximate Analytical Solution for Injection in a Multicomposite reservoir

In this section, we derive an approximate analytical solution for water injection in a radially heterogeneous reservoir.

We assume an infinite cylindrical reservoir with a fully penetrating injection well of radius r_w at the center of the reservoir. Wellbore storage effects are neglected. Water is injected into the reservoir at a constant rate, q_w RB/d. Except for connate water, the reservoir is initially assumed to be filled with oil of a small and constant compressibility. The reservoir is made up of $N+1$ concentric cylinders having radii of $r_1, r_2, \ldots r_N, \infty$ with corresponding permeability values of $k_1, k_2, \ldots k_N, k_{N+1}$ respectively. The initial reservoir pressure (p_i) and the initial connate water saturation (S_{wi}) are assumed to be constant everywhere. The reservoir consists of a single layer, and gravitational effects have been neglected.

Figure 2.2.1 illustrates schematically a cross-section of the reservoir after constant-rate injection has been in progress for some time. As in Ref. 13, there is an annular region extending out from the wellbore where the total reservoir rate is essentially constant and equal to the injection rate. Within the constant-total-rate region, a water-flooded annular region also extends out from the wellbore. Both the constant-total-rate region and the water-flooded regions increase in areal extent during the injection process; however, the rate of increase of the constant-total-rate zone is much more rapid than that of the flooded zone. As a function of radial distance from the well, the water saturation changes from $1-S_{or}$ in the water zone to S_{wi} just ahead of the front. Thus, it is clear that the constant total reservoir rate zone consists of only flowing water in the flushed zone,

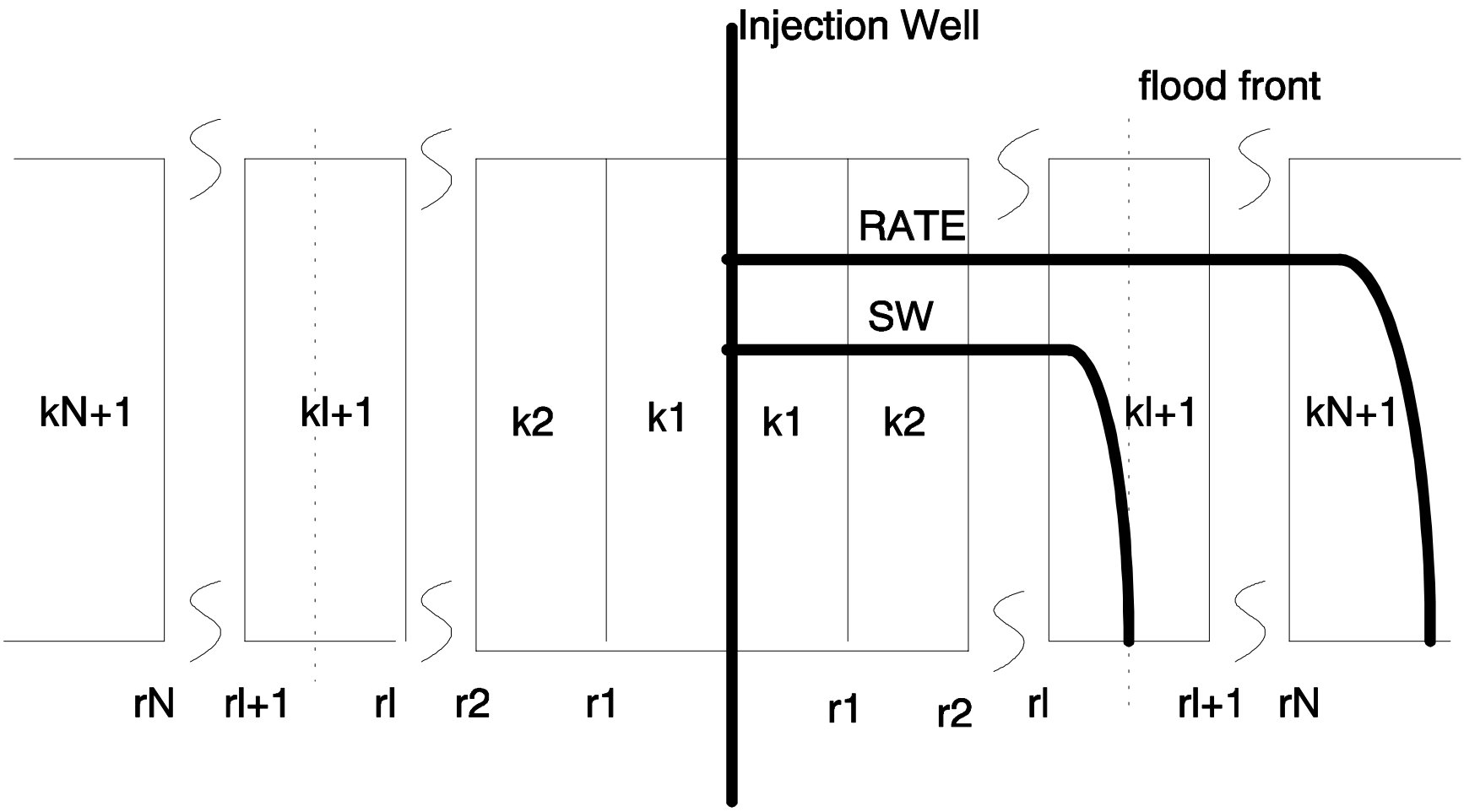
Injection Well
flood front
RATE
SW
kN+1
kl+1
k2
k1
k1
k2
kl+1
kN+1
rN
rl+1
rl
r2
r1
r1
r2
rl
rl+1
rN

flowing oil and water in the transition zone and only flowing oil in the oil bank ahead of the flood front.

Assume that the constant total reservoir rate zone extends up to radius r_N at a particular instant of time. Consider flow across the surface of a cylinder centered at the well, and with radius r_o, such that $r_o = r_N$ and r_o is beyond the water-invaded zone. Since r_o is within the constant-total-rate zone, the volumetric oil rate at r_o must be the same as the water injection rate at r_w, i.e.,

$$q_w\big|_{rw} = q_o\big|_{ro}. \qquad (2.2.1)$$

That is, for reservoir regions at $r > r_o$, the flow behavior is the same as if the reservoir region for $r \le r_o$ were replaced by well of radius r_o at which oil is injected at a constant rate of q_o RB/D. If we were to observe pressure and pressure derivative data at r_o, the pressure p_o and its derivative would show typical single phase pressure transient behavior. In other words, at long times, the pressure derivative at r_o would be given by

$$\frac{d\Delta p_o}{d\ln t} = \frac{70.6q_o}{k_{N+1}\lambda_o h} = \frac{70.6q_w}{k_{N+1}\lambda_o h} = \frac{70.6q_{inj}B_w}{k_{N+1}\lambda_o h}. \qquad (2.2.2)$$

Now let us consider the system within the region $r < r_o = r_N$. Considering r_o to be the outer radius of this "inner reservoir" we can rewrite Eq. 2.1.4 as

$$\int_{r_w}^{r_N} \frac{\partial p}{\partial r}\partial r = \frac{1}{C_1}\int_{r_w}^{r_N} \frac{q_t(r',t)}{r' k(r')\lambda_t(r',t)} dr' \qquad (2.2.3)$$

Integrating the left hand side of Eq. 2.2.3 we have

$$p_o(t) - p_{wf}(t) = \frac{1}{C_1}\int_{r_w}^{r_N} \frac{q_t(r',t)}{r'k(r')\lambda_t(r',t)}dr' \,. \qquad (2.2.4)$$

Let us assume that the flood front is at a position $r_l < r_f < r_{l+1}$. Since the rate everywhere in the region $r_w < r \le r_N$ is constant and equal to $q_{inj}B_w$ RB/day we can rewrite Eq. 2.2.4 as

$$p_o(t) - p_{wf}(t) = \frac{q_{inj}B_w}{C_1}\left[\sum_{j=1}^{l}\int_{r_{j-1}}^{r_j} \frac{1}{r'k(r')\lambda_t(r',t)}dr' + \int_{r_l}^{r_f(t)} \frac{1}{r'k(r')\lambda_t(r',t)}dr' + \int_{r_f(t)}^{r_{l+1}} \frac{1}{r'k(r')\lambda_t(r',t)}dr' + \sum_{j=l+2}^{N+1}\int_{r_{j-1}}^{r_j} \frac{1}{r'k(r')\lambda_t(r',t)}dr'\right] \,. \qquad (2.2.5)$$

If we denote the average mobility in each flooded region to be λ_{tj}, the average mobility in the region $r_l < r < r_{l+1}$ (behind the flood front) by λ_f^-, the average mobility ahead of the front (in the same region) as λ_f^+ and the mobility in the unflooded oil zone as λ_o we can evaluate Eq. 2.2.5 as

$$p_o(t) - p_{wf}(t) = \frac{q_{inj}B_w}{C_1}\left[\sum_{j=1}^{l}\frac{1}{k_j\lambda_{tj}}\ln\left(\frac{r_j}{r_{j-1}}\right) + \frac{1}{k_{l+1}\lambda_f^-}\ln\left(\frac{r_f(t)}{r_l}\right) + \frac{1}{k_{l+1}\lambda_f^+}\ln\left(\frac{r_{l+1}}{r_f(t)}\right) + \sum_{j=l+2}^{N+1}\frac{1}{k_j\lambda_o}\ln\left(\frac{r_j}{r_{j-1}}\right)\right] \,. \qquad (2.2.6)$$

Taking the derivative of Eq. 2.2.6 with respect to natural logarithm of time we have

$$\frac{d\Delta p_{wf}}{d\ln t}-\frac{d\Delta p_o}{d\ln t}=\frac{q_{inj}B_w}{C_1}\left[\sum_{j=1}^{l}\frac{1}{k_j}\ln\left(\frac{r_j}{r_{j-1}}\right)\frac{\partial\left(\frac{1}{\lambda_{tj}}\right)}{\partial\ln t}+\frac{1}{k_{l+1}}\ln\left(\frac{r_f(t)}{r_l}\right)\frac{\partial\left(\frac{1}{\lambda_f^-}\right)}{\partial\ln t}\right.$$
$$+\frac{1}{k_{l+1}\lambda_f^-}\frac{\partial\ln\left(\frac{r_f(t)}{r_l}\right)}{\partial\ln t}-\frac{1}{k_{l+1}}\ln\left(\frac{r_f(t)}{r_{l+1}}\right)\frac{\partial\left(\frac{1}{\lambda_f^+}\right)}{\partial\ln t} \qquad (2.2.7)$$
$$\left.-\frac{1}{k_{l+1}\lambda_f^+}\frac{\partial\ln\left(\frac{r_f(t)}{r_{l+1}}\right)}{\partial\ln t}\right].$$

If the flood front is entirely contained in the region $r_l < r < r_{l+1}$, and saturation in the surrounding regions is changing only very slowly, we can approximate Eq. 2.2.7 as

$$\frac{d\Delta p_{wf}}{d\ln t}-\frac{d\Delta p_o}{d\ln t}=\frac{q_{inj}B_w}{C_1}\left[\frac{1}{k_{l+1}}\ln\left(\frac{r_f(t)}{r_l}\right)\frac{\partial\left(\frac{1}{\lambda_f^-}\right)}{\partial\ln t}+\frac{1}{k_{l+1}\lambda_f^-}\frac{\partial\ln\left(\frac{r_f(t)}{r_l}\right)}{\partial\ln t}\right.$$
$$\left.-\frac{1}{k_{l+1}}\ln\left(\frac{r_f(t)}{r_{l+1}}\right)\frac{\partial\left(\frac{1}{\lambda_f^+}\right)}{\partial\ln t}-\frac{1}{k_{l+1}\lambda_f^+}\frac{\partial\ln\left(\frac{r_f(t)}{r_{l+1}}\right)}{\partial\ln t}\right]. \qquad (2.2.8)$$

Finally, as the flood front moves through the region $r_l < r < r_{l+1}$, we expect that the average mobilities behind (λ_f^-) and beyond (λ_f^+) the flood front will approach mobilities λ_f, (close to λ_w) and λ_o respectively. In this case Eq. 2.2.8 becomes

$$\frac{d\Delta p_{wf}}{d\ln t} - \frac{d\Delta p_o}{d\ln t} = \frac{q_{inj} B_w}{C_1}\left[\frac{1}{k_{l+1}\lambda_f}\frac{\partial \ln\left(\frac{r_f(t)}{r_l}\right)}{\partial \ln t} - \frac{1}{k_{l+1}\lambda_o}\frac{\partial \ln\left(\frac{r_f(t)}{r_{l+1}}\right)}{\partial \ln t}\right] . \qquad (2.2.9)$$

Performing the differentiation in the right hand side of Eq. 2.2.9, we have

$$\frac{d\Delta p_{wf}}{d\ln t} - \frac{d\Delta p_o}{d\ln t} = \frac{q_{inj} B_w}{C_1}\left[\frac{1}{k_{l+1}\lambda_f} - \frac{1}{k_{l+1}\lambda_o}\right]\frac{1}{r_f(t)}\frac{\partial r_f(t)}{\partial \ln t} . \qquad (2.2.10)$$

We now turn our attention to the movement of the flood front in the reservoir. From material balance, we can write an equation for water injected into the reservoir as

$$5.615 q_{inj} B_w t = 2\pi h \int_{r_w}^{r_f(t)} \phi(r)\left[S_w(r,t) - S_{wi}\right] r dr . \qquad (2.2.11)$$

If we consider the average saturation in each region as S_{wj} for j = *1* to *l* and the average saturation behind the flood front in the region $r_l < r < r_f$ as S_{wf} we can evaluate Eq. 2.2.11 as

$$5.615 q_{inj} B_w t = \pi h \left[\sum_{j=1}^{l} \phi_j \left(S_{wj} - S_{wi} \right) \left(r_j^2 - r_{j-1}^2 \right) + \phi_{l+1} \left(S_{wf} - S_{wi} \right) \left(r_f(t)^2 - r_l^2 \right) \right]. \tag{2.2.12}$$

Solving for $r_f(t)$ we have

$$r_f(t)^2 = \frac{5.615 q_{inj} B_w t}{\pi h \phi_{l+1} \left(S_{wf} - S_{wi} \right)} - \frac{\sum_{j=1}^{l} \phi_j \left(S_{wj} - S_{wi} \right) \left(r_j^2 - r_{j-1}^2 \right) - \phi_{l+1} \left(S_{wf} - S_{wi} \right) r_l^2}{\pi h \phi_{l+1} \left(S_{wf} - S_{wi} \right)} . \tag{2.2.13}$$

As oil is flushed from the flooded zone, S_{wj} will approach a value close to $1\text{-}S_{or}$. Also, after the flood front has resided in the block $r_l < r < r_{l+1}$ for some time, the average water saturation in the block behind the front S_{wf}, will also approach $1\text{-}S_{or}$. Under these conditions Eq. 2.2.13 becomes

$$r_f(t)^2 = \frac{5.615 q_{inj} B_w t}{\pi h \phi_{l+1} \left(\overline{S_w} - S_{wi} \right)} - \frac{\sum_{j=1}^{l} \phi_j \left(r_j^2 - r_{j-1}^2 \right) - \phi_{l+1} r_l^2}{\pi h \phi_{l+1}} , \tag{2.2.14}$$

where $\overline{S_w} = 1 - S_{or}$.

For a system with constant porosity, the second term in the right hand side of Eq. 2.2.14 clearly disappears if we neglect the wellbore radius and we have

$$r_f(t) = \sqrt{\frac{5.615 q_{inj} B_w}{\pi h \left(\overline{S_w} - S_{wi}\right)\phi}}\sqrt{t}\,, \tag{2.2.15}$$

or

$$r_f(t) = \alpha\sqrt{t}\,, \tag{2.2.16a}$$

where α is a constant given by

$$\alpha = \sqrt{\frac{5.615 q_{inj} B_w}{\pi h \left(\overline{S_w} - S_{wi}\right)\phi}}\,. \tag{2.2.16b}$$

In order to explore the effect of change in porosity, let us consider a reservoir whose porosity changes from ϕ_1 to ϕ_2, with the zone interface being at radius r_1. In this case, neglecting the wellbore radius, Eq. 2.2.14 becomes

$$r_f(t)^2 = \frac{5.615 q_{inj} B_w t}{\pi h \phi_2 \left(\overline{S_w} - S_{wi}\right)} - \left(\frac{\phi_1 - \phi_2}{\phi_2}\right) r_1^2\,. \tag{2.2.17}$$

If we inject for long enough time and/or the porosity contrast is low so that $r_f(t)^2 >> \frac{\phi_1 - \phi_2}{\phi_2} r_1^2$, Eq. 2.2.17 degenerates to Eq. 2.2.16. In other words Eq. 2.2.16 will not be valid immediately when the flood front crosses a porosity change interface. We would instead have an equation of the form

$$r_f(t) = \alpha\sqrt{t+\gamma}\,, \tag{2.2.18}$$

where α is given by Eq. 2.2.16b, and γ is a constant given by

$$\gamma = -\left(\frac{\phi_1 - \phi_2}{\phi_2}\right)\frac{r_1^2}{\alpha^2}. \tag{2.2.18a}$$

The above observation has been also validated through two-phase numerical simulation of slightly compressible oil water system. Figure 2.2.2 shows a plot of the radial distance to the flood front (defined as the maximum radius at which $S_w = 1\text{-}S_{or}$

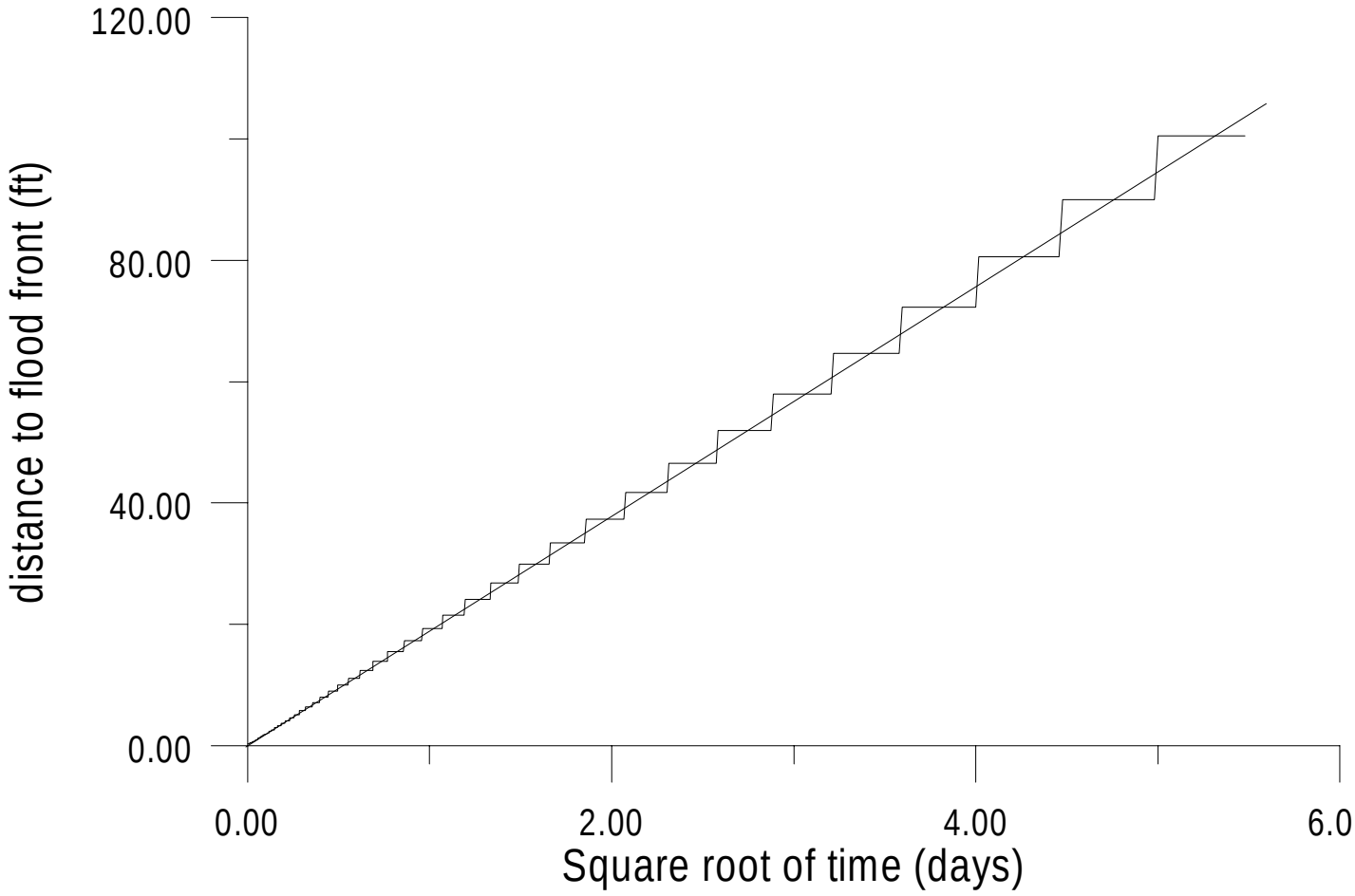

Figure 2.2.2 :Radial Distance to the Flood Front versus Square Root of Time

versus square root of injection time generated by simulating water injection into a heterogeneous reservoir (k = 50 md for $r_w \le r \le 500$ ft ; k = 20 md for $r > 500$ ft and porosity constant at 0.10 thorough out the reservoir.). It is obvious from the plot that a constant slope is maintained. That is the flood front position is directly proportional to the square root of time. Note that the step structure of the plot is due to the block sizes in the finite difference simulator. On the other hand, if the heterogeneity is in terms of changing porosity as well as permeability (ϕ = 0.1 for $r_w \le r \le 500$ ft ; ϕ = 0.2 for $r > 500$ ft), we have a plot of radial distance to the flood front versus square root of injection time showing different slopes for the different zones (see Fig. 2.2.3). However, given a particular zone of constant porosity the slope is practically constant.

Returning to our system, if we assume the position of the flood front as given by Eq. 2.2.16a to be valid we have, after replacing the value of C_1 and performing the differentiation in the right hand side of Eq. 2.2.10

$$\frac{d\Delta p_{wf}}{d\ln t} - \frac{d\Delta p_o}{d\ln t} = \frac{70.6 q_{inj} B_w}{k_{l+1}} \left[\frac{1}{\lambda_f} - \frac{1}{\lambda_o} \right] . \qquad (2.2.19)$$

However, when the flood front crosses a porosity interface we would have to use Eq. 2.2.18 in Eq. 2.2.10. This would result in

$$\frac{d\Delta p_{wf}}{d\ln t} - \frac{d\Delta p_o}{d\ln t} = \frac{70.6 q_{inj} B_w}{k_{l+1}} \left[\frac{1}{\lambda_f} - \frac{1}{\lambda_o} \right] \frac{t}{t+\gamma} . \qquad (2.2.20)$$

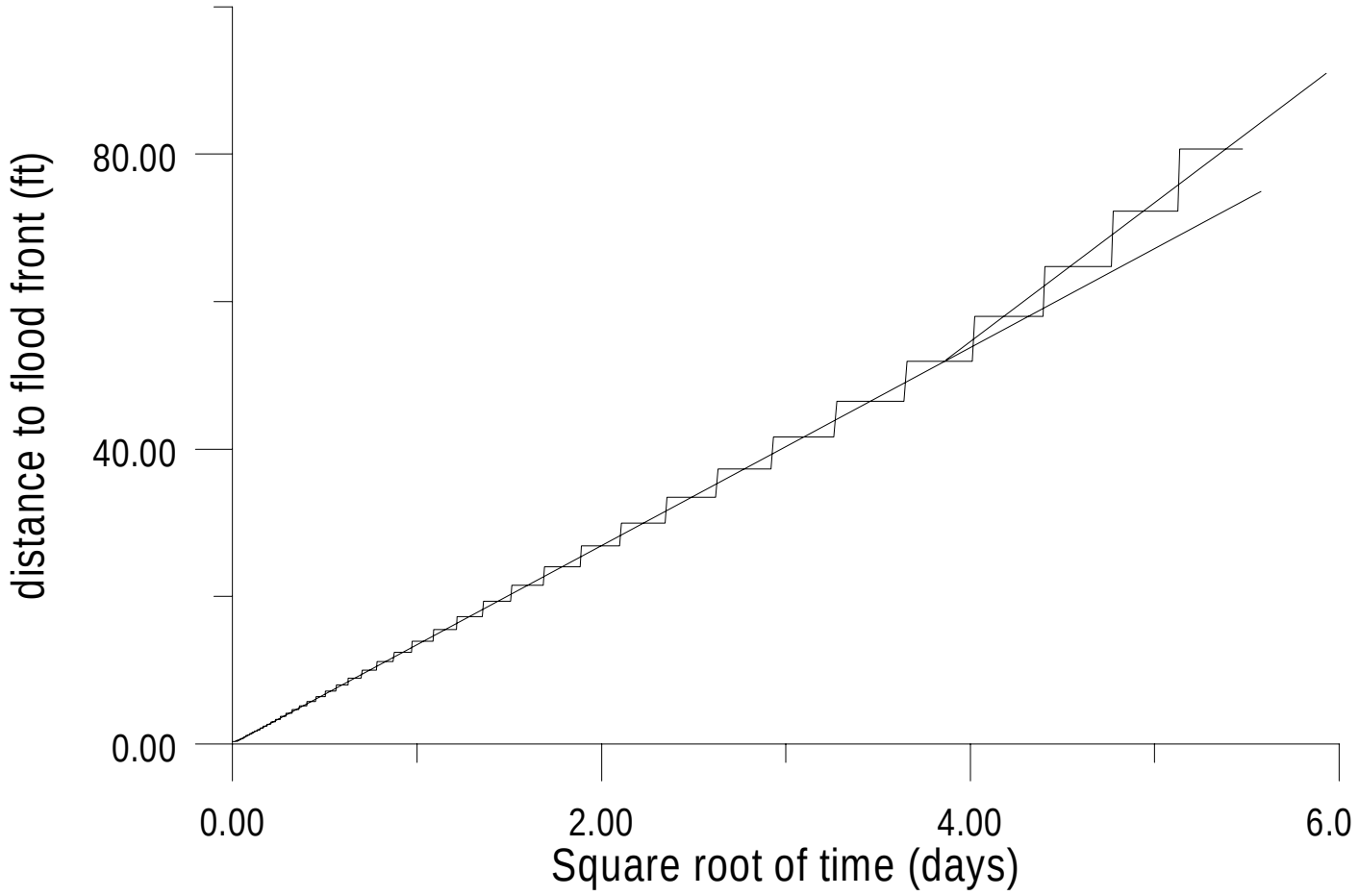

Figure 2.2.3 : Radial distance to flood front versus square root of time

For $\phi_2 > \phi_1$, γ, (Eq. 2.2.18a) is positive and evaluating Eq. 2.2.20 we would obtain a value less than that obtained from evaluating Eq. 2.2.19. On the other hand, for $\phi_2 < \phi_1$, γ is negative Eq. 2.2.20 would yield a value higher than Eq. 2.2.19.

Note that if the large diameter well pressure derivative reflects mobility in the unflooded zone with absolute permeability k_{N+1}, we can replace Eq. 2.2.2 directly into Eq. 2.2.19 to obtain

$$\frac{d\Delta p_{wf}}{d\ln t} = \frac{70.6 q_{inj} B_w}{h}\left[\frac{1}{k_{l+1}\lambda_f} - \frac{1}{\lambda_o}\left[\frac{1}{k_{l+1}} - \frac{1}{k_{N+1}}\right]\right]. \qquad (2.2.21)$$

For a homogeneous reservoir with permeability k Eq. 2.2.21 reduces to

$$\frac{d\Delta p_{wf}}{d\ln t} = \frac{70.6 q_{inj} B_w}{k\lambda_f h} \quad . \qquad (2.2.22)$$

This is the well established result for injection tests in homogeneous reservoirs which gave rise to the belief that it is impossible to see beyond the flood front in an injection test. If the reservoir were a two zone system as shown in Fig. 2.2.4 and the pressure derivative at the large diameter well were constant with the value reflecting permeability of the first zone, k_1, Eq. 2.2.22 would still be valid. However, if the pressure

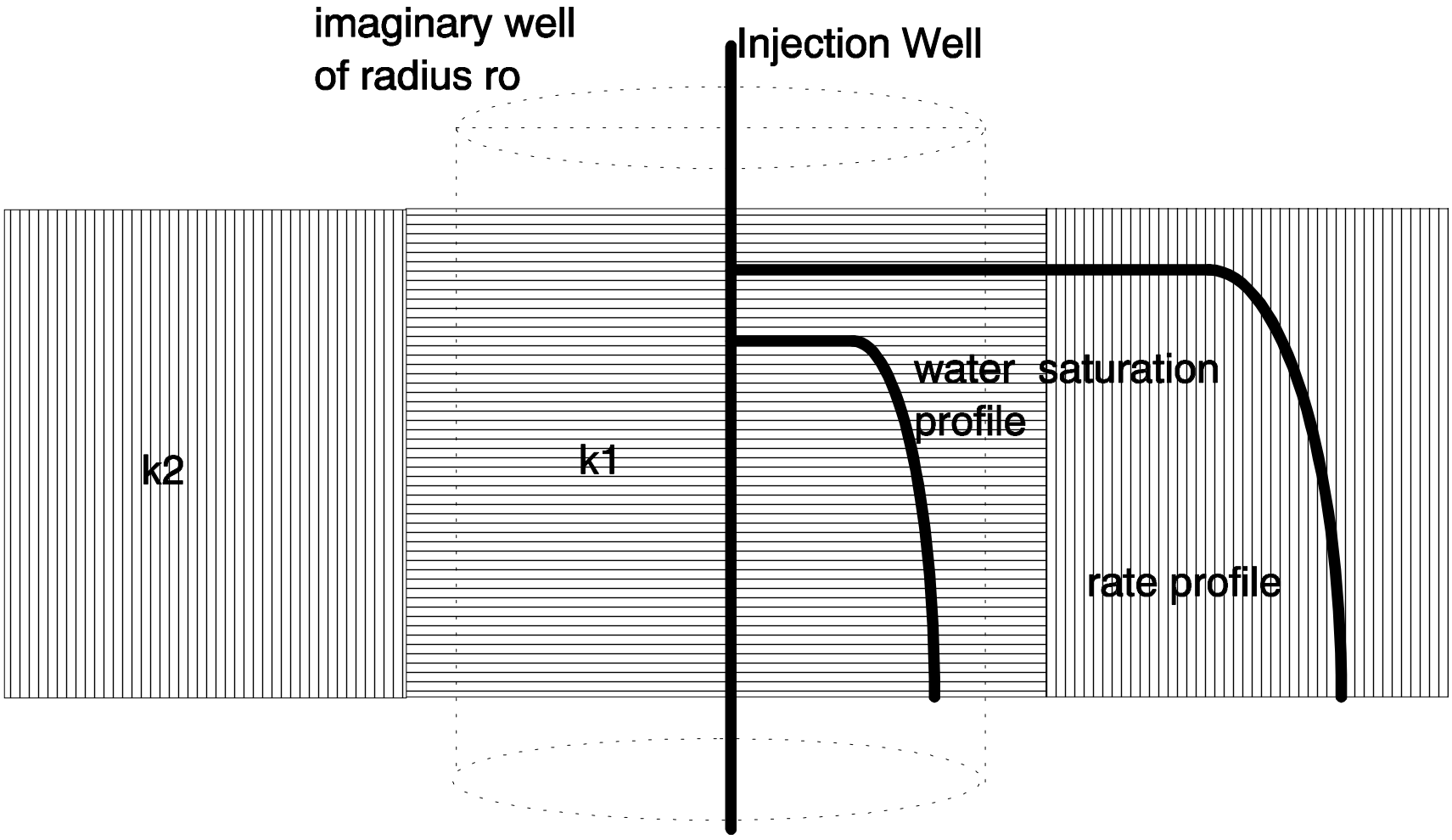
imaginary well
of radius ro
Injection Well
water saturation
profile
k2
k1
rate profile

derivative at the large diameter well were constant with slope reflecting permeability of the outer zone, k_2, Eq. 2.2.21 becomes

$$\frac{d\Delta p_{wf}}{d\ln t} = \frac{70.6 q_{inj} B_w}{h}\left[\frac{1}{k_1\lambda_f} - \frac{1}{\lambda_o}\left[\frac{1}{k_1} - \frac{1}{k_2}\right]\right]. \qquad (2.2.23)$$

Equation 2.2.23 suggests that if end-point mobilities are known and distinct sets of semilog data are available at the injection well, it would be possible to compute permeabilities corresponding to the various semilog straight lines.

Let us consider what happens when the flood front moves to the second zone as illustrated in Fig. 2.2.5. Putting $k_{l+1} = k_{N+1} = k_2$ we have

$$\frac{d\Delta p_{wf}}{d\ln t} = \frac{70.6 q_{inj} B_w}{k_2 h \lambda_f} \ . \qquad (2.2.24)$$

Equation 2.2.24 suggests that if the flood front is in the second zone, the corresponding straight line obtained from the semilog plot gives us the mobility-permeability product of the second zone. However, note that the derivative will deviate from the value evaluated using Eq. 2.2.24 at the time when the flood front just crosses over the heterogeneity interface. We have already explained that Eq. 2.2.19 would not be strictly valid at the instant when the flood front crosses over a heterogeneity interface, hence, Eq. 2.2.24, which is derived from Eq. 2.2.19, would also deviate at that situation.

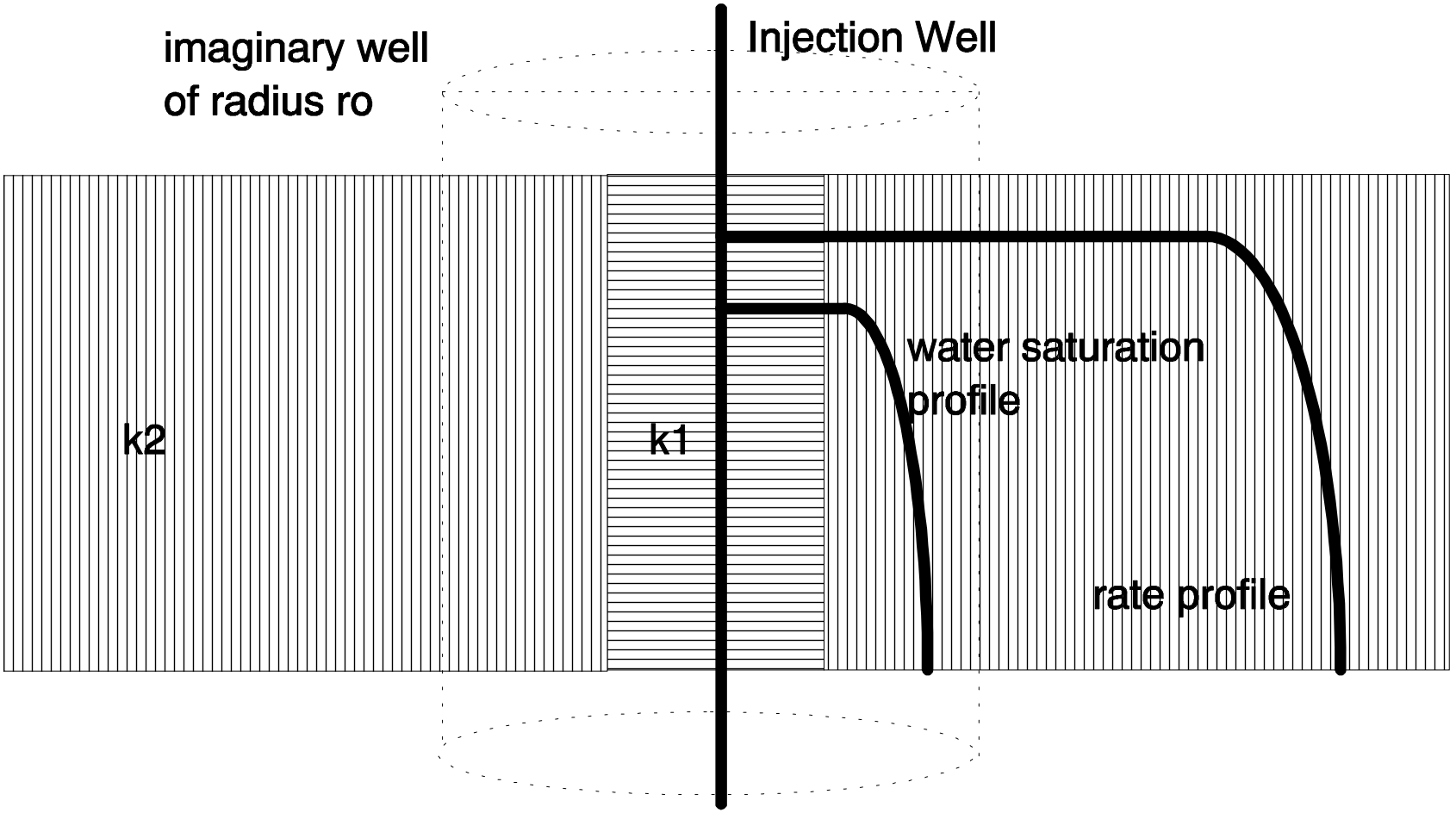
imaginary well
of radius ro
Injection Well
water saturation
profile
k2
k1
rate profile

The equations developed above are consistent with the theory of multiphase pressure transient analysis discussed in Section 2.1. We had obtained Eq. 2.1.7 which is repeated here as

$$\frac{d\Delta p_{wf}(t)}{d\ln t} = \frac{1}{C_1}\int_{r_w}^{\infty}\frac{1}{k(r')}\frac{1}{r'}\left[\frac{1}{\lambda_t(r',t)}\frac{\partial q_t(r',t)}{\partial \ln t} - \frac{q_t(r',t)}{\lambda_t^2(r',t)}\frac{\partial \lambda_t(r',t)}{\partial \ln t}\right]dr' . \qquad (2.2.25)$$

For the imaginary observation well of radius r_o, Eq. 2.1.12 which describes the single-phase pressure derivative would be valid. Therefore, rewriting Eq. 2.1.12 in general form we have

$$\frac{d\Delta p_o(t)}{d\ln t} = \frac{1}{\lambda_t C_1}\int_{r_o}^{\infty}\frac{1}{k(r')}\frac{1}{r'}\left[\frac{\partial q_t(r',t)}{\partial \ln t}\right]dr' . \qquad (2.2.26)$$

Using Eq. 2.2.26 and 2.2.25 we have

$$\begin{aligned}\frac{d\Delta p_{wf}}{d\ln t} - \frac{d\Delta p_o}{d\ln t} = &-\frac{1}{C_1}\int_{r_w}^{\infty}\frac{1}{k(r')r'}\left[\frac{q_t(r',t)}{\lambda_t^2(r',t)}\frac{\partial \lambda_t(r',t)}{\partial \ln t}\right]dr' \\ &+\frac{1}{C_1}\int_{r_w}^{r_o}\frac{1}{k(r')r'}\left[\frac{1}{\lambda_t}\frac{\partial q(r',t)}{\partial \ln t}\right]dr' .\end{aligned} \qquad (2.2.27)$$

Since we have "steady state" flow in the region $r_w < r < r_o$, $\frac{\partial q(r',t)}{\partial \ln t} = 0$ and Eq. 2.2.27 reduces to

$$\frac{d\Delta p_{wf}}{d\ln t}-\frac{d\Delta p_o}{d\ln t}=-\frac{1}{C_1}\int_{r_w}^{\infty}\frac{1}{k(r')r'}\left[\frac{q_t(r',t)}{\lambda_t^2(r',t)}\frac{\partial\lambda_t(r',t)}{\partial\ln t}\right]dr'. \qquad (2.2.28)$$

Note that mobility changes rapidly at the flood front where the total reservoir rate is constant. We can rewrite Eq. 2.2.28 as

$$\frac{d\Delta p_{wf}}{d\ln t}-\frac{d\Delta p_o}{d\ln t}=\frac{q_{inj}B_w}{C_1}\int_{r_w}^{\infty}\frac{1}{k(r')\lambda_t(r',t)r'}\left[-\frac{1}{\lambda_t(r',t)}\frac{\partial\lambda_t(r',t)}{\partial\ln t}\right]dr'. \quad (2.2.29)$$

Eq. 2.2.29 indicates that the well test pressure derivative data are highly influenced by the mobility at the flood front, since it is at this radius that mobility is changing most rapidly. Eqs. 2.2.19 and 2.2.29 present alternative expressions for pressure derivative data in identical systems. This suggests that the function $\frac{1}{\lambda_t(r',t)}\frac{\partial\lambda_t(r',t)}{\partial\ln t}$ must resemble the function depicted in Fig. 2.2.6; i.e., it must display the following properties:

1. $\int_{r_w}^{r_f}\frac{1}{\lambda_t(r',t)}\frac{\partial\lambda_t(r',t)}{\partial\ln t}dr'=-\frac{1}{2}$

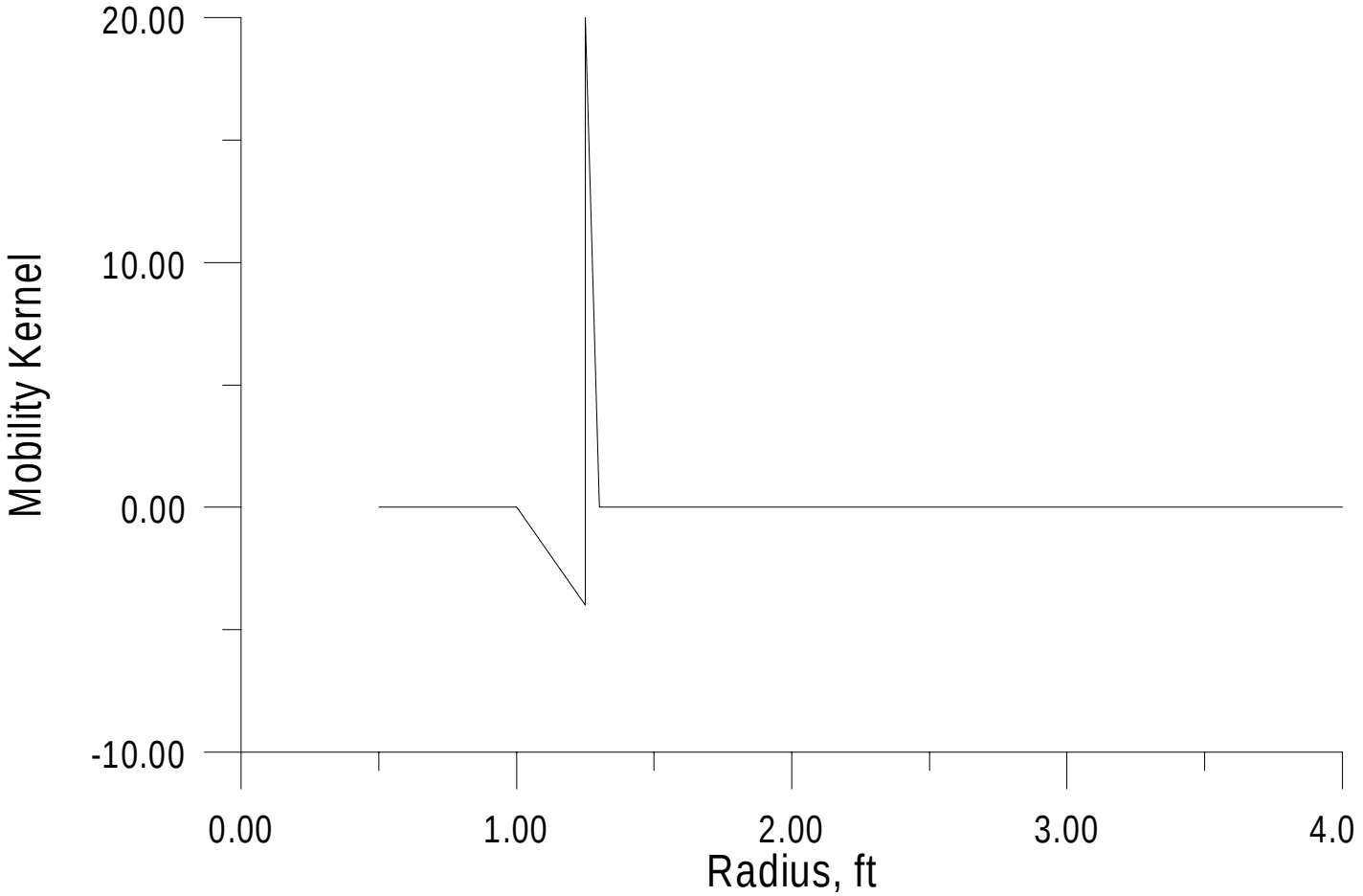
20.00
10.00
0.00
-10.00
Mobility Kernel
0.00
1.00
2.00
3.00
4.0
Radius, ft

2. $$\int_{r_f}^{\infty} \frac{1}{\lambda_t(r',t)} \frac{\partial \lambda_t(r',t)}{\partial \ln t} dr' = \frac{1}{2}$$

In subsequent sections, we show that the numerical mobility kernels computed from our simulation runs qualitatively support this conclusion.

2.3 Calculation of skin

Wellbore damage or improvement is the steady-state pressure drop at the wellface in excess of the "normal" pressure drop in the undamaged reservoir. The additional pressure drop is called the "skin effect" because it occurs in a thin "skin" zone around the wellbore. The degree of damage or improvement is expressed in terms of a dimensionless "skin factor", *s*, which is positive for damage and negative for improvement. It can vary from about -5 for a hydraulically fractured well to typically 10-20 or even more for a badly damaged well. In this section, we present a methodology for calculation of skin factor for the special case of water injection in a homogeneous reservoir. In the heterogeneous case, if the radius of the zone nearest the well were large enough, we would see a distinct semilog straight line reflecting the zone properties, and the analytical solution we developed in the previous section would be valid. In this section, we focus on thin skin zones - i.e., such that no distinct semilog straight line is available for the zone. For this case, we develop a relationship between the true mechanical skin factor, *s*, and apparent skin factor, $s_{app,}$ obtained from conventional semilog analysis. Note s_{app} incorporates the effect of the moving water flood front.

Pressure drop due to skin is given by the following equation:

$$\Delta p_s = \frac{141.2qB}{kh} s \ . \qquad (2.3.1)$$

If skin is viewed as a zone of radius r_s with permeability k_s then skin factor can be expressed as[15]

$$s = \left(\frac{k}{k_s} - 1 \right) \ln \left(\frac{r_s}{r_w} \right) . \qquad (2.3.2)$$

For the purpose of calculation of skin let us consider a homogeneous reservoir of permeability k and a damaged zone of permeability k_s extending from the wellbore to a radius r_s. Let us assume that water is injected into the reservoir through an injection well of radius r_w at a rate of q_{inj} STB/D. Figure 2.3.1 illustrates schematically a cross-section of the reservoir after injection has been in progress for some time. As already explained in Section 2.2, we have a zone of a constant reservoir rate propagating into the reservoir. Behind this we have the flood front propagating at a much slower rate. Let the flood front be at a radial distance r_f from the wellbore at some time t. Physically, three distinct reservoir regions will exist after a short injection time: a near-wellbore flooded region where only water is mobile, a transition region where both oil and water are flowing, and an unflooded region where only oil is mobile. For the purpose of model development, we

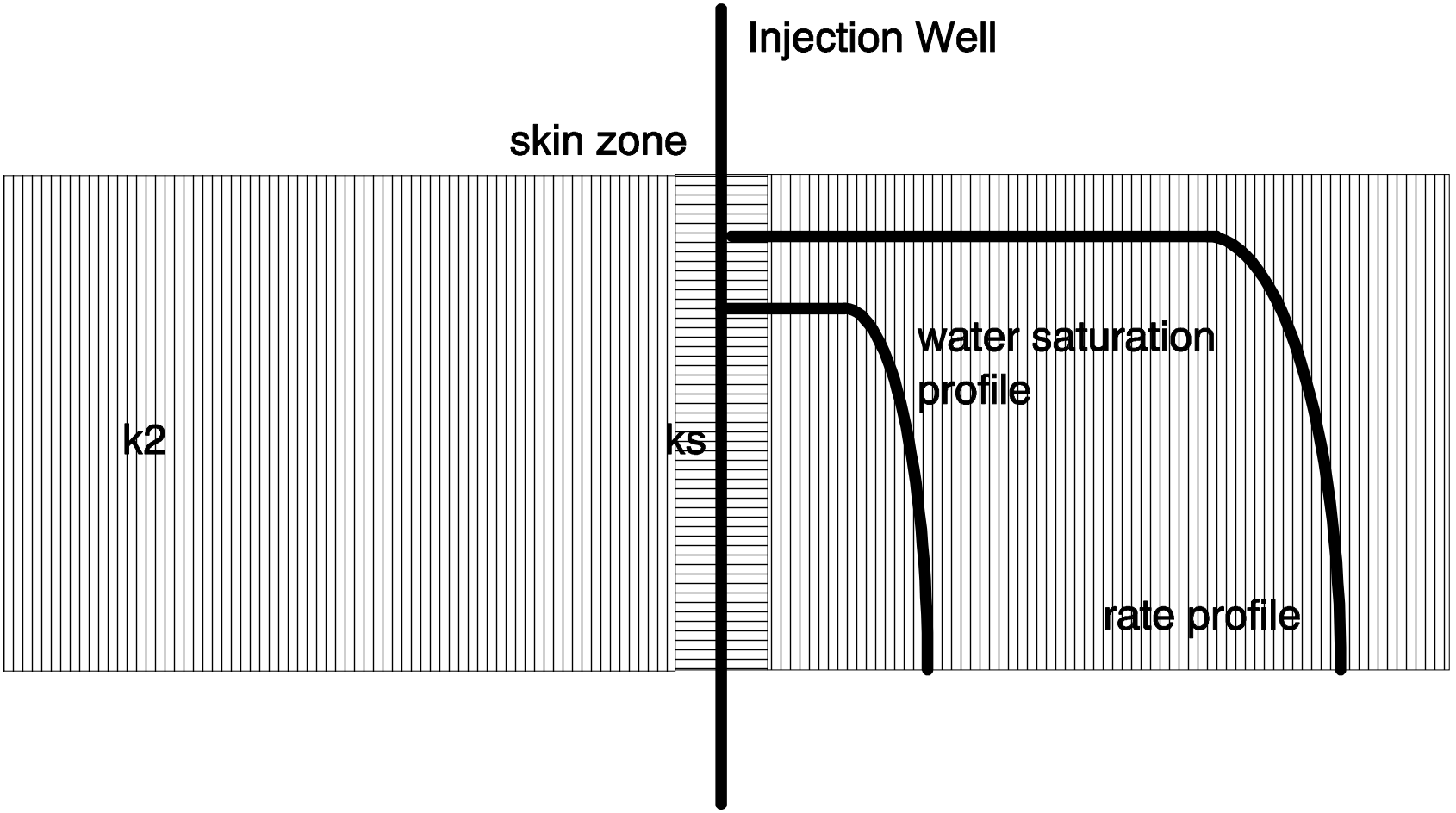
Injection Well
skin zone
k2
ks
water saturation
profile
rate profile

assume that after a short period, the transition region will be small when compared to the other regions. Since the flooded region is in the “steady-state” zone we can write

$$p_{wf} - p_f = \frac{141.2 q_{inj} B_w}{h \lambda_w} \left[\frac{1}{k_s} \ln\left(\frac{r_s}{r_w} \right) + \frac{1}{k} \ln\left(\frac{r_f}{r_s} \right) \right], \qquad (2.3.3)$$

where p_f is the pressure at the flood front.

Combining Eqs. 2.3.3 and Eq. 2.3.2 and eliminating the damaged zone permeability k_s, we have

$$p_{wf} - p_f = \frac{141.2 q_{inj} B_w}{k h \lambda_w} \left[s + \ln\left(\frac{r_s}{r_w} \right) + \ln\left(\frac{r_f}{r_s} \right) \right]. \qquad (2.3.4)$$

Simplifying Eq. 2.3.4 further we have

$$p_{wf} - p_f = \frac{141.2 q_{inj} B_w}{k h \lambda_w} \left[\ln\left(\frac{r_f}{r_w} \right) + s \right]. \qquad (2.3.5)$$

Let us now consider the region to the right of the front, $r \geq r_f$. Here r_f not only denotes a fixed radial location but also denotes the radius of the front at a specific time $t = t_f$. Since the constant zone rate propagates further than the front, $q_t(r_f, t) = q_w$ for all $t \geq t_1$ where t_1 is the earliest time at which $q_t(r_f, t) = q_w$ and $t_1 < t_f$. For $t < t_1$, $q_t(r_f, t) < q_w$. If we consider an imaginary well with wellbore radius r_f, then in essence

the time period $t < t_1$ corresponds to a wellbore storage period. However, similar to the wellbore storage solution, once t is sufficiently greater than t_1, the pressure response at r_f will be given by the equation

$$p_f - p_i = \frac{141.2 q_{inj} B_w}{kh\lambda_o}\left[\frac{1}{2}\left(\ln\left(t_D\right) + 0.80907\right)\right], \qquad (2.3.6)$$

where

$$t_D = \frac{0.0002637 k\lambda_o t}{\phi c_{to} r_f^2} \quad . \qquad (2.3.7)$$

In Eq. 2.3.7 time, t, is in hours and c_{to} is the total compressibility in the oil zone ($c_f + c_o(1-S_{wi}) + c_w S_{wi}$).

Eq. 2.3.6 can also be derived by assuming that the pressure response at r_f is only influenced by the total flow rate profile that occurs in the reservoir. As this profile does not appear to be influenced by multiphase flow effects, we expect that

$$p_f - p_i = \frac{141.2 q_o}{kh\lambda_o}\left[-\frac{1}{2} Ei\left(\frac{-1}{4t_D}\right)\right] \quad , \qquad (2.3.8)$$

where t_D is given by Eq. 2.3.7. Thus, for $t_D > 50$, Eq. 2.3.8 can also be approximated by the semi-log equation given by Eq. 2.3.6.

Adding Eqs. 2.3.5 and 2.3.6 we have

$$p_{wf} - p_i = \frac{141.2 q_{inj} B_w}{kh}\left[\frac{1}{2\lambda_o}\ln\left(\frac{0.0002637 kt\lambda_o}{\phi c_{to} r_f^2}\right) + \frac{0.80907}{2\lambda_o} + \frac{1}{\lambda_w}\ln\left(\frac{r_f}{r_w}\right) + \frac{s}{\lambda_w}\right]. \quad (2.3.9)$$

The radial distance to the flood front, r_f, can be determined from Eq 2.2.16, viz.,

$$r_f = \alpha\sqrt{t}\,, \quad (2.3.10)$$

where α is the Boltzman's constant which can be determined by

$$\alpha = \sqrt{\frac{5.615 q_{inj} B_w}{\pi h(\overline{S_w} - S_w)\phi}}\,. \quad (2.3.11)$$

Using Eq. 2.3.10 into Eq. 2.3.9 and simplifying we have

$$p_{wf} - p_i = \frac{162.6 q_{inj} B_w}{kh}$$
$$\left[\frac{1}{\lambda_o}\log\left(\frac{k\lambda_o}{\phi c_{to}\alpha^2}\right) - \frac{3.2275}{\lambda_o} + \frac{1}{\lambda_w}\log\left(\frac{\alpha^2}{r_w^2}\right) + \frac{1}{\lambda_w}\log(t) + \frac{0.86859 s}{\lambda_w}\right]. \quad (2.3.12)$$

At time t = 1 hour Eq. 2.3.12 becomes

$$p_{1hr} - p_i = \frac{162.6 q_{inj} B_w}{kh}\left[\frac{1}{\lambda_o}\log\left(\frac{k\lambda_o}{\phi c_{to}\alpha^2}\right) - \frac{3.2275}{\lambda_o} + \frac{1}{\lambda_w}\log\left(\frac{\alpha^2}{r_w^2}\right) + \frac{0.86859 s}{\lambda_w}\right]. \quad (2.3.13)$$

Subtracting Eq. 2.3.13 from Eq. 2.3.12 we have

$$p_{wf} - p_{1hr} = \frac{162.6 q_{inj} B_w}{kh}\left[\frac{1}{\lambda_w}\log(t)\right]. \quad (2.3.14)$$

The semi-log slope can then be represented as

$$m = \frac{162.6 q_{inj} B_w}{kh\lambda_w} \ . \quad (2.3.15)$$

Writing Eq. 2.3.13 in terms of *m* and rearranging the terms we obtain

$$s = 1.151\left[\frac{p_{1hr} - p_i}{m} - \frac{\lambda_w}{\lambda_o}\log\left(\frac{k\lambda_o}{\phi c_{to}\alpha^2}\right) + 3.2275\frac{\lambda_w}{\lambda_o} - \log\left(\frac{\alpha^2}{r_w^2}\right)\right]. \quad (2.3.16)$$

Eq. 2.3.16 gives the mechanical skin due to near wellbore damage or improvement. The apparent skin, s_{app}, due to near wellbore effects as well as mobility changes at the flood front is given by the conventional formula, i.e.,

$$s_{app} = 1.151\left[\frac{p_{1hr} - p_i}{m} - \log\left(\frac{k\lambda_w}{\phi c_t r_w^2}\right) + 3.2275\right]. \qquad (2.3.17)$$

In order to get a relationship between s and s_{app} we subtract Eqs. 2.3.17 from 2.3.16 which gives us

$$s = s_{app} + 1.151\left[\log\left(\frac{k\lambda_w}{\phi c_{to}\alpha^2}\right) - \frac{\lambda_w}{\lambda_o}\log\left(\frac{k\lambda_o}{\phi c_t \alpha^2}\right) + 3.2275\left(\frac{\lambda_w}{\lambda_o} - 1\right)\right]. \quad (2.3.18)$$

2.4 Model Validation

The objective of this work was to determine whether pressure transient data obtained from an injection test could be affected by heterogeneity beyond the flood front. In Section 2.2 we had argued that it is indeed possible to "see" beyond the flood front in an injection test. Furthermore, we presented an analytical model which can be used to determine the absolute permeability ahead of the flooded zone. Also in Section 2.3, we had presented a formula for calculation of skin. In this section, we present results obtained from analysis of synthetic well test data generated using a two-phase radial flow simulator. Details of the simulator are provided in Appendix 1.

- Case I:

We simulated water injection at 250 STB/day into a multi-composite oil reservoir containing two zones: k = 50 md for $0.25 < r \leq 500$ ft and k=20 md for $500 < r \leq 5000$ ft.

The relative permeability curves are depicted in Fig. 2.4.1, and other pertinent reservoir and fluid data are presented in Table 2.4.1. When water is injected into a reservoir at constant rate, a zone of constant total injection rate, q_t (i.e., $q_oB_o+q_wB_w$ RB/D) propagates out from the wellbore, in addition to the propagation of a zone from which oil has been flushed. Figs. 2.4.2 - 2.4.5 show rate and saturation profiles as functions of radius at various times during the injection process. If we consider the zone in which the total rate is constant as a "steady state" zone, we see that the flooded zone is always within the steady state zone. We calculated the distance to the flood front using Eq. 2.2.15 for 10 days of injection. We obtained a value of 44.62 ft compared to 50 ft obtained by simulation (Fig. 2.4.4).

Figures 2.4.6 - 2.4.9 show plots of rate and mobility kernels (see Eqs. 2.1.10 and 2.1.11) corresponding to Figs. 2.4.2 - 2.4.5. A plot of total mobility-permeability product at the end of the injection test and absolute permeability is presented in Figs. 2.4.10 - 2.4.13. Considering Figs. 2.4.6 - 2.4.9, as we proceed out from the wellbore, the mobility kernel becomes slightly negative, then in the immediate neighborhood of the flood front, it increases rapidly to a large value and thereafter declines rapidly to zero. Note that the mobility kernel is larger in magnitude than the rate kernel and is also nearer to the wellbore than the rate kernel. Recall that pressure derivative reflects a weighted harmonic average of permeability. The weighting function is the total kernel $K(r,t)$, which depends upon the magnitude of the rate and mobility kernels (K_R , K_λ). Therefore, at a first glance, it seems that pressure derivative data must be influenced primarily by mobility kernel. In other words, pressure derivative data should only reflect average permeability/mobility behind the flood front. However, a closer look at Figs. 2.4.6 - 2.4.9

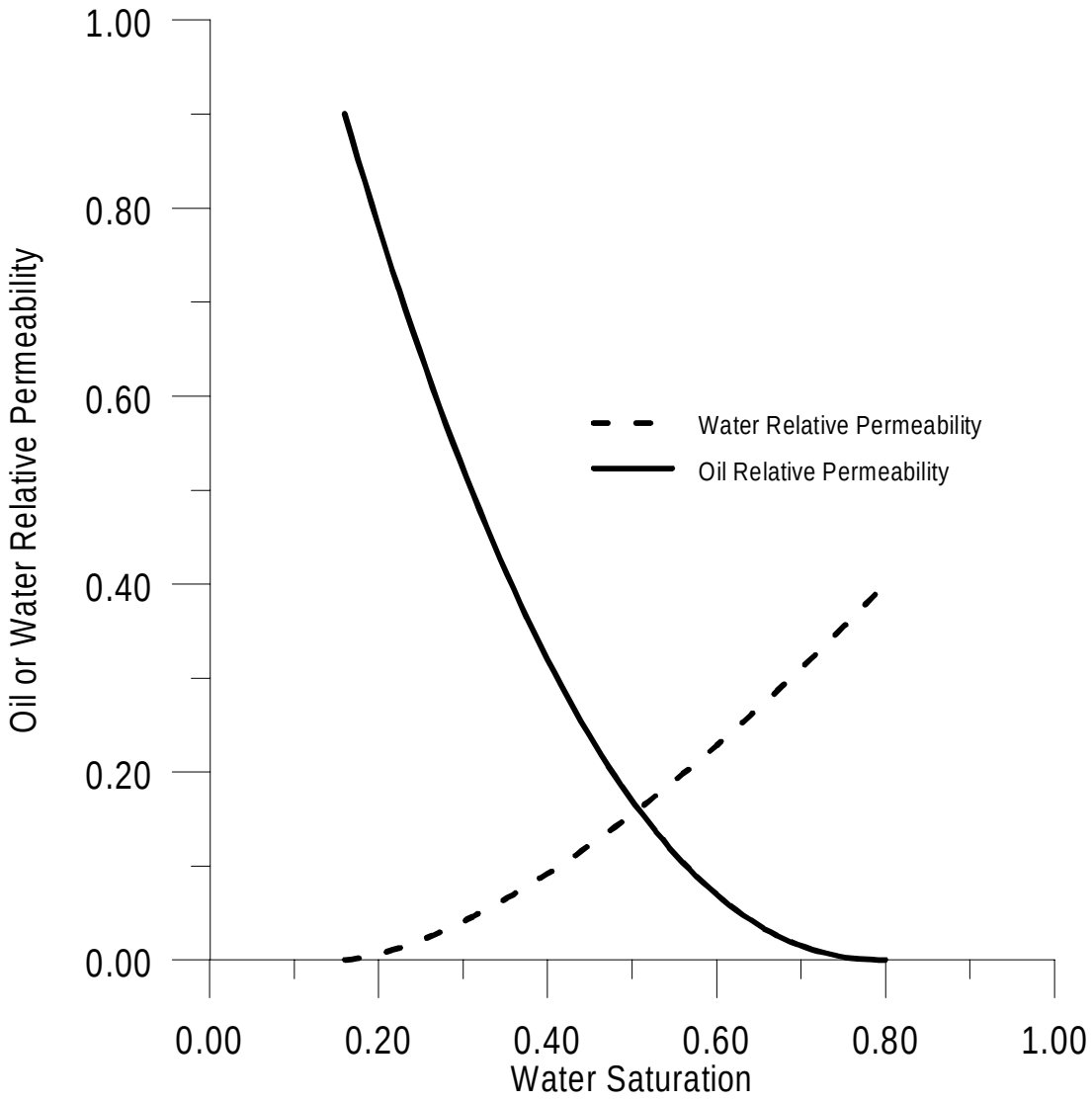

Figure 2.4.1: Relative Permeability Curves

Reservoir/Fluid Data	
Wellbore Radius	0.25 ft
Reservoir Radius	5000.00 ft
Oil Viscosity	0.64 cp
Water Viscosity	1.0 cp
Oil Compressibility	10.0 E-06 psi^{-1}
Water Compressibility	3.0 E-06 psi^{-1}
Porosity	10.0 %
Connate Water Saturation	16.0 %
Irreducible Oil Saturation	20.0 %
Initial Pressure	2000.0 psia
Injection Rate	250.0 barrels/day

Table 2.4.1: Reservoir and Fluid Data

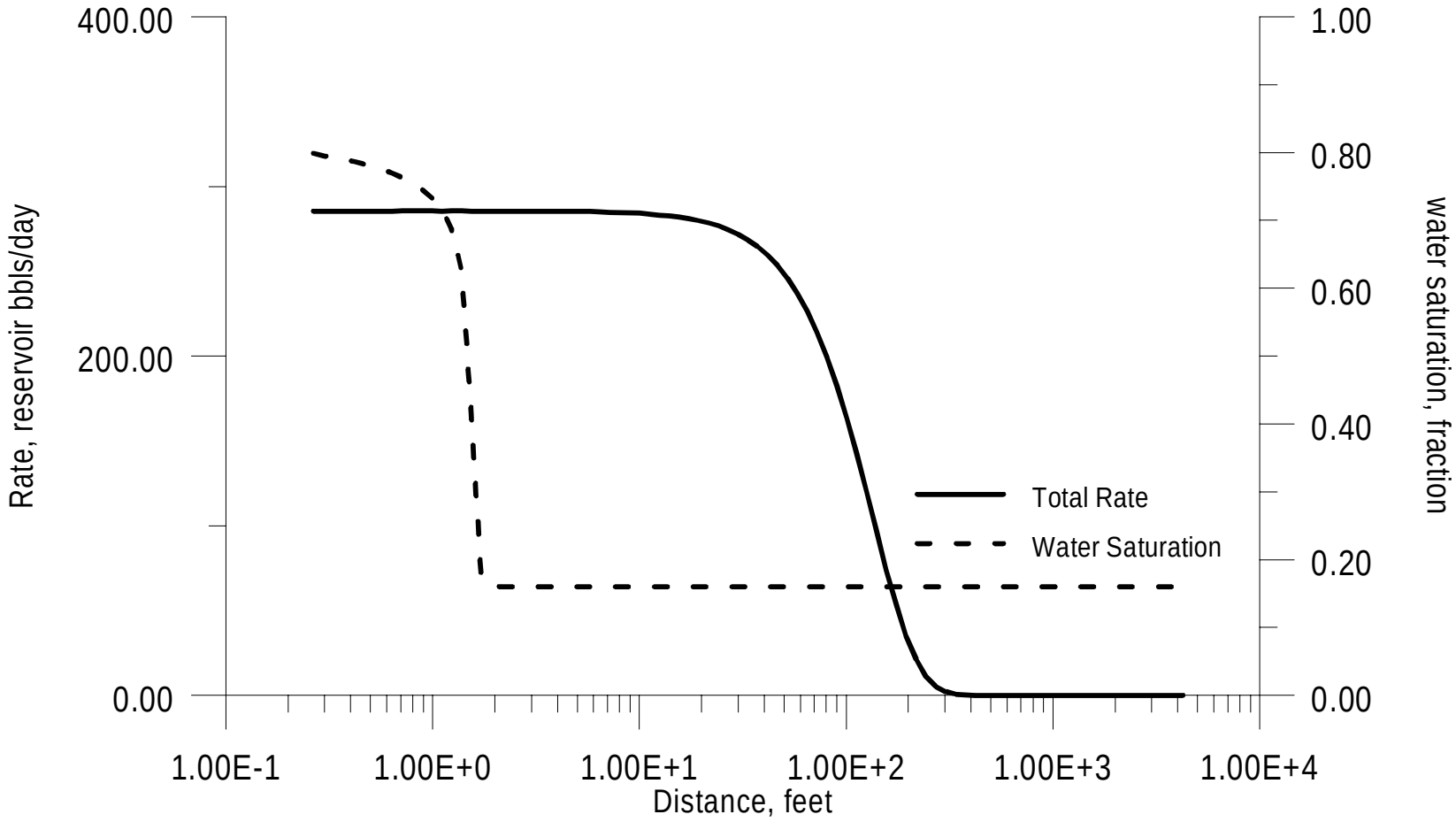

Figure 2.4.2: Rate and Saturation Profiles as a function of Radius

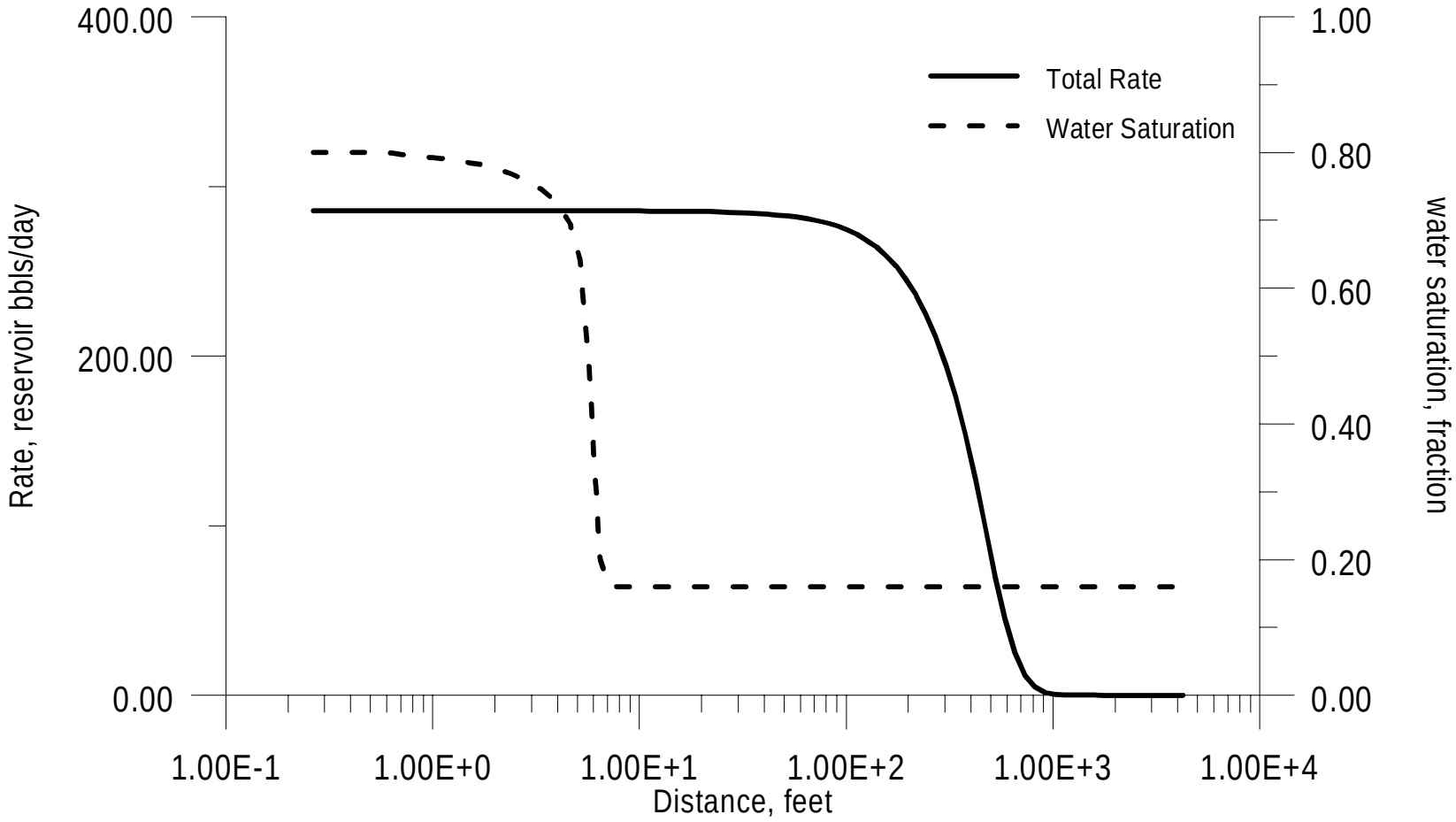

Fig. 2.4.3: Rate and Saturation Profiles as a function of Radius

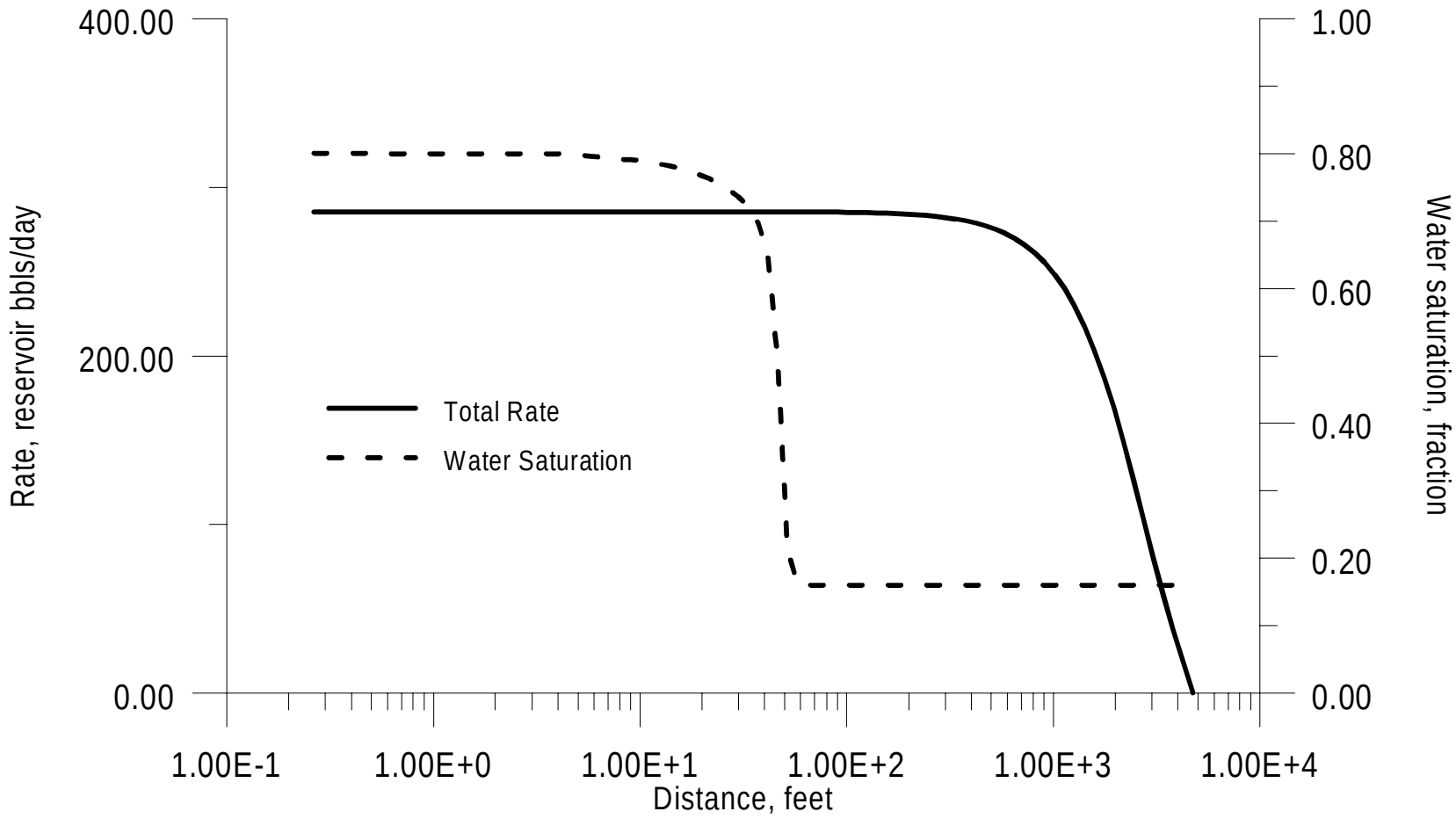

Fig. 2.4.4: Rate and Saturation Profiles as a function of Radius

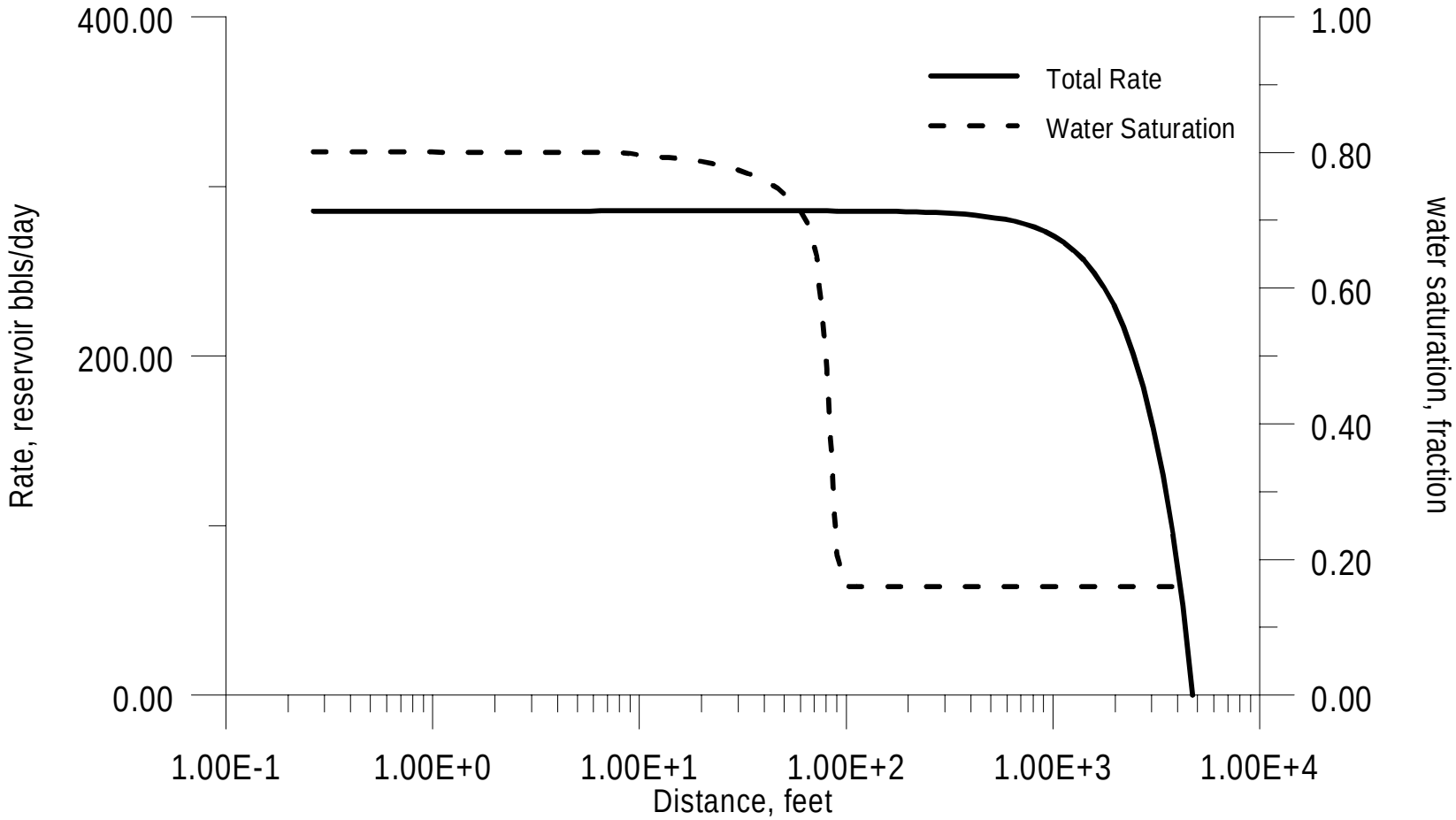

Fig. 2.4.5: Rate and Saturation Profiles as a function of Radius

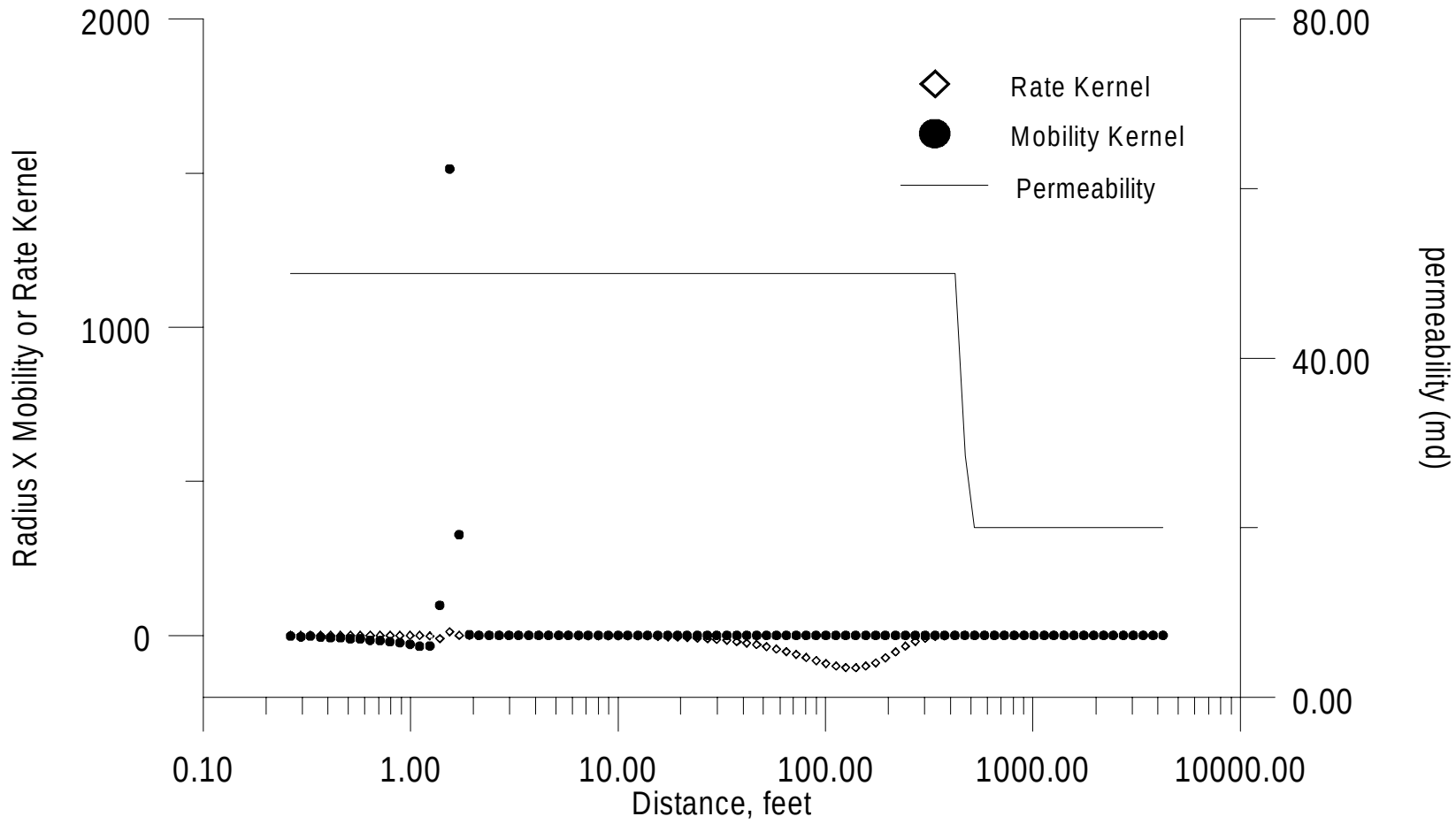

Fig. 3.4.6 Mobility and Rate Kernels at 0.01 dp (Case I)

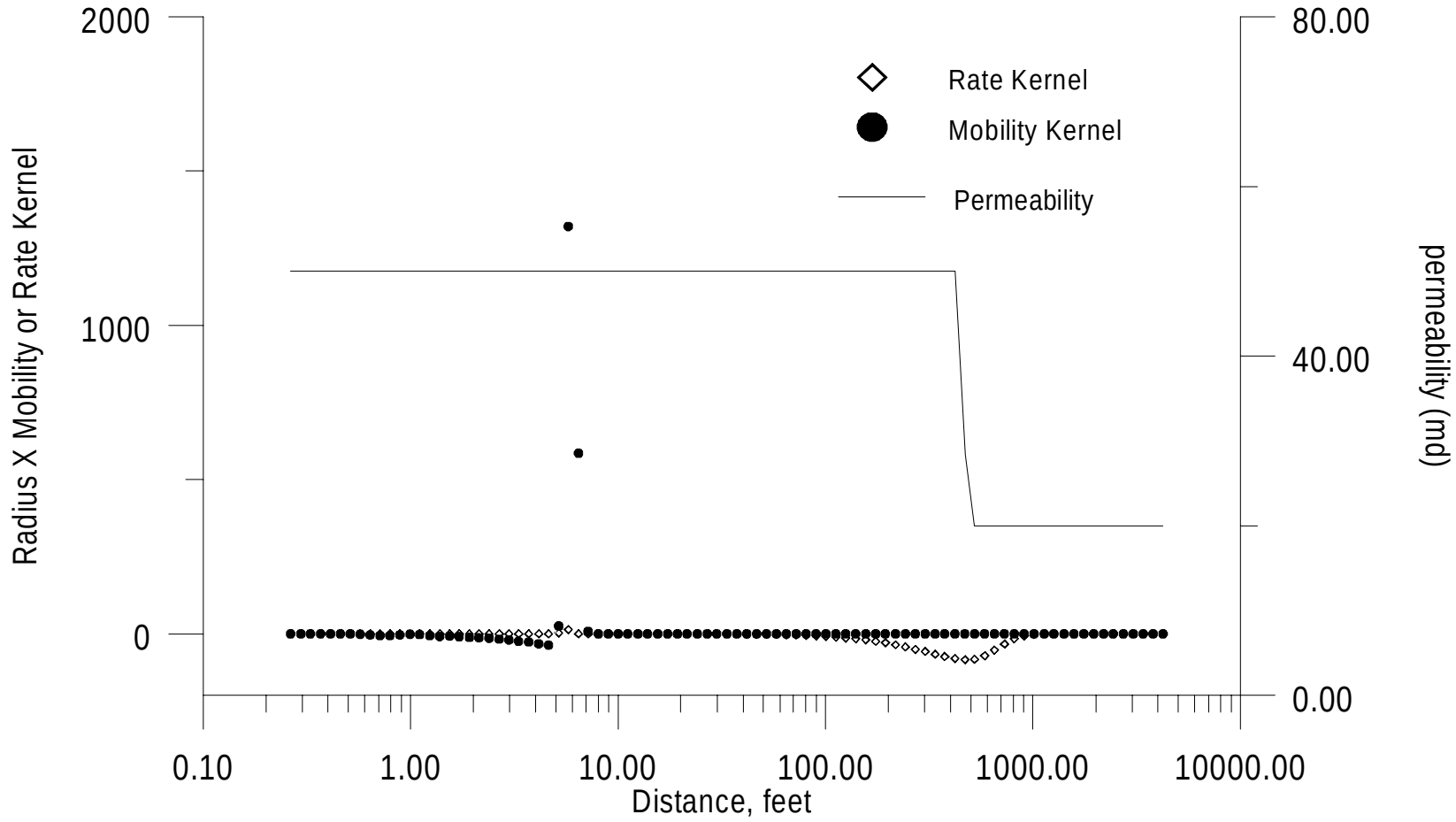

Fig. 2.4.7 :Mobility and Rate Kernels at 0.15 da (Case I)

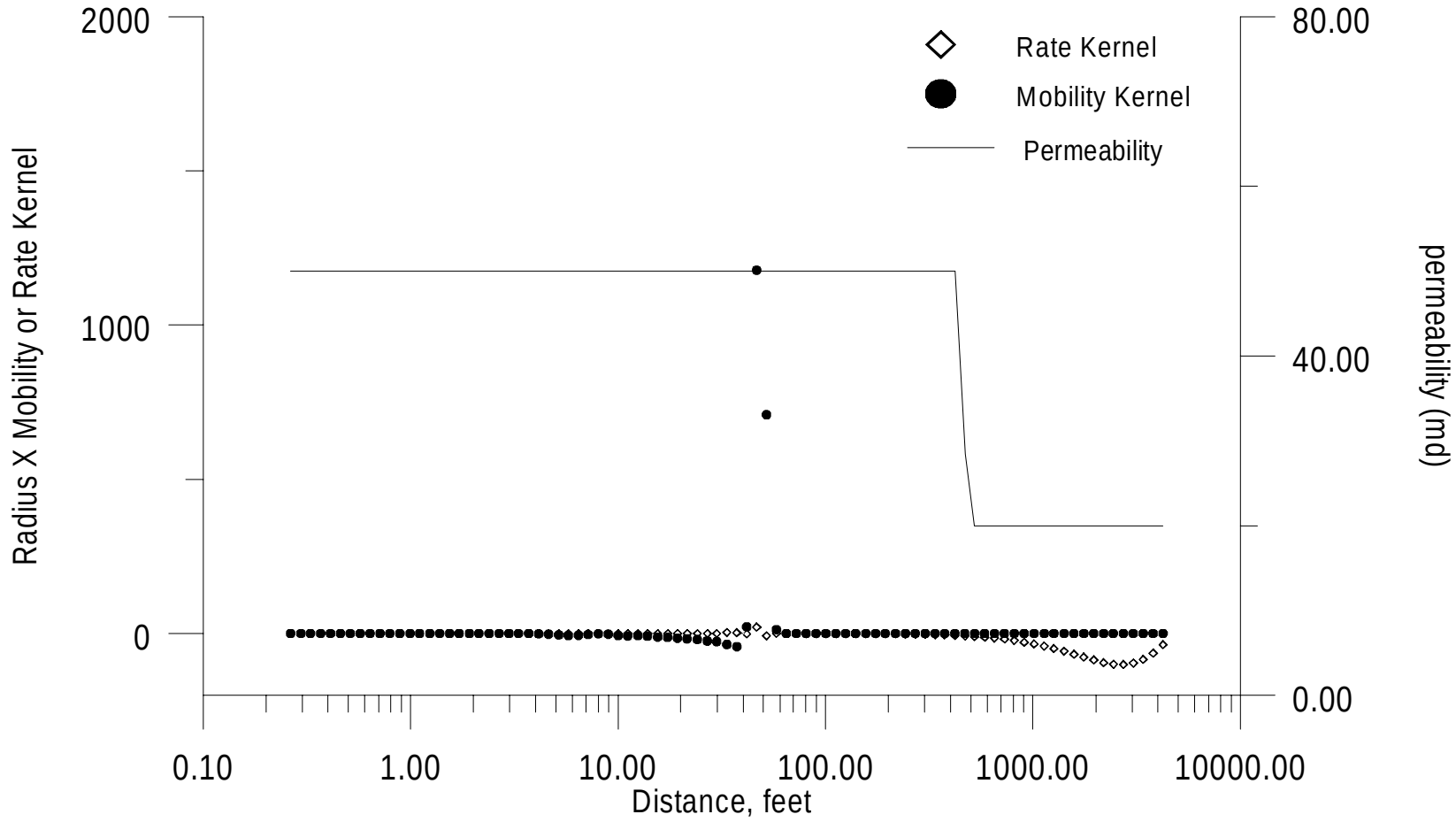

Fig. 2.4.8 :Mobility and Rate Kernels at 10.0 days. (Case I)

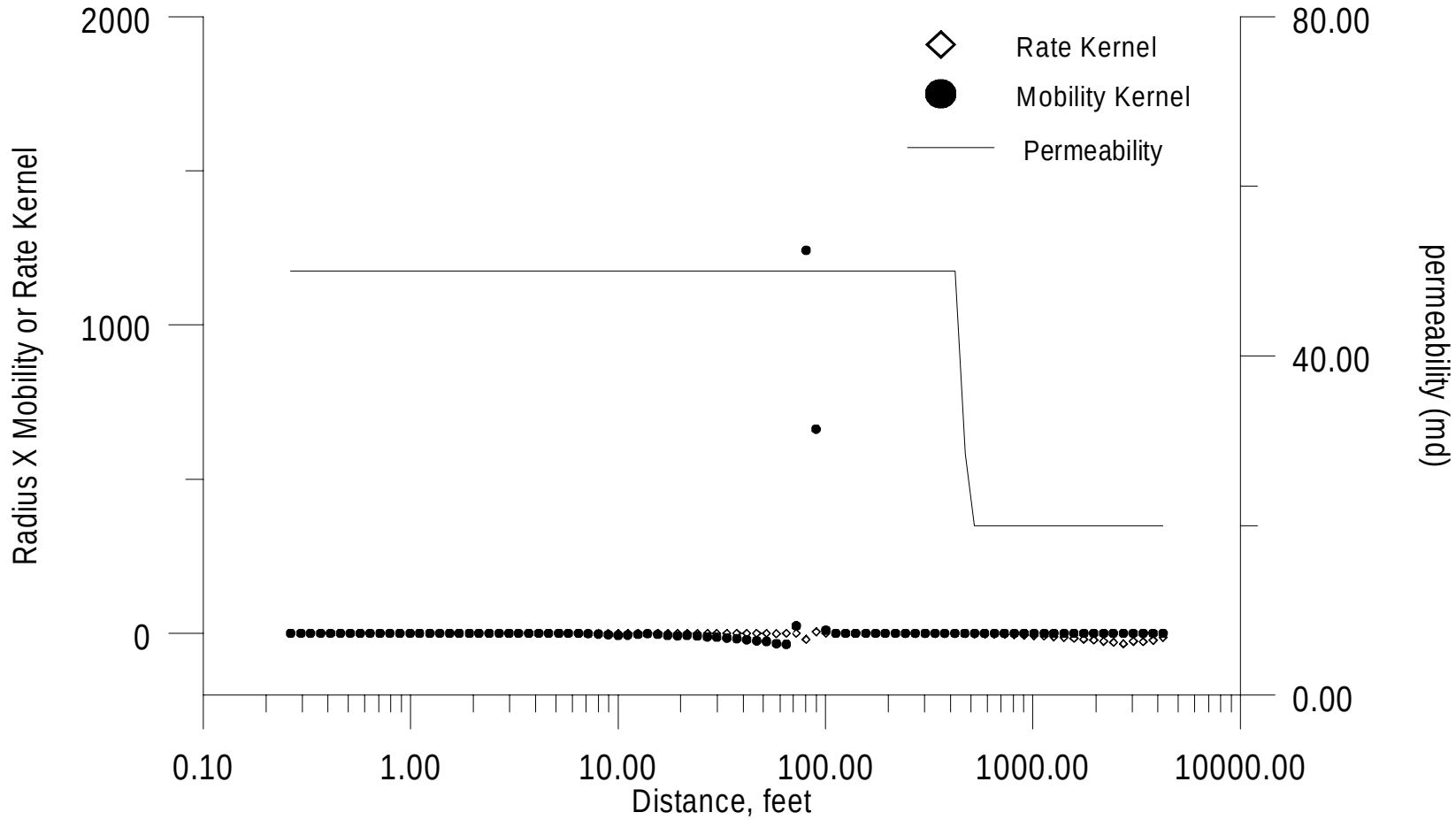

Fig. 2.4.9 :Mobility and Rate Kernels at 20.0 days. (Case I)

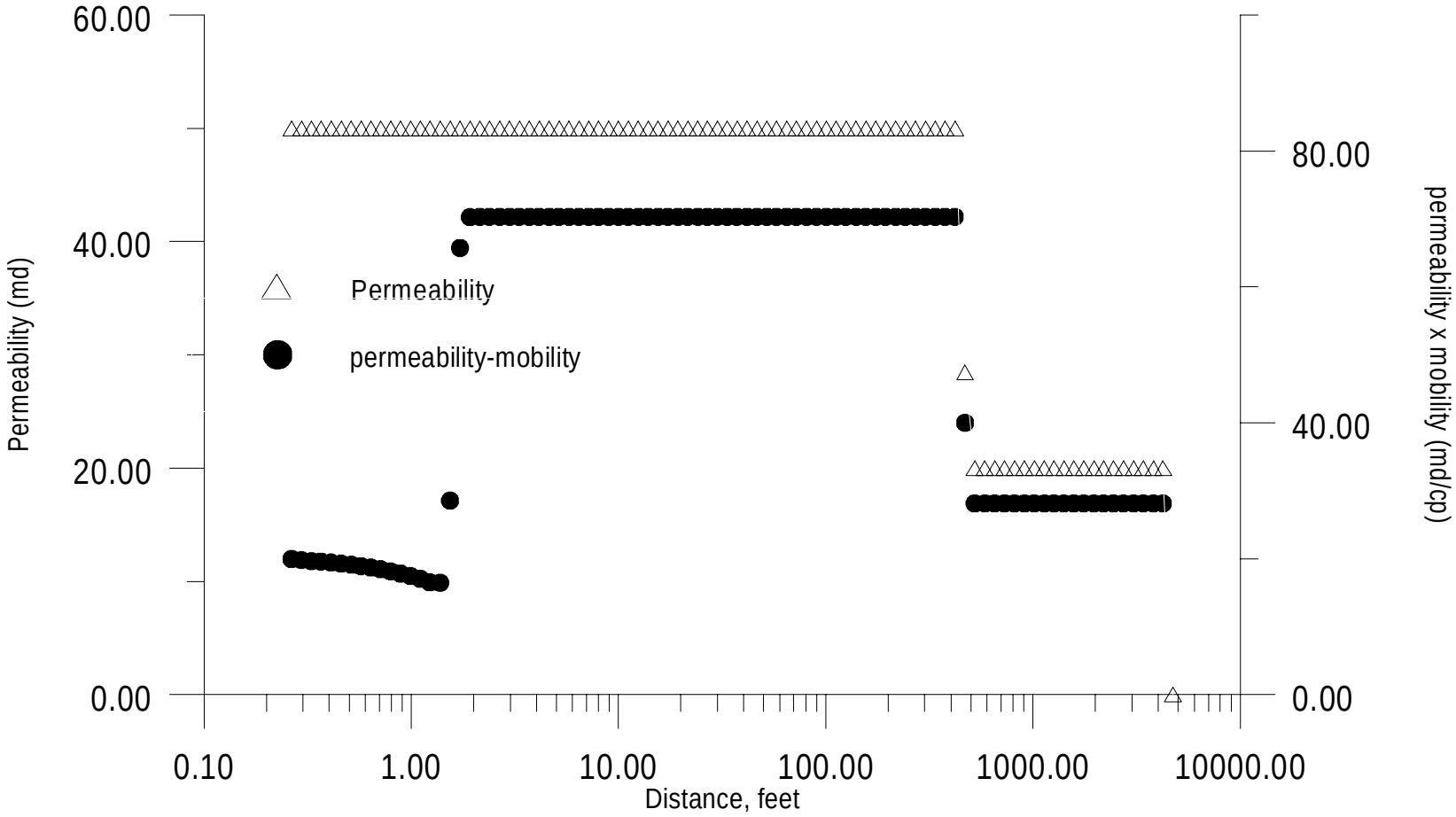

Figure 2.4.10 : Absolute Permeability and Permeability Mobility Product at 0.01 days

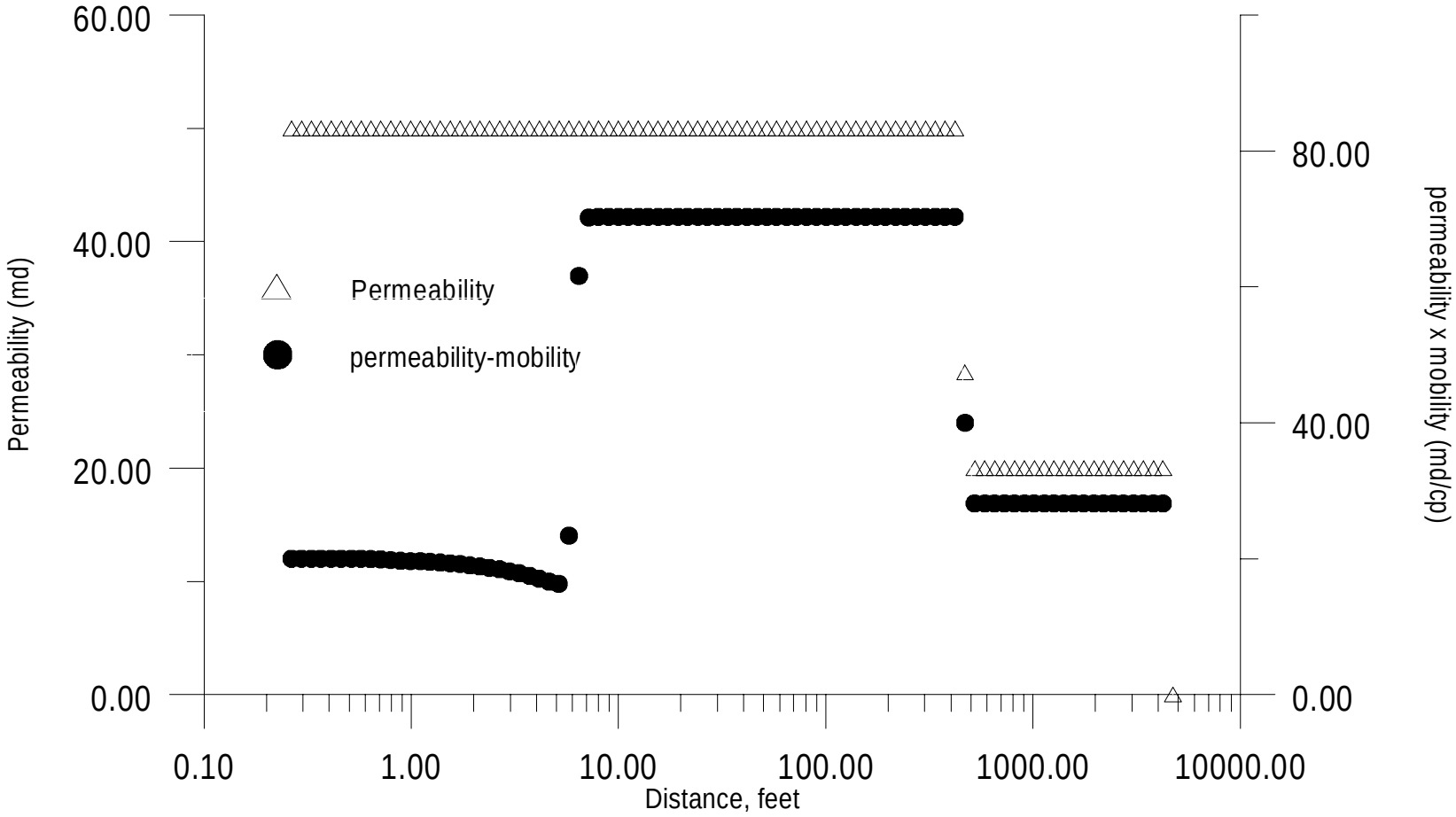

Figure 2.4.11 : Absolute Permeability and Permeability Mobility Product at 0.15 days

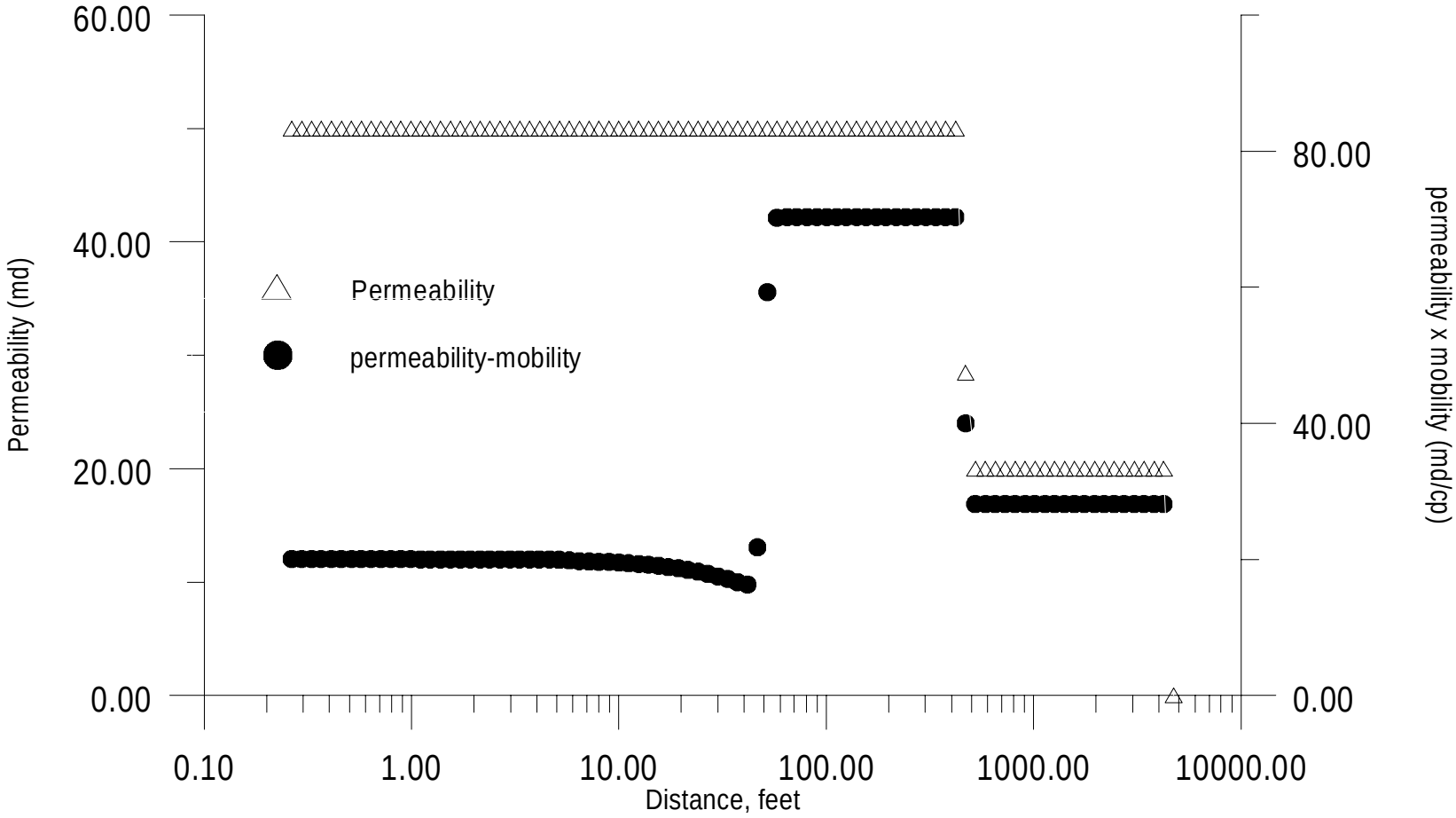

Figure 2.4.12 : Absolute Permeability and Permeability Mobility Product at 10.0 days

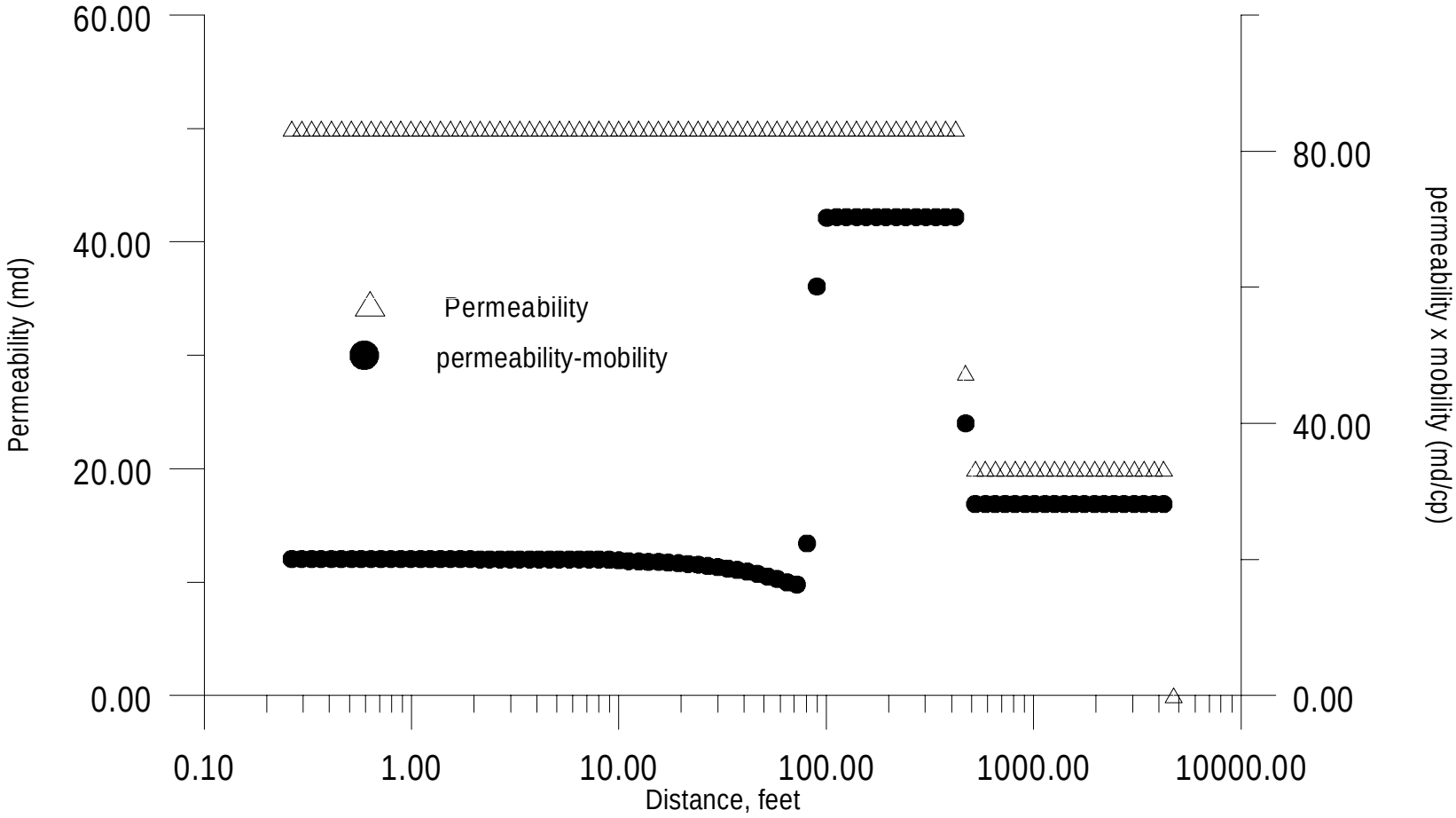

Figure 2.4.13 : Absolute Permeability and Permeability Mobility Product at 30.0 days

indicates that the mobility kernel, K_λ, is valid over a very small reservoir area whereas the rate kernel, K_R, is valid over a large area (note that radius is in logarithmic scale). Thus, the relative influence of each of these kernels in the weighting process may be comparable.

Figure 2.4.14 shows log-log plots of pressure and pressure derivative at the injection well and at a point (henceforth referred to as the imaginary well) located 125 ft away. The imaginary well pressure derivative data are clearly influenced by both permeability zones and although the effect is somewhat damped in the injection well pressure derivative, it also appears to show some influence of the permeability heterogeneity, even though the flood front never extends beyond the first permeability zone. Based on the injection well pressure derivative data in Fig. 2.4.14, we picked horizontal straight lines for $7\times10^{-3} < t < 0.2$ days and $7 < t < 21$ days. We obtained values of the derivatives as 25.36 and 35.38. Recall from Eq. 2.2.22 we have

$$\frac{d\Delta p_{wf}}{d\ln t} = \frac{70.6 q_{inj} B_w}{k_1 \lambda_f h}. \qquad (2.4.1)$$

Approximating λ_f to be the water mobility at water saturation 1-S_{or} and using the first value of the horizontal straight line, we obtained the first zone permeability, k_1 = 49.58 md compared to the input value of 50 md. We had derived Eq. 2.2.23 as

$$\frac{d\Delta p_{wf}}{d\ln t} = \frac{70.6 q_{inj} B_w}{h}\left[\frac{1}{k_1 \lambda_f} - \frac{1}{\lambda_o}\left[\frac{1}{k_1} - \frac{1}{k_2}\right]\right]. \qquad (2.4.2)$$

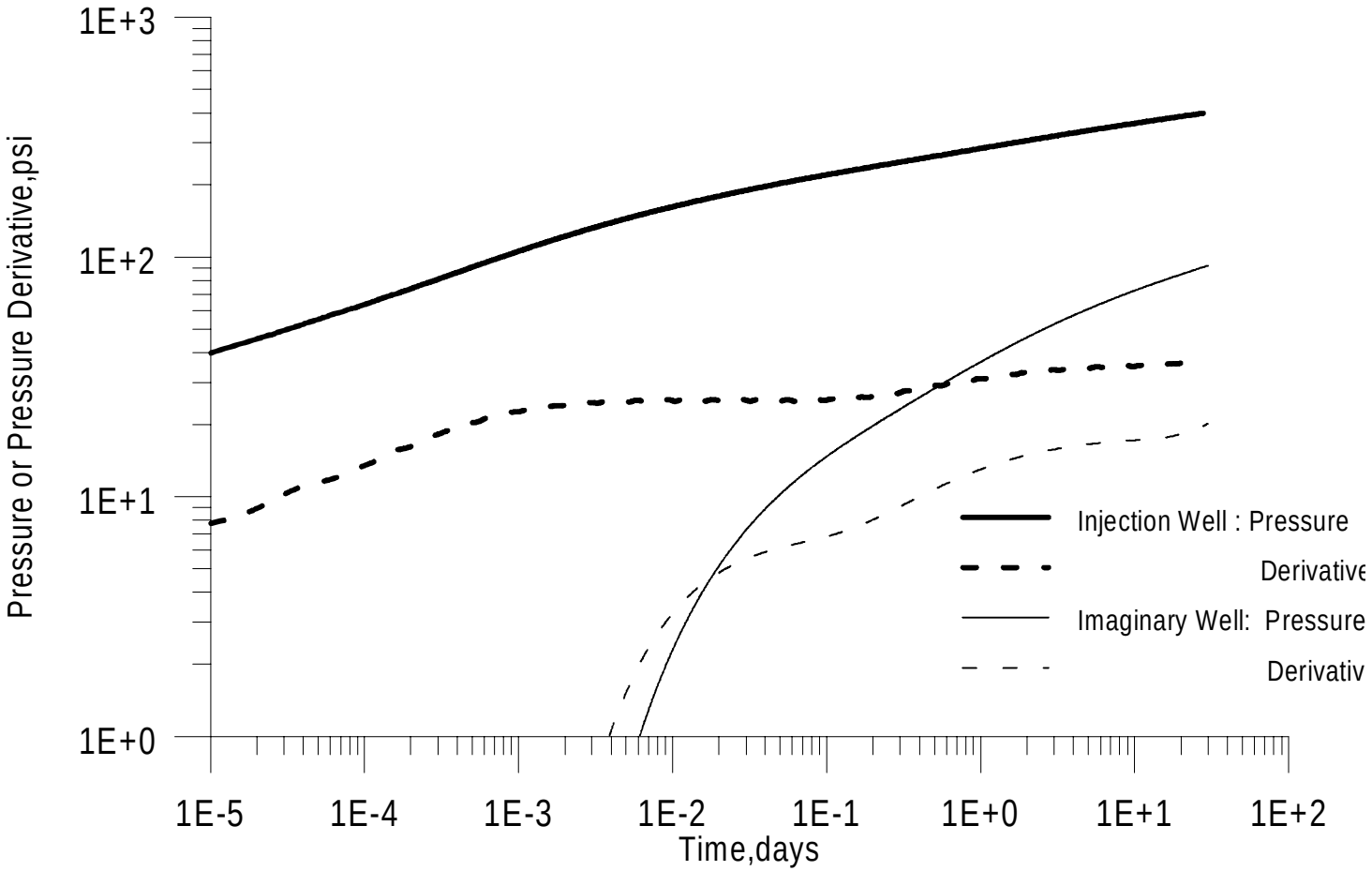

Figure 2.4.14: Pressure/Pressure Derivative Response at Injection & Observation Wells

Assuming λ_o as the oil mobility at connate water saturation, S_{wi}, and using the value of the second horizontal straight line and the calculated first zone permeability we obtained the second zone permeability, k_2 = 20.76 md which matches well with the input value of 20 md.

Figure 2.4.15 shows a log-log plot of the difference in pressure derivative data at the injection and observation wells obtained from simulation, as well as the result of calculating the right hand side of Eq. 2.2.19, repeated here as

$$\frac{d\Delta p_{wf}}{d\ln t} - \frac{d\Delta p_o}{d\ln t} = \frac{70.6 q_{inj} B_w}{k_1 h}\left[\frac{1}{\lambda_f} - \frac{1}{\lambda_o}\right]. \qquad (2.4.3)$$

Clearly the curves agree after the time at which the rate between the injection and observation wells attains a constant value ($t \approx 0.1$ days, see Fig. 2.4.3). Note also that the difference in pressure derivative, does not show any influence of the reservoir heterogeneity, and that it attains an approximately constant value after a short time (t ≈ 0.1 day). Thus, there is excellent agreement between the theory and the computed result.

- Case II:

In this example, the same data were used as in Case I. However, the zone interface was considered at 5.0 ft, viz., k = 50 md for $0.25 < r \leq 5$ ft and k = 20 md for $5 < r \leq 5000$ ft. This was to assure that the flood front would have advanced well into the second zone by the end of the test.

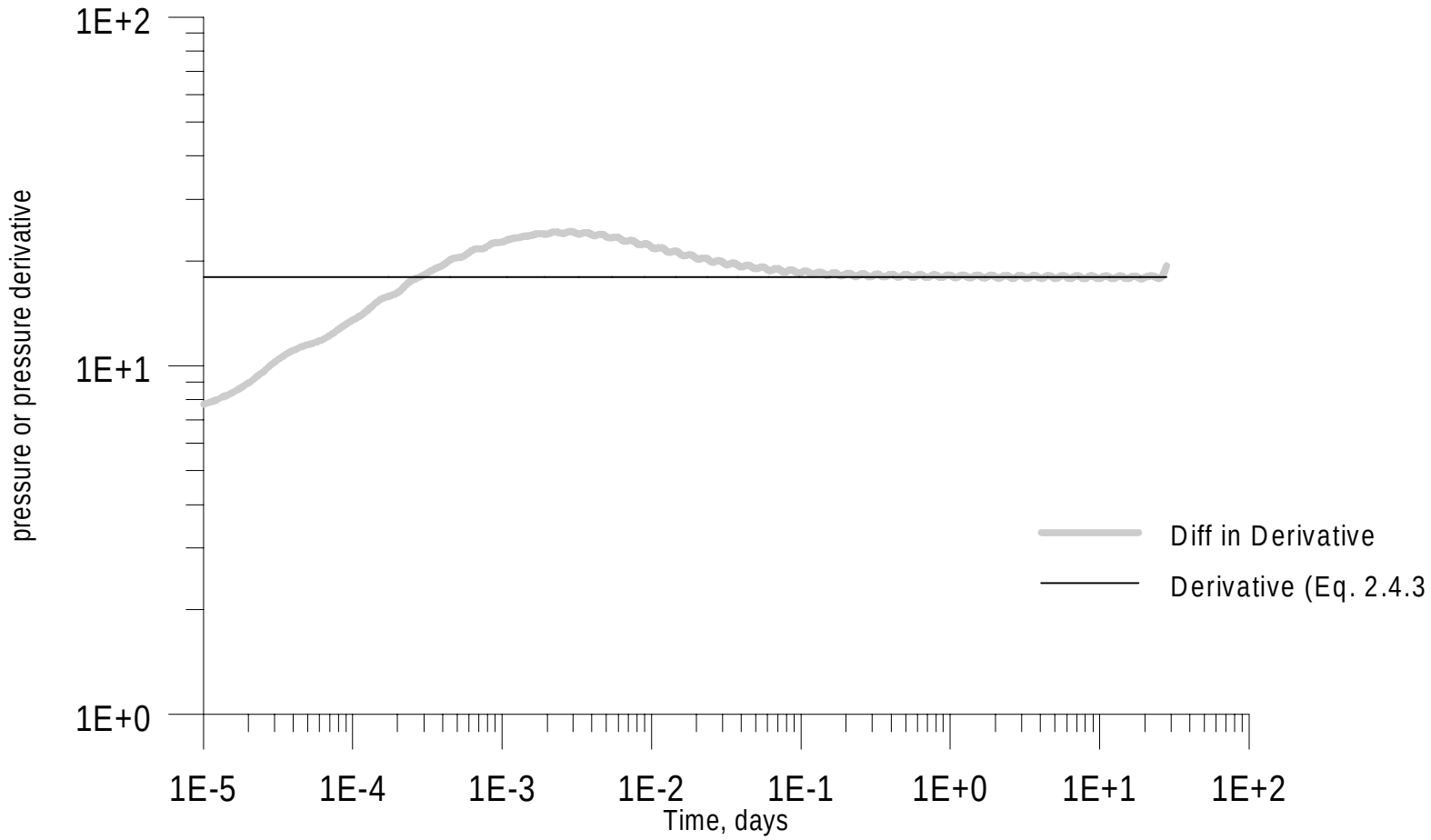

Figure 2.4.15: Comparison of Difference in Pressure Derivatives and Pressure Derivative

Figures 2.4.16 - 2.4.18 show rate and saturation profiles as functions of radius at various times during the injection process. Here too, we see that the flooded zone is always within the “steady state” zone. Figures 2.4.19 - 2.4.21 show plots of rate and mobility kernels (see Eqs. 2.1.10 and 2.1.11) corresponding to Figs. 2.4.16 - 2.4.18.

Figure 2.4.22 gives a log-log plot of pressure / pressure derivative versus time. The small hump in the pressure derivative data at 0.15 days characterizes the time at which the flood front crosses the zone interface. This can be qualitatively deduced by observing Figs. 2.4.17 and 2.4.20. While deriving our general equation for injection test we had seen that (see Eq. 2.2.8) when the flood front crosses over a zone interface, the change in mobility with time cannot be assumed to be negligible. Therefore, the pressure derivative deviates from the constant value predicated by Eq. 2.2.19 and we see a hump.

From the pressure derivative plot in Fig 2.4.22 we obtained two horizontal straight lines for $3\times10^{-3} < t < 3\times10^{-2}$ and $1 < t < 20$ days. The value of the derivatives corresponding to these lines were 63.06 and 36.13 respectively. We used the latter value of the derivative to calculate the second zone permeability from Eq. 2.2.24 repeated here as

$$\frac{d\Delta p_{wf}}{d\ln t} = \frac{70.6 q_{inj} B_w}{k_2 h \lambda_f} . \qquad (2.4.4)$$

We obtained a value of 19.95 md which compares well with the input value of 20 md.

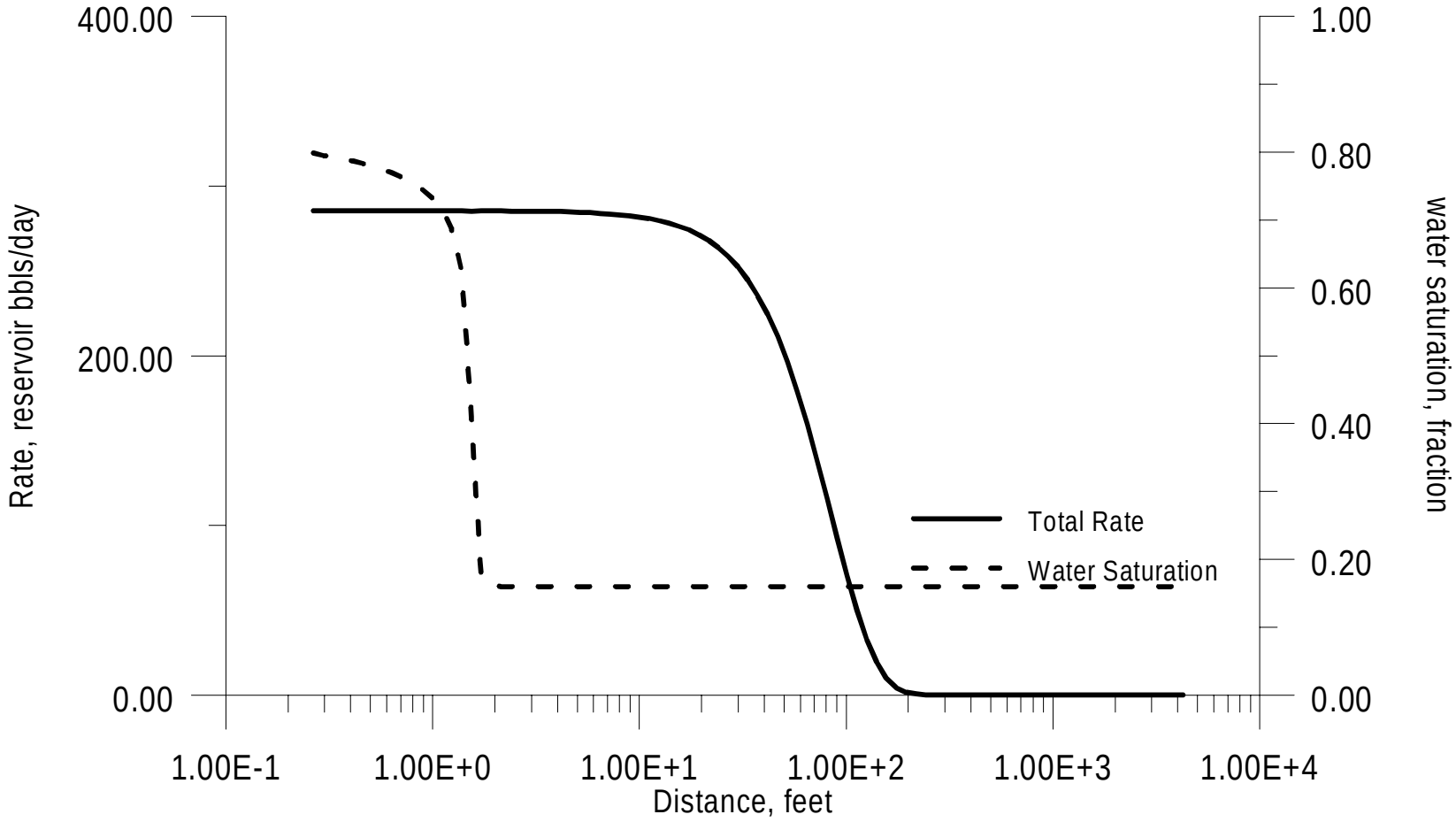

Fig. 2.4.16: Rate and Saturation Profiles as a function of Radius

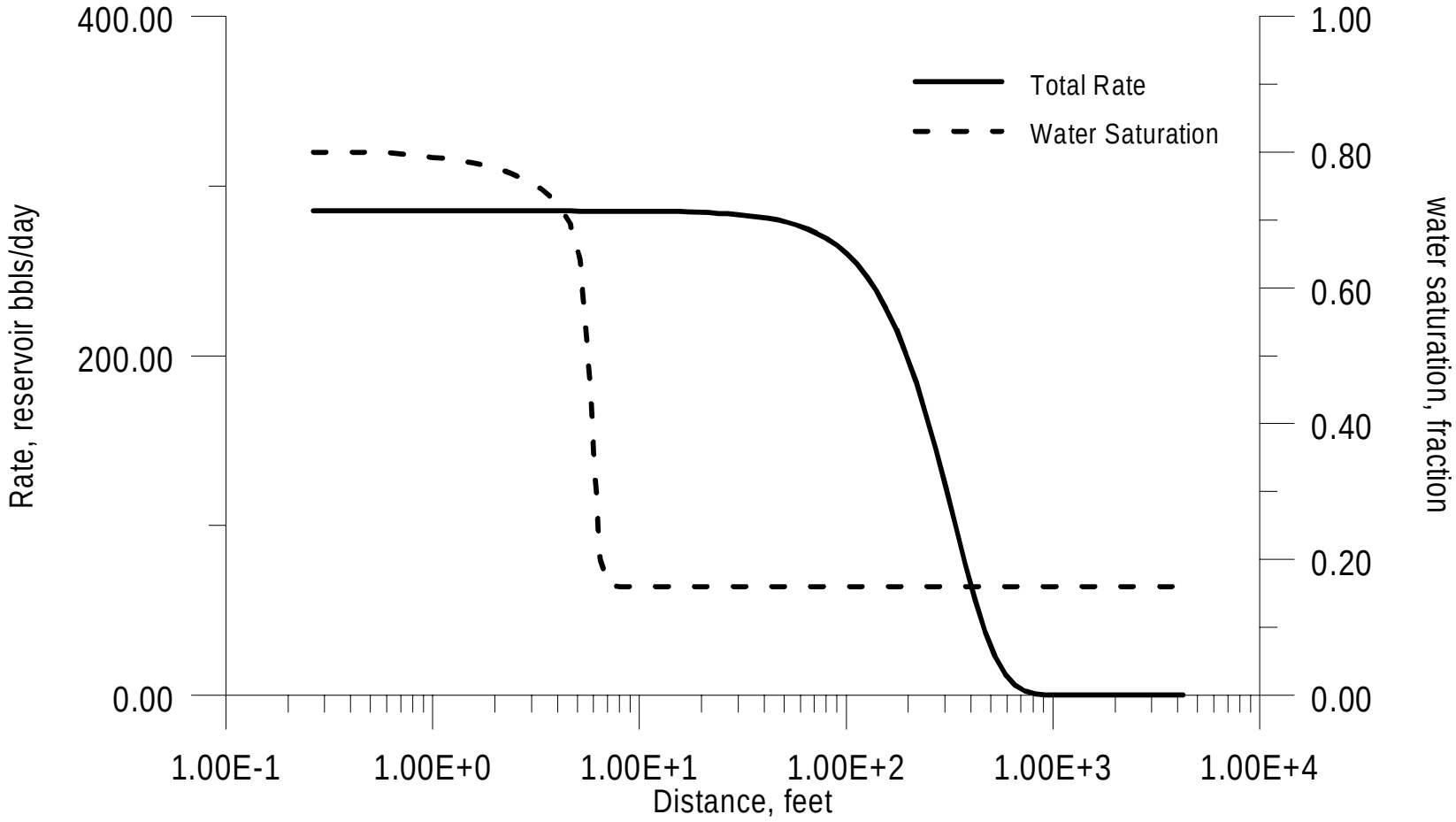

Fig. 2.4.17: Rate and Saturation Profiles as a function of Radius

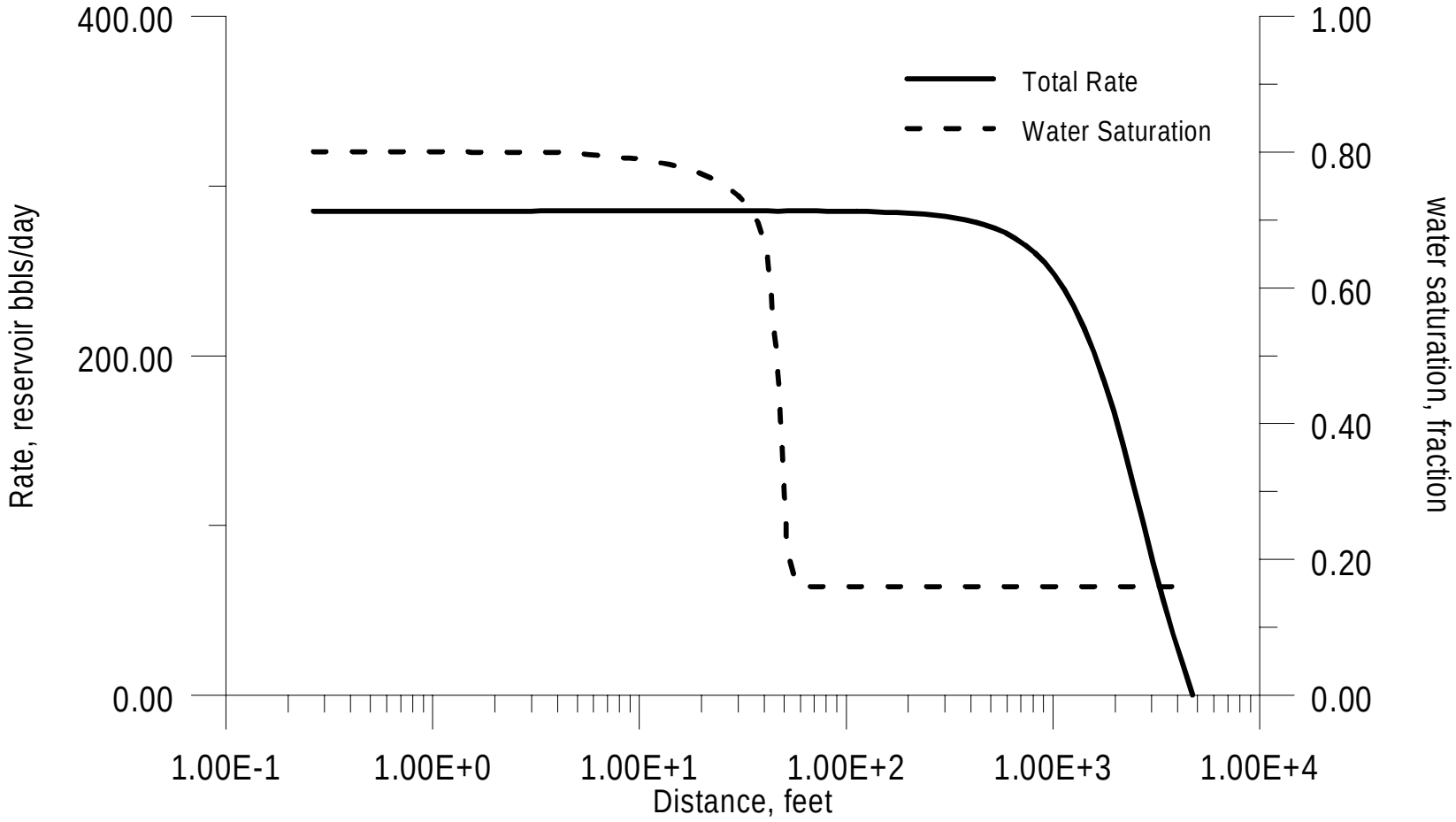

Fig. 2.4.18: Rate and Saturation Profiles as a function of Radius

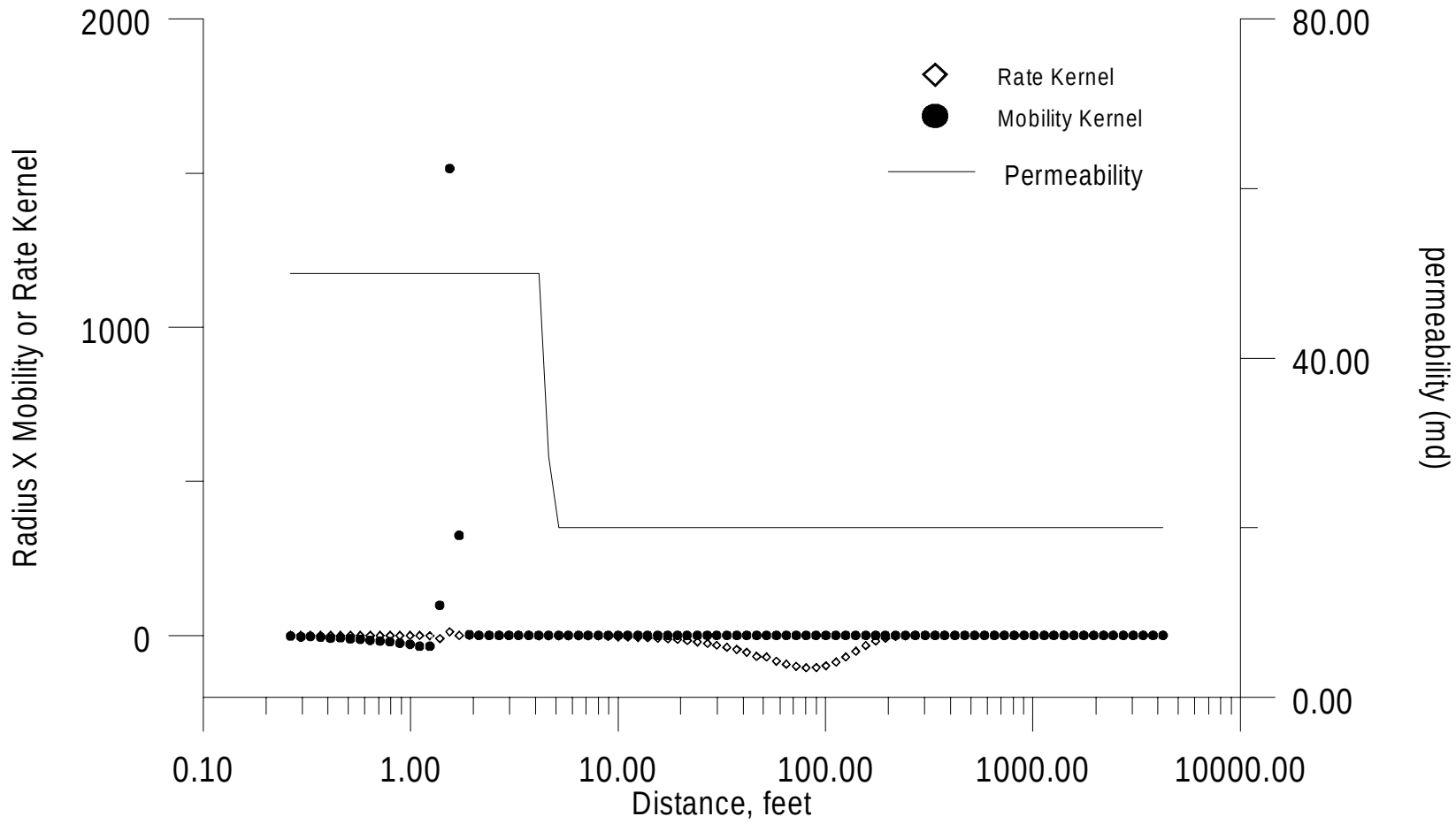

Fig. 3.4.10 Mobility and Rate Kernels at 0.01 day (Case II)

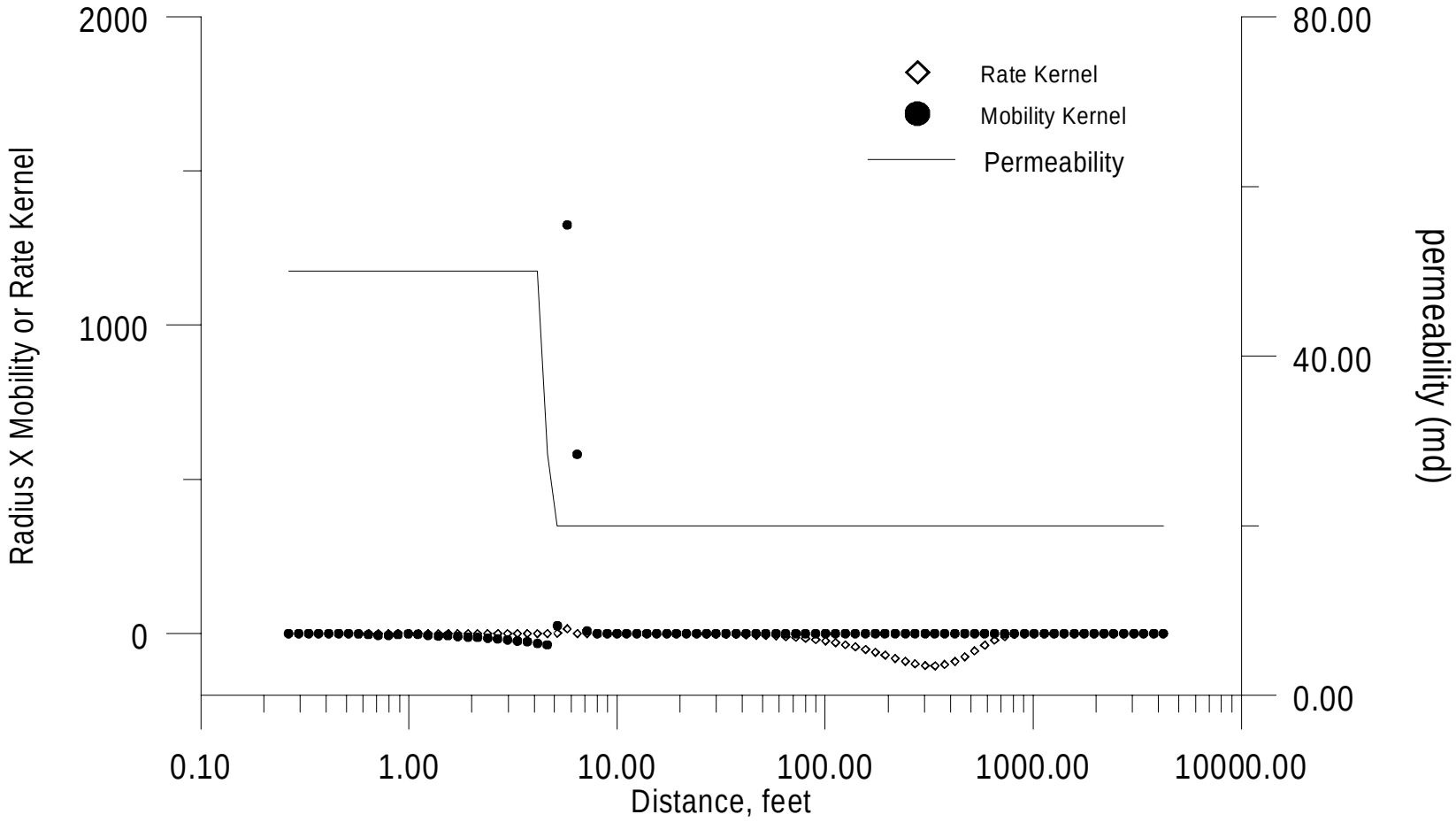

Fig. 2.4.20 :Mobility and Rate Kernels at 0.15 dp (Case II)

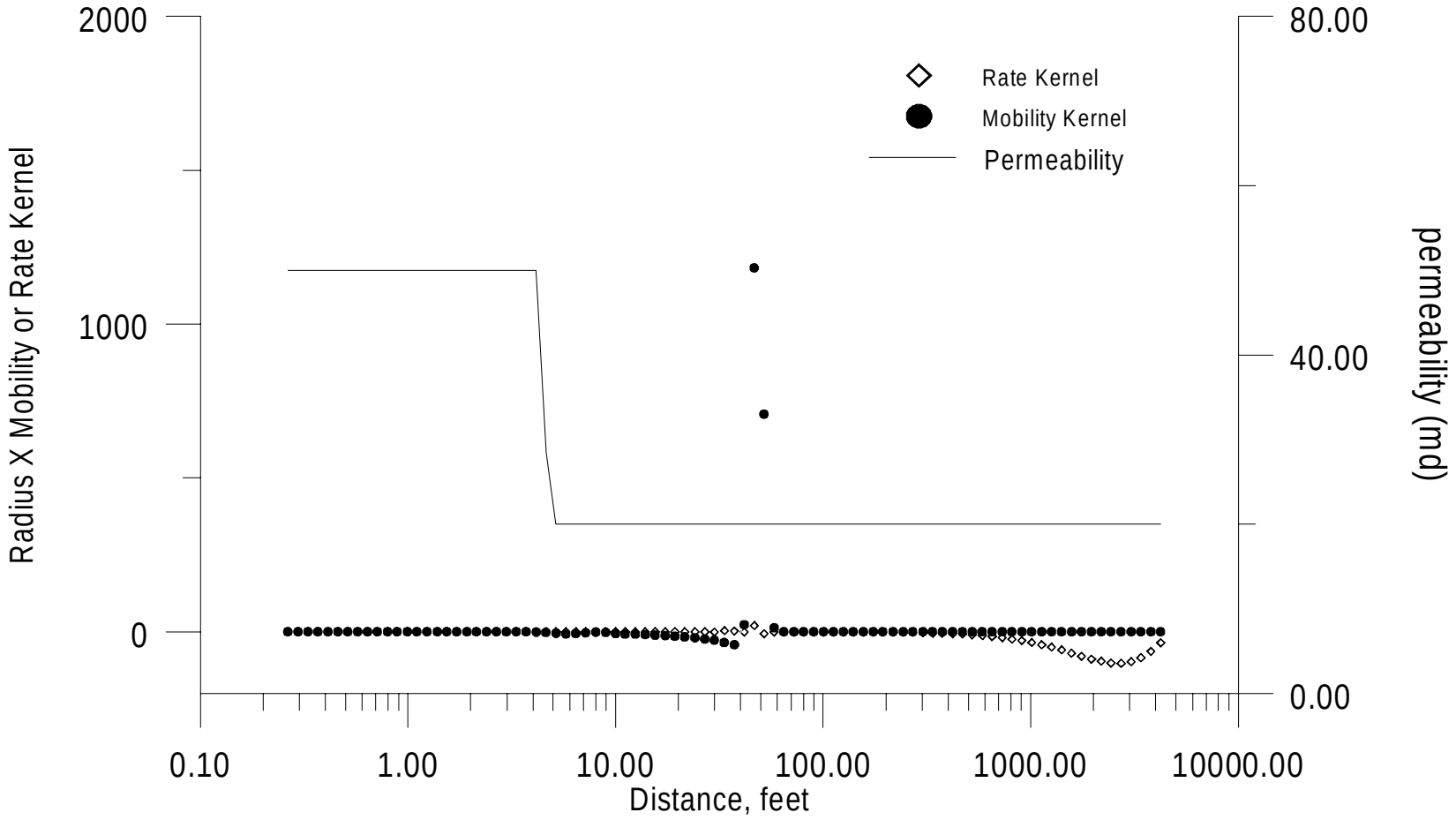

Fig. 2.4.21 :Mobility and Rate Kernels at 10.0 days (Case II)

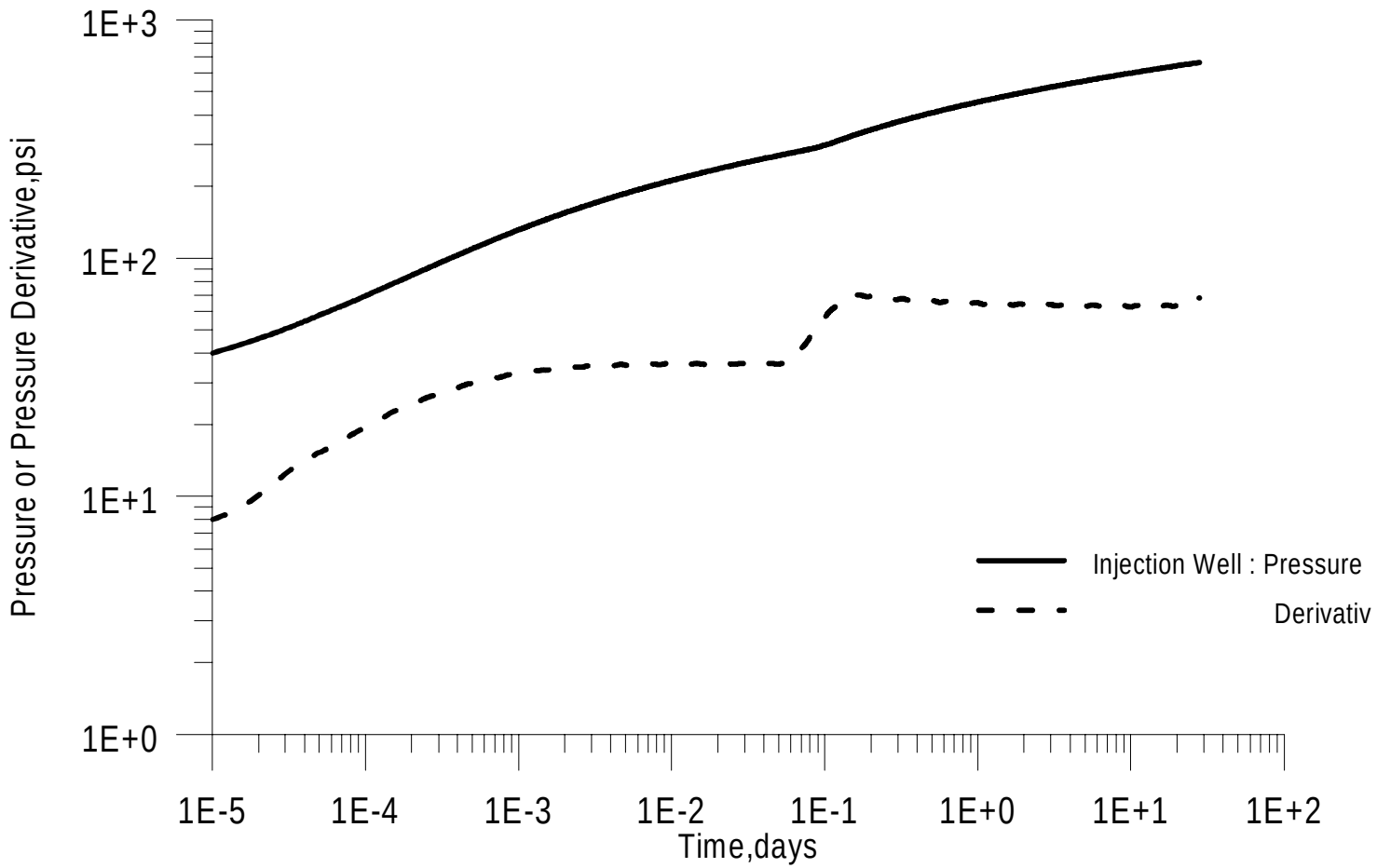

Figure 2.4.22: Pressure/Pressure Derivative Response at Injection Well

Further, from the first horizontal straight line in the pressure derivative log-log plot (Fig. 2.4.22) we calculated the permeability of the first zone using Eq. 2.4.2. Here, too, the calculated value, 49.45 md compared well with the input value of 50.0 md.

In this case, the pressure derivative data did not reflect a horizontal line corresponding to the first horizontal straight line obtained in Fig. 2.4.14 of Case I. This is due to the fact that the rate kernel did not reside in the first zone long enough for the effect to be seen in the derivative plot.

A study of the rate and mobility kernels, e.g., Figs. 2.4.6 - 2.4.9 and Figs. 2.4.19 - 2.4.21 shows that derivative plot remains horizontal when both rate and mobility kernels are within the same zone or each completely within different zones. This is in agreement with our generalized equation (see Eq. 2.2.21). Rewriting this equation we have

$$\frac{d\Delta p_{wf}}{d\ln t} = \frac{70.6 q_{inj} B_w}{h}\left[\frac{1}{k\lambda_f} - \frac{1}{\lambda_o}\left[\frac{1}{k} - \frac{1}{k'}\right]\right], \qquad (2.4.5)$$

where k is the permeability of that zone where mobility kernel resides and k' is the permeability of that zone where the rate kernel resides.

Obviously, when both the kernels are in the same zone

$$\frac{d\Delta p_{wf}}{d\ln t} = \frac{70.6 q_{inj} B_w}{kh\lambda_f}, \qquad (2.4.6)$$

where k represents permeability of that zone where both the kernels are present.

- Case III:

To illustrate the concept explained in the previous paragraphs, we considered a three zone system with k = 50 md for $0.25 < r \leq 5.0$; k = 100 md for $5.0 < r \leq 500.0$ ft and k = 20 md for $500.0 < r \leq 5000.0$ ft.

Plots of rate and mobility kernel at different times are presented in Figs. 2.4.23 - 2.4.25. These times correspond to the points of interest in the log-log plot of pressure / pressure derivative given in Fig. 2.4.26. It is clear from Fig. 2.4.23 that the first horizontal line in the pressure derivative (for $4\times10^{-3} < t < 4\times10^{-2}$) corresponds to the situation when the mobility kernel is in the first zone and the rate kernel is in the second zone. Indeed, putting k = 50 md and k' = 100 md in Eq. 2.4.5, we obtained $\frac{d\Delta p_{wf}}{d\ln t} = 21.57$ which closely matches the value 21.63 obtained from Fig. 2.4.26.

We considered the value of pressure derivative at the trough at $t \approx 0.15$ days (see Figs 2.3.24 and 2.4.26). No clear semilog data are available, because both the kernels do not stay in the second zone long enough. Putting $k = k'$ = 100 md in Eq. 2.4.6 we obtained $\frac{d\Delta p_{wf}}{d\ln t} = 12.57$ which closely matches the value 12.61 at the minimum of the trough in Fig. 2.4.26. Note that the typical hump in the derivative plot caused by the flood front crossing over to the second zone is not visible as the rate kernel moves over the second zone very quickly.

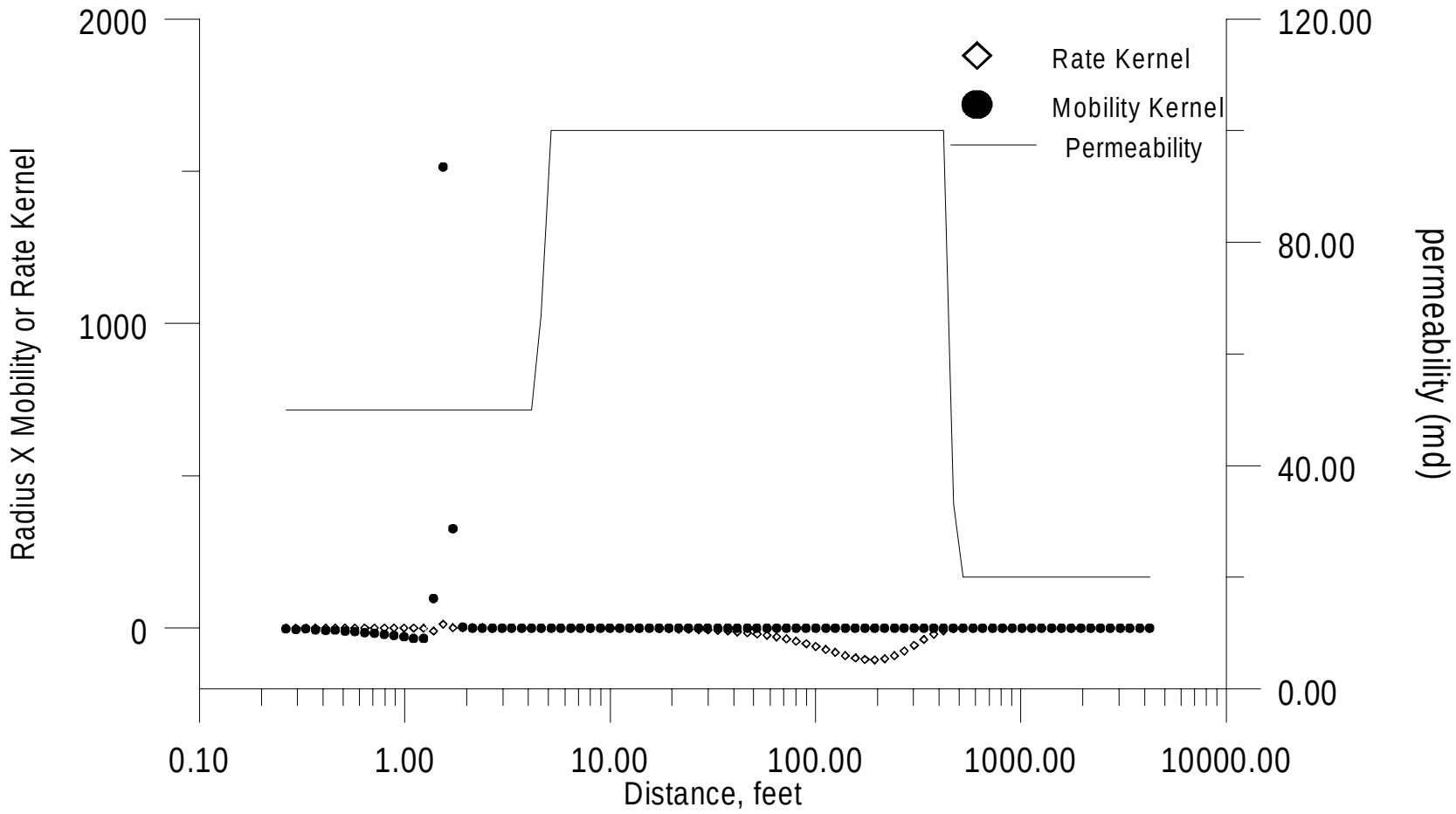

Fig. 2.4.22 :Mobility and Rate Kernels at 0.01 da (Case III)

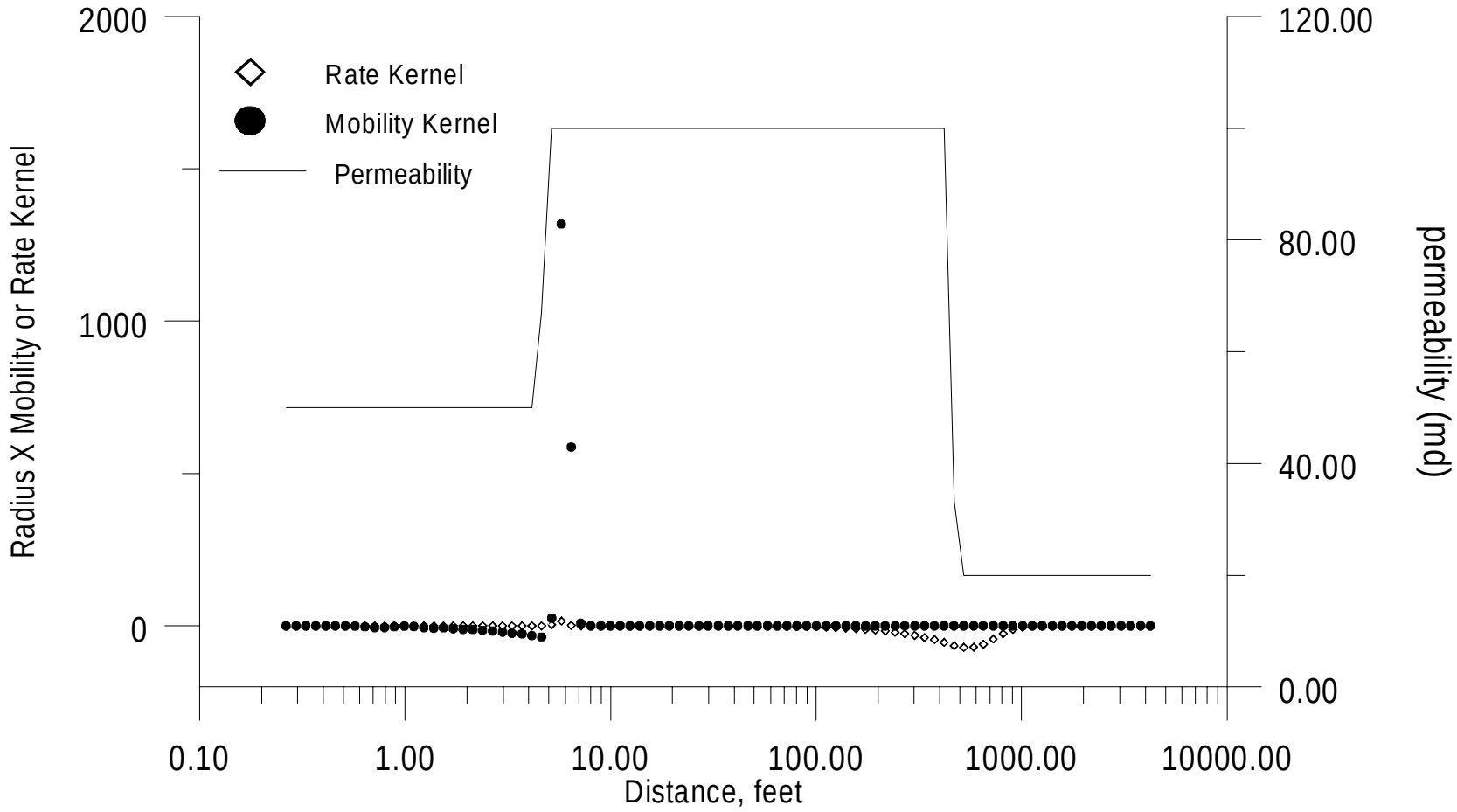

Fig. 2.4.24 :Mobility and Rate Kernels at 0.15 da (Case III)

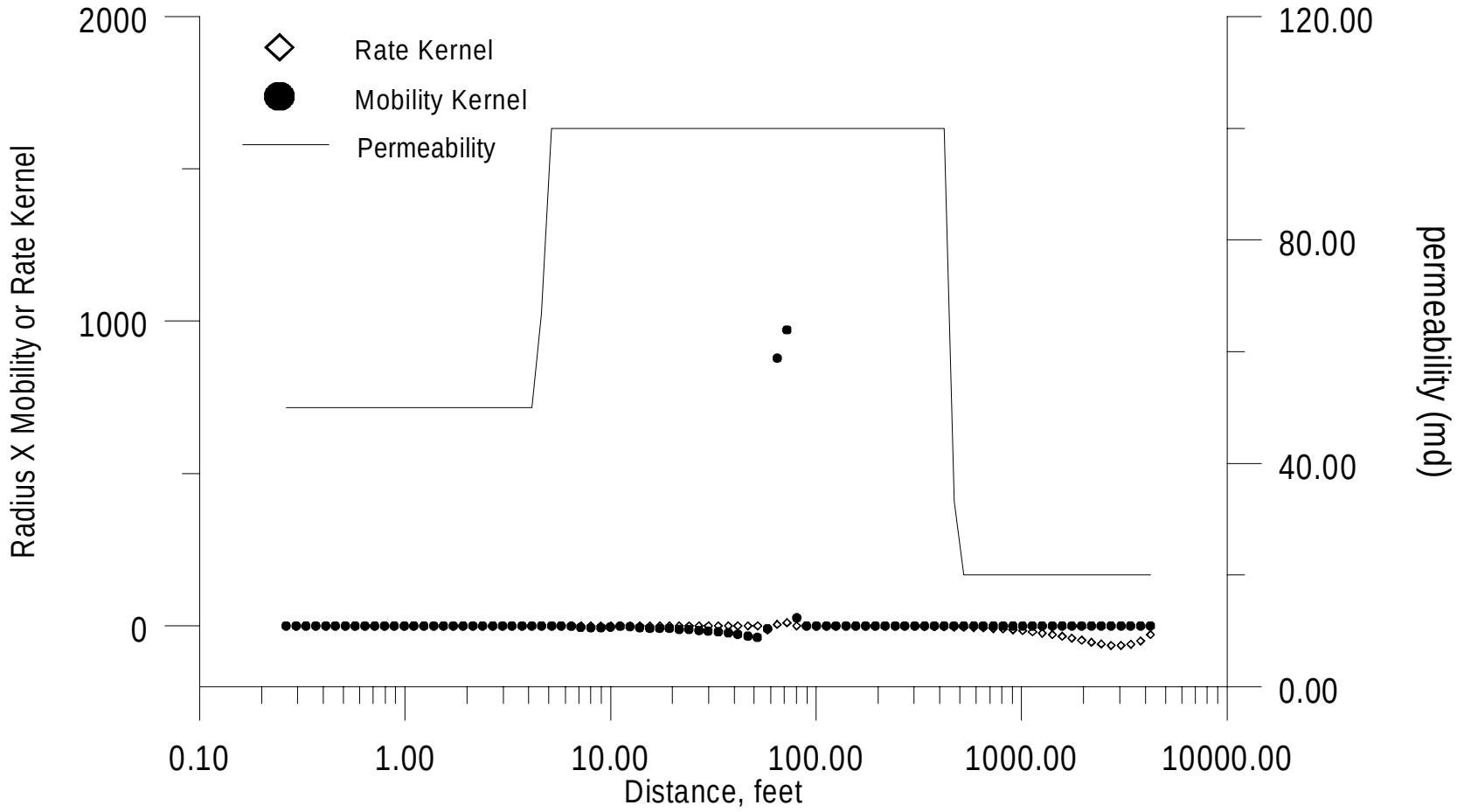

Fig. 2.4.25 :Mobility and Rate Kernels at 20.0 days (Case III)

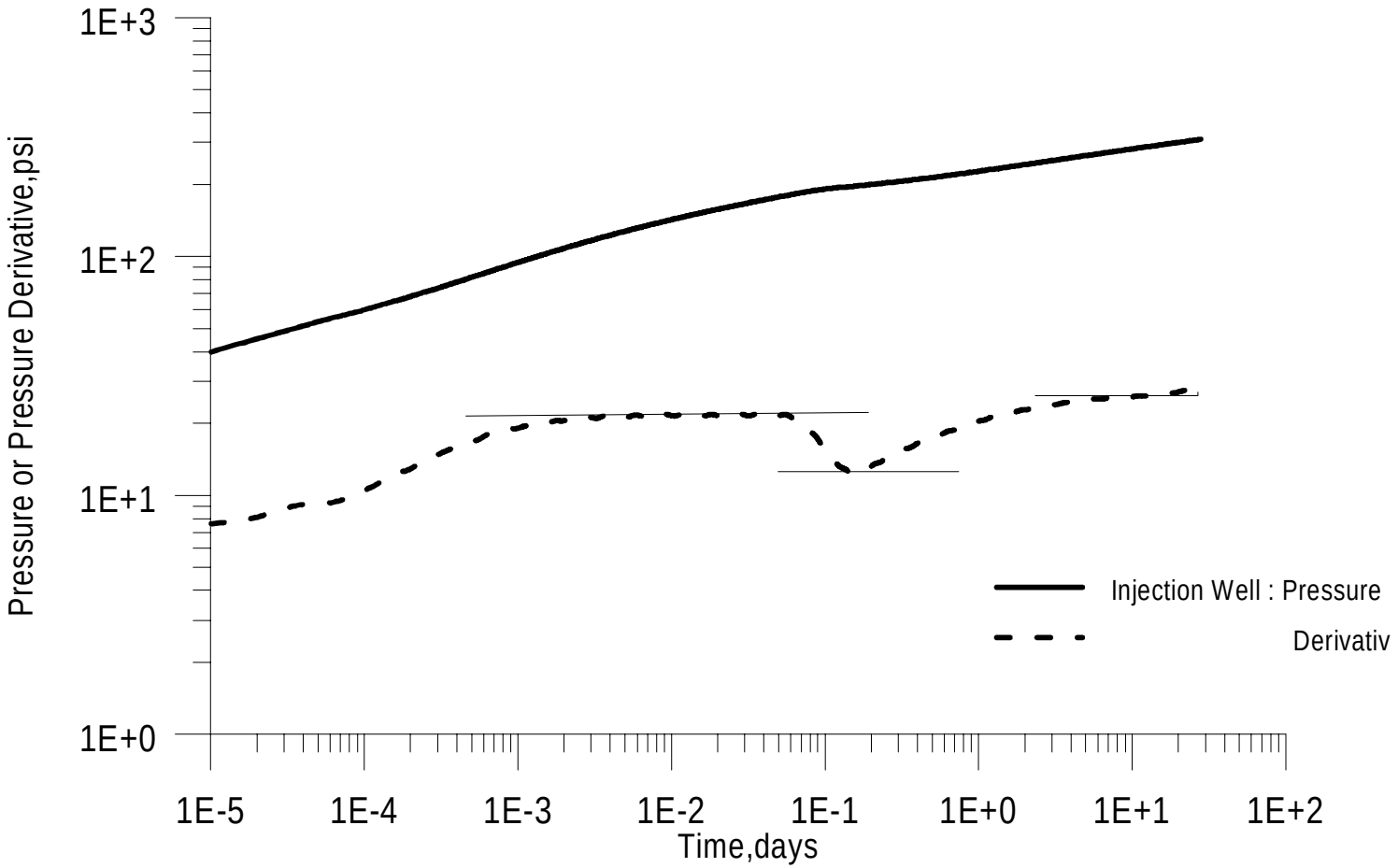

Figure 2.4.26 : Pressure/Pressure Derivative Response at Injection Well

Similarly, we see that the apparent horizontal straight line for 10 < t < 20 days represents the case where the mobility kernel is in the second zone and the rate kernel is in the third zone (see Fig. 2.4.25). Putting k = 100 md and k' = 20 md in Eq. 2.4.5 we obtained $\frac{d\Delta p_{wf}}{d\ln t} = 26.88$. From the pressure derivative plot we obtained 26.42.

- Case IV:

In this case, we demonstrate the effect of changing porosity between zones. We considered a reservoir with porosity = 0.2 and k = 50 md for 0.25 < r < 500.0 ft; and porosity = 0.1 and k = 20 md for 500.0< r < 5000.0 ft. The other properties were same as that of Case I. As has been predicted in Section 2.2, different porosity values in the two regions had no effect in the horizontal straight lines (Fig. 2.4.27) which showed the same trend as the lines in Fig. 2.4.14 of Case I. We were able to apply the same formulae and obtained the same values of permeability as in the earlier case. Note that in this case the flood front was always in the first zone. However, if the flood front had crossed over to the second zone, we would have obtained a hump (as seen in Case II), the shape of which would depend on both permeability and porosity difference in the two zones.

- Case V:

We have explained in Section 2.2 that Eq. 2.2.10 and, therefore, Eq. 2.2.21 would be invalid for a period of time when the flood front crosses a permeability and/or porosity change interface and we would observe a hump corresponding to that period.

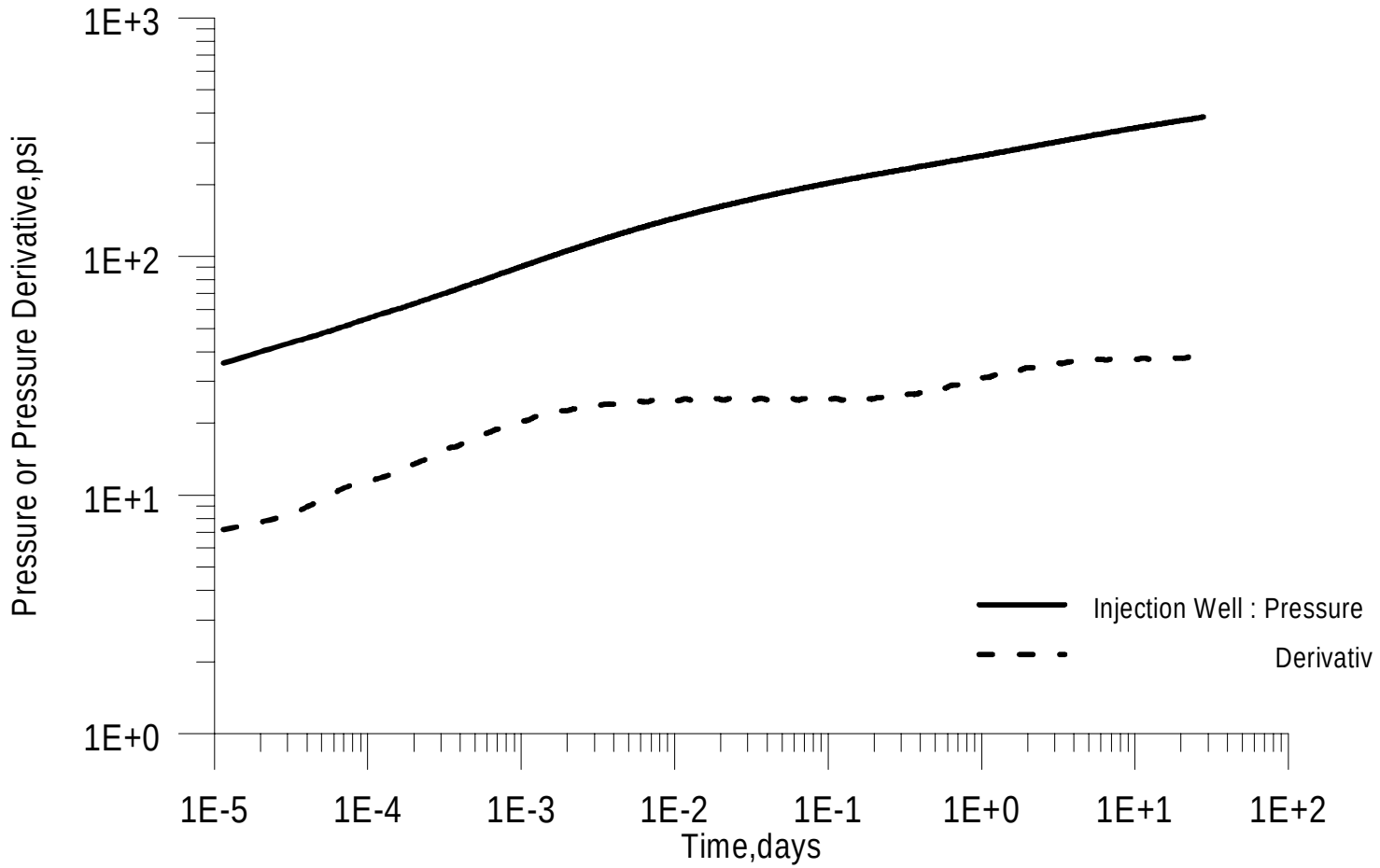

Figure 2.4.27: Pressure/Pressure Derivative Response at Injection Well

We have also explained that the direction of the deviation in case of porosity interface would depend upon the direction of porosity change. In this case, we studied the effect of changing porosity on the size of the hump observed when the mobility kernel crosses a permeability discontinuity. Here we demonstrate an instance when the hump completely disappears. As seen in Fig. 2.4.28, the hump completely disappears when the permeability-porosity product remains constant at the zone interface. Recall that the sign of the porosity difference affects the direction of deviation from our water flood equation (Eq. 2.2.20).

This hump should not be confused with the characteristic hump seen in single phase composite reservoir model with very high diffusivity coefficient contrast between zones. In the multiphase flow case, we may expect to see a hump when the rate kernel crosses a zone interface; however, we do not. The reason for this is that the mobility kernel completely masks minor changes in pressure derivative caused by the rate kernel crossing a permeability-porosity boundary.

- Case VI

Finally we show the effect of changing the mobility ratio. If we approximate the water saturation behind the flood front to be 1-S_{or} we can define mobility ratio as,

$$M = \frac{\left(k_w / \mu_w\right)_{1-S_{or}}}{\left(k_o / \mu_o\right)_{S_{wi}}} \qquad (2.4.7)$$

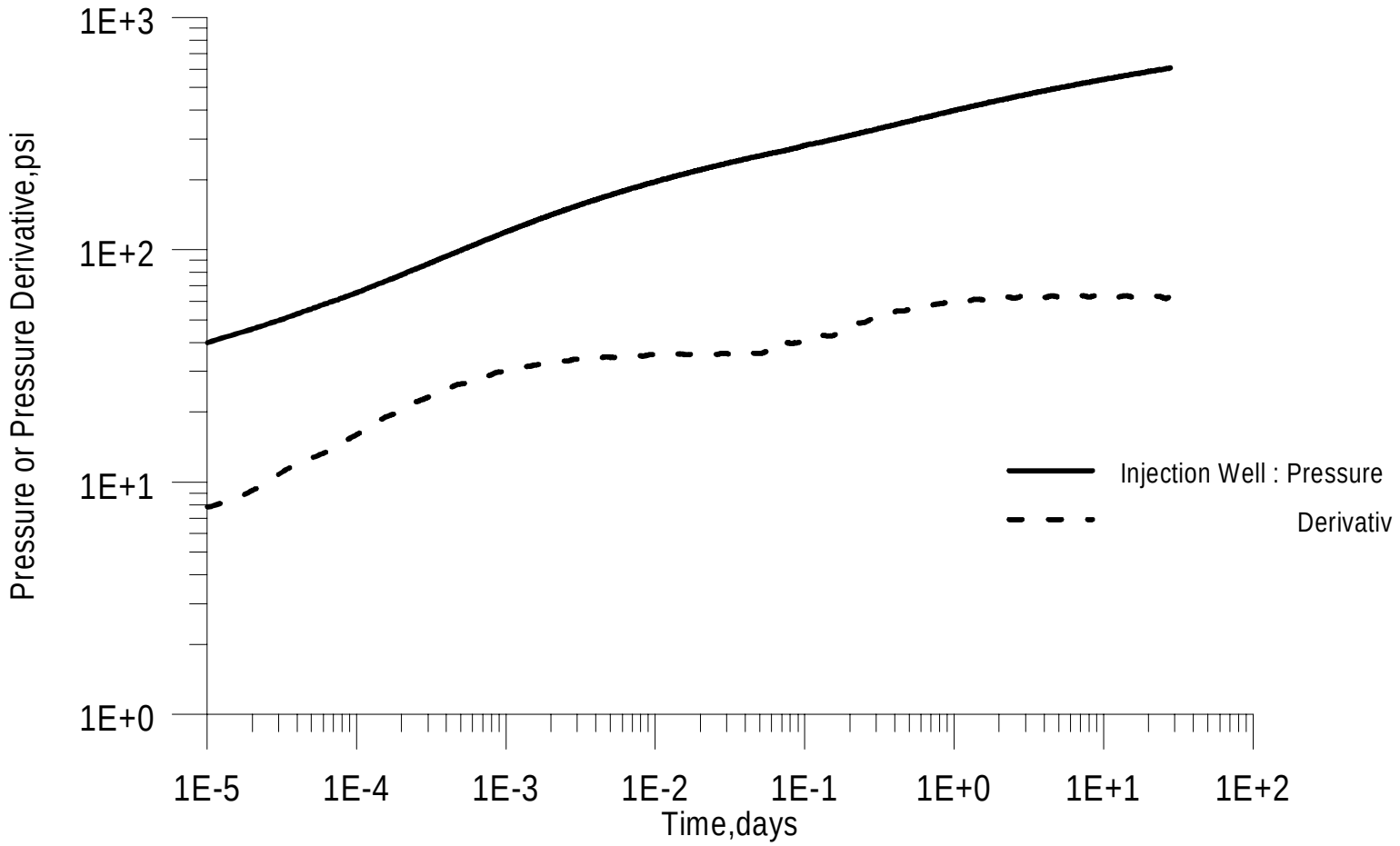

Figure 2.4.28: Pressure/Pressure Derivative Response at Injection Well

In all the cases considered previously, we used a favorable mobility ratio, viz., 0.28. In this case we change the mobility ratio to a value greater than unity in order to test the validity of our model for unfavorable mobility ratio. We assumed oil viscosity of 3.0 cp and water viscosity of 1.0 cp, i.e., M = 1.33, while keeping the other parameters the same as in Case I. Fig 2.4.29 gives log-log plot of pressure derivative versus time. If we consider the first and the second straight lines as the ranges $0.1 < t < 0.6$ and $15 < t < 30$ days respectively, we have, by applying Eqs. 2.4.1 and 2.4.2 , the first and second zone permeability values as 49.32 md and 21.33 md respectively. Thus we see that we get excellent results irrespective of the value of mobility ratio.

- Case VII

In order to test the validity of our equation for skin (Eq. 2.3.16), we simulated water injection at 250 STB/day into a homogeneous reservoir having a permeability of 30 md. We used the same relative permeability curves (Fig. 2.4.1) and the other reservoir and fluid properties (Table 2.4.1) discussed previously. In this case, however, we assumed a skin of 10. In order to incorporate this skin in our simulator we, assumed a damaged zone radius of 0.51 ft and arrived at a damaged zone permeability of 2.0 md using Eq. 2.3.2. Thus, effectively we had a composite system with k = 2 md for $0.25 < r \leq 0.51$ ft and k = 30 md for $0.51 < r \leq 5000$ ft. Figure 2.4.30 presents a semi-log plot of pressure versus injection time. We calculated skin factor using Eq. 2.3.16 and obtained a value of 10.32 compared to the input value of 10.0. Using the conventional equation, viz., Eq.2.3.17, we arrived at a value of 8.02.

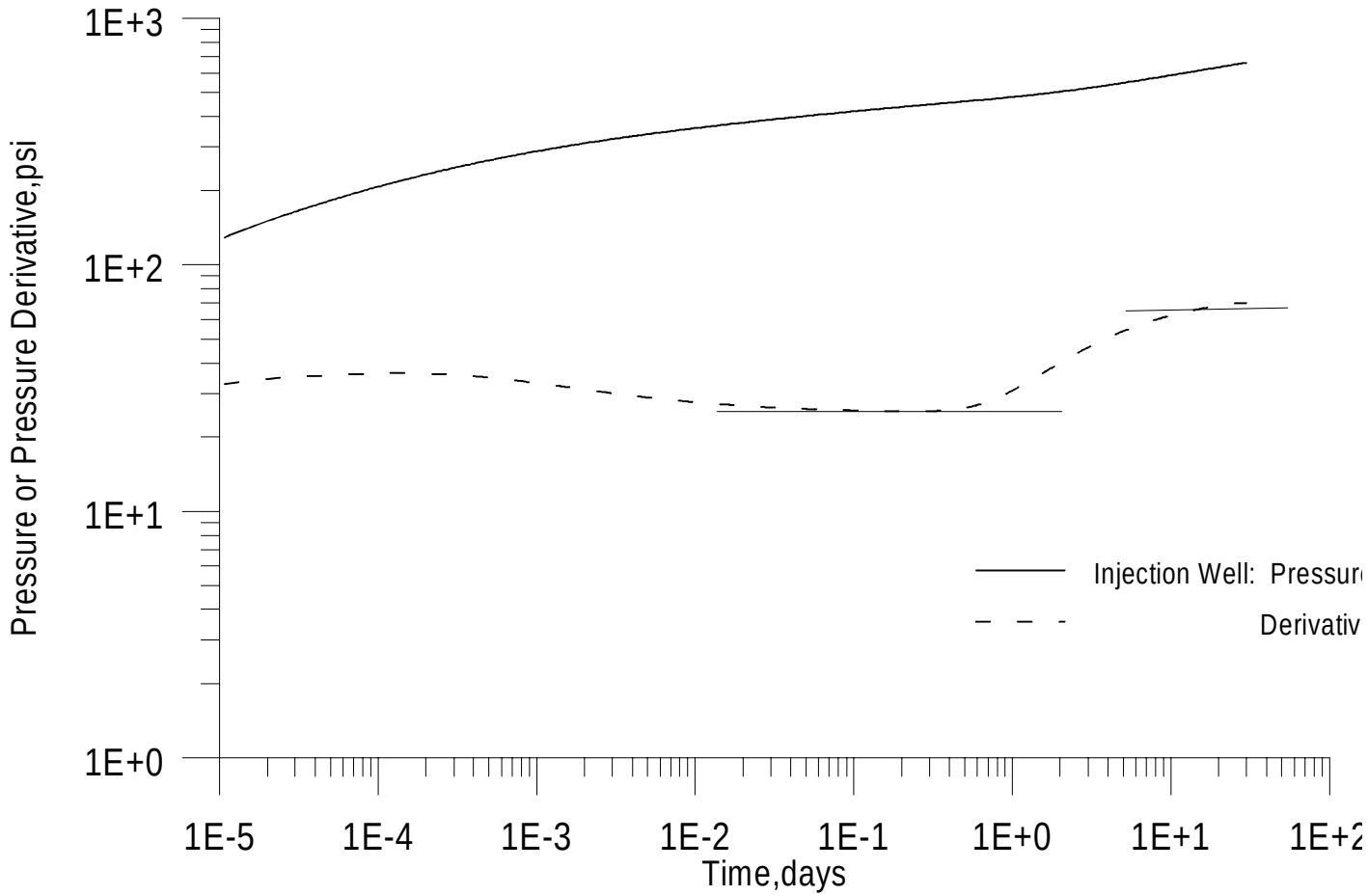

Figure 2.4.29: Pressure/Pressure Derivative Response at Injection Well

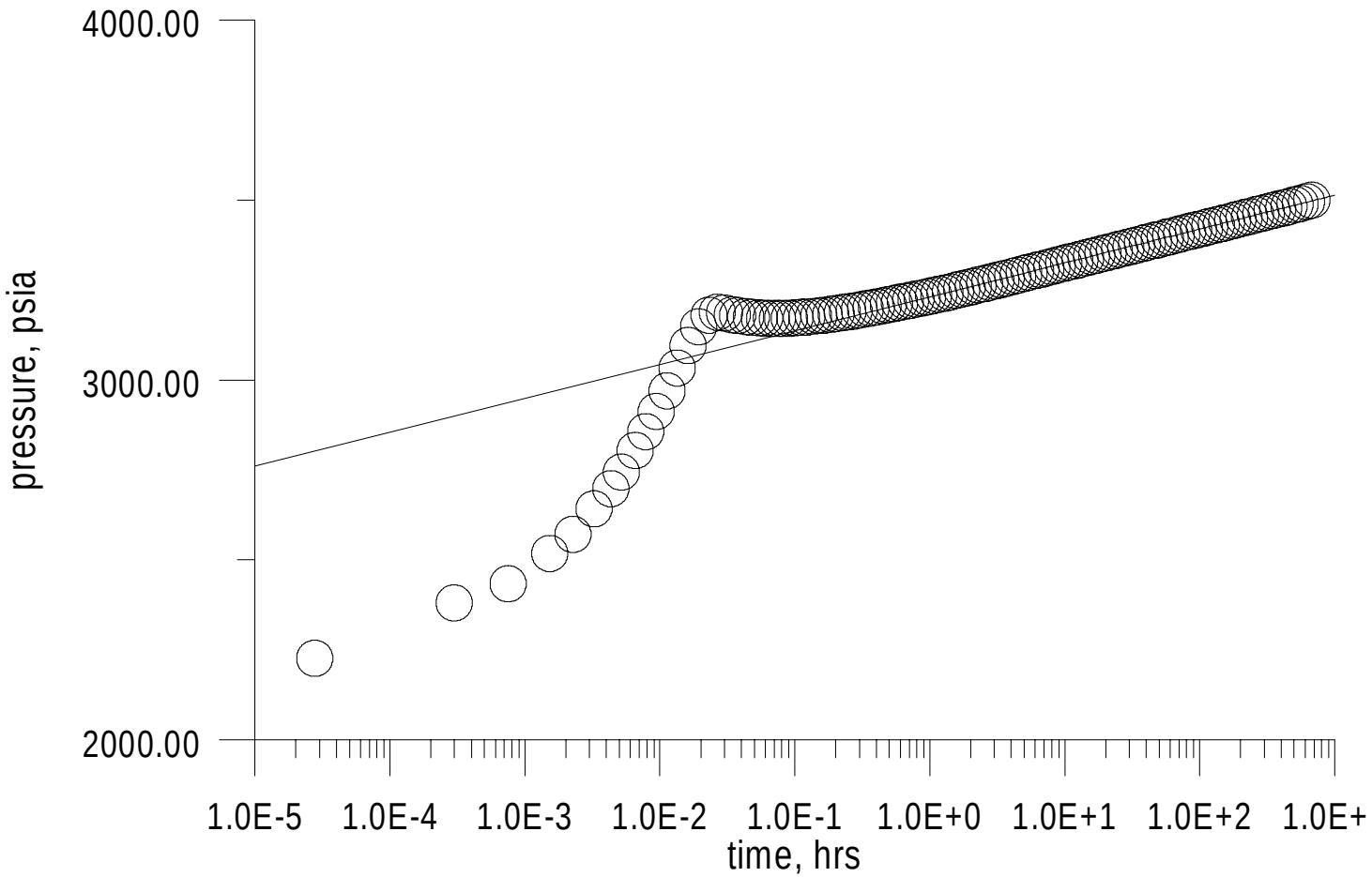
4000.00
3000.00
2000.00
pressure, psia
1.0E-5
1.0E-4
1.0E-3
1.0E-2
1.0E-1
1.0E+0
1.0E+1
1.0E+2
1.0E+
time, hrs

We repeated the run for negative skin with s = -2. In order to incorporate this skin in our simulator we assumed a modified zone radius of 5.75 ft and arrived at a modified zone permeability of 82.76 md using Eq. 2.3.2. Figure 2.4.31 presents a semi-log plot of pressure versus injection time. We calculated skin factor using Eq. 2.3.16 and obtained a value of -2.9 compared to the input value of -2.0. The value of apparent skin factor obtained using Eq. 2.3.17 was -4.415.

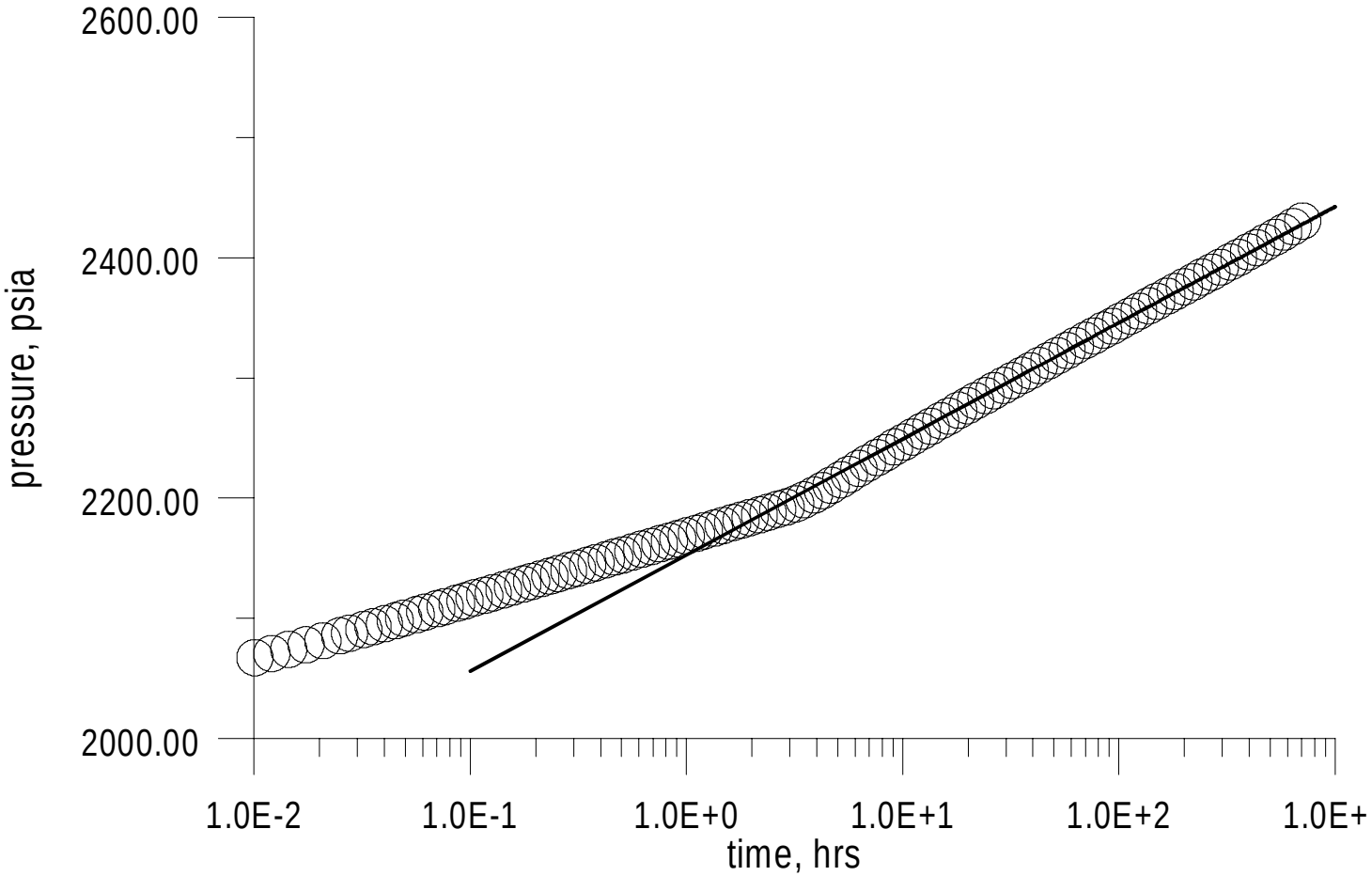
2600.00
2400.00
2200.00
2000.00
pressure, psia
1.0E-2
1.0E-1
1.0E+0
1.0E+1
1.0E+2
1.0E+
time, hrs

CHAPTER III

PRESSURE FALLOFF AND MULTI-RATE TESTING IN HETEROGENEOUS RESERVOIRS

Petroleum engineering literature is replete with references on falloff testing (see Chapter I) and the analysis techniques are well founded. In this chapter we discuss falloff tests in light of the multiphase flow theory of Ref. 13 (see also Section 2.1). We also present an equation for calculation of mechanical skin factor. We investigate the nature of multirate tests. Finally, we analyze synthetic data to demonstrate our results.

3.1 Pressure Falloff Testing

A pressure falloff test involves shutting off water injection into a well and observing the change in pressure with shut-in time. In Ref. 13, it was shown that during pressure falloff the pressure derivative reflects permeability of that region where rate changes rapidly and that single phase techniques may be used to analyze these tests. Indeed, falloff tests are amenable to classical analysis methods applied to a composite reservoir model. More specifically, the Inverse Solution Algorithm (ISA)[12] may be used to obtain permeability-mobility profile of a radially heterogeneous reservoir. While an

excellent discourse on ISA is given in Ref. 12 we discuss here the salient features of its application to injection falloff testing.

We define the instantaneous well-test permeability-mobility product, $(k\lambda)_{in}$, as the apparent instantaneous permeability-mobility product reflected by well test pressure derivative data; i.e., for a falloff test we can write

$$\frac{d\Delta p_{ws}(\Delta t)}{d\ln\Delta t} = \frac{70.6 q_{inj} B_w}{(k\lambda)_{in} h}, \tag{3.1.1}$$

where

$$\Delta p_{ws} = p_{wf}\Big|_{\Delta t=0} - p_{ws}(\Delta t). \tag{3.1.2}$$

Note that $(k\lambda)_{in}$ represents the weighted harmonic average of the permeability-mobility product in an annular region of the reservoir that moves away from the wellbore with shut-in time. The weight function that is applied to the permeability-mobility product in the averaging process closely resembles our rate kernel (see Eq.2.1.12) and is a function of radial distance and time. We can write

$$\frac{1}{(k\lambda)_{in}} = \int_1^{\infty} K_1\left(r_D, \Delta t_D\right)\left[\frac{1}{k\lambda\left(r_D\right)}\right] dr_D \ , \tag{3.1.3}$$

where

$$\Delta t_D = \frac{2.637 \times 10^{-4} (k\lambda)_{in} \Delta t}{\phi c_t r_w^2}, \qquad (3.1.4)$$

and Δt is in hours.

Thus, theoretically, the reservoir permeability-mobility profile can be obtained from pressure derivative data if we have an analytical expression for the rate kernel. The ISA algorithm uses a modification of Oliver's analytical expression for the kernel to obtain the radial permeability-mobility distribution. Note that in Eq. 3.1.4 c_t refers to the total compressibility of the system. Our investigations show that having a small variation in porosity and compressibility has only a small effect on the accuracy of our estimates. Therefore, we have considered the flooded zone compressibility as the total system compressibility in our calculations. Furthermore, we have used ISA in the drawdown mode, i.e., we consider the falloff data as equivalent drawdown data.

In a heterogeneous reservoir, if the kernel function is fully within a zone having constant mobility and permeability the instantaneous permeability actually represents the true permeability of the zone. In the derivative plot this would show as a horizontal straight line represented by the equation

$$\frac{d\Delta p_{ws}}{d \ln t} = \frac{70.6 q_{inj} B_w}{k\lambda_t h} \qquad (3.1.5)$$

Constant mobility is obtained in the regions where we have single phase flow, i.e., flow of either only oil or only water. We suggest a simple method for determination of permeability in a heterogeneous reservoir.

- Obtain the mobility-permeability profile using ISA and note the radii where the permeability-mobility product experiences sharp changes.
- Determine the radial distance of the flood front using the piston displacement approximation given in Eq. 2.2.15,viz.,

$$r_f(t) = \sqrt{\frac{5.615 q_{inj} B_w}{\pi h \left(\overline{S_w} - S_w\right)\phi}}\sqrt{t}\,. \qquad (3.1.6)$$

- Determine the point in the ISA plot approximately matching the flood front radius obtained from Eq. 3.1.6.
- Obviously each straight line in the derivative plot corresponds to a zone of constant permeability-mobility value in the ISA plot. For straight lines in the derivative plot corresponding to constant mobility-permeability values in the ISA plot behind the flood front use end-point water mobility to determine permeability using Eq. 3.1.5. Similarly for straight lines corresponding to values beyond the flood front use the end-point oil mobility.

3.2 Calculation of Skin

In this section we provide a relation between mechanical skin factor, *s*, and apparent skin factor, s_{app}. Since single phase analysis techniques can be applied to falloff

tests, semilog analysis using the first constant slope line, viz., the line representing permeability-mobility product of the flooded zone, will yield the actual mechanical skin factor[7]. The formula for skin factor is repeated here for convenience

$$s = 1.151\left[\frac{p_{1hr} - p_i}{m} - \log\left(\frac{k\lambda_w}{\phi c_t r_w^2}\right) + 3.2275\right]. \qquad (3.2.1)$$

Note that this early time constant slope line may be obscured by wellbore storage effects during actual field tests. Therefore, we endeavor to find a method to determine mechanical skin factor using the second constant slope line, viz., the line representing constant mobility-permeability value beyond the flood front. The proposed equation is analogous to an equation derived for pressure buildup analysis of gas-condensate data. In a recent work by Thompson and Reynolds[18], the authors derived such a relationship for buildup, viz.,

$$s_{app} = \frac{s}{\hat{k}_{rg}} + \left[\frac{1}{\hat{k}_{rg}} - 1\right]\ln\left(\frac{\lambda\sqrt{t_p}}{r_w}\right). \qquad (3.2.2)$$

where $\hat{k}_{rg}$ denotes near-wellbore gas relative permeability, λ is a constant relating the position of the critical oil saturation front to producing time and the other terms have their usual significance.

Based on Eq. 3.2.1, we can write the equation for determination of skin factor in a falloff test as

$$s_{app} = \frac{s\lambda_o}{\lambda_w} + \left[\frac{\lambda_o}{\lambda_w} - 1\right]\ln\left(\frac{\alpha\sqrt{t_{in}}}{r_w}\right), \qquad (3.2.3)$$

where s is the actual mechanical skin factor, t_{in} is the injection time, and s_{app} the apparent skin factor determined using the second constant slope line and Eq. 3.2.1.

Equation 3.2.3 can be derived by assuming steady-state pressure drop. If we consider the apparent skin as the sum of the actual skin and the skin due to difference in mobilities of oil and water we can write

$$\Delta p_{sapp} = \Delta p_{skin} + \Delta p_{flood,water} - \Delta p_{flood,oil}\,. \qquad (3.2.4)$$

Applying the formulae for skin and steady-state pressure drop in Eq. 3.2.4 we have

$$\frac{141.2q_{inj}B_w}{k\lambda_o}s_{app} = \frac{141.2q_{inj}B_w}{k\lambda_w}s + \frac{141.2q_{inj}B_w}{k\lambda_w}\ln\left(\frac{r_f}{r_w}\right) - \frac{141.2q_{inj}B_w}{k\lambda_o}\ln\left(\frac{r_f}{r_w}\right). \qquad (3.2.5)$$

Simplifying Eq. 3.2.5 we obtain

$$\frac{1}{\lambda_o}s_{app} = \frac{1}{\lambda_o}s + \left(\frac{1}{\lambda_w} - \frac{1}{\lambda_o}\right)\ln\left(\frac{r_f}{r_w}\right). \qquad (3.2.6)$$

Clearly, rearranging Eq. 3.2.6 and replacing the value of r_f we obtain Eq. 3.2.3.

In the presence of heterogeneity, our results are still valid. If the permeability change interface is far enough so that flood front is in the first zone and we are able to get the first or, at least, the second constant slope line, we can apply our methodology. If the zone interface is very near the wellbore, we can view the first zone as a part of the damaged zone and use the constant slope lines corresponding to the second zone permeability for our calculations. However, given the condition that the first zone is large, but the flood front is in the second zone and the constant slope line corresponding to the first zone permeability is obscured by wellbore storage effects, our method will fail. Clearly the likelihood of this condition is extremely remote.

3.3 Multirate Tests

A multi-rate test of an injection well involves changing the injection rate and observing the change in pressure response with time. This type of test is uncommon in oilfield practice, but we review them here in the interest of completeness and in order to determine whether they offer any advantages in terms of quality of information available from the test.

We postulate that when the injection rate is changed, another rate kernel propagates into the reservoir in addition to the existing rate and mobility kernels. Since this second kernel is nearer to the wellbore, its effect is more pronounced than the kernels further away. However, since the rate kernel propagates into the reservoir at a faster rate than the mobility kernel, the new rate kernel will cross the original mobility kernel after some period of time. Thus, while the rate kernel is dominant in the permeability-mobility averaging procedure, we could apply single phase techniques. While we observed that the

mobility kernel becomes dominant only after the second rate kernel overtakes it we could not determine exactly how long after the crossover this phenomena occurs. Our observations in Section 3.1 pertaining to falloff testing would be valid subject to the above mentioned restriction. Note that in using ISA we would have to use the difference in rate in place of the actual injection rate. In Cases X and XI we demonstrate our theory on multirate testing using synthetic well test data.

3.4 Analysis of Falloff and Multirate Data.

- Case VIII

We considered the same model as in Case 1, viz., k=50 md for $0.25 < r \leq 500$ ft and k=20 md for $500 < r \leq 5000$ ft and simulated a falloff test of 10 days after an injection period of 30 days. Figures 3.4.1-3.4.4 gives plots of the mobility and rate kernels as functions of the radial distance from the wellbore. Note that the characteristic sharply peaked shape of the mobility kernel observed during injection tests (see Figs. 2.4.6 - 2.4.9) is absent in the falloff test. This is to be expected since the flood front is stagnant during the test. However, it should be noted that the rate kernel behaves as it does in single phase systems.

Figure 3.4.5 presents a log-log plot of pressure change / pressure change derivative versus shut-in time.

We ran ISA (Inverse Solution Algorithm, see Ref. 12) with the pressure and pressure derivative data of Fig. 3.4.5. A comparison of the mobility-permeability product obtained from ISA is plotted against that obtained from the simulation results at the end

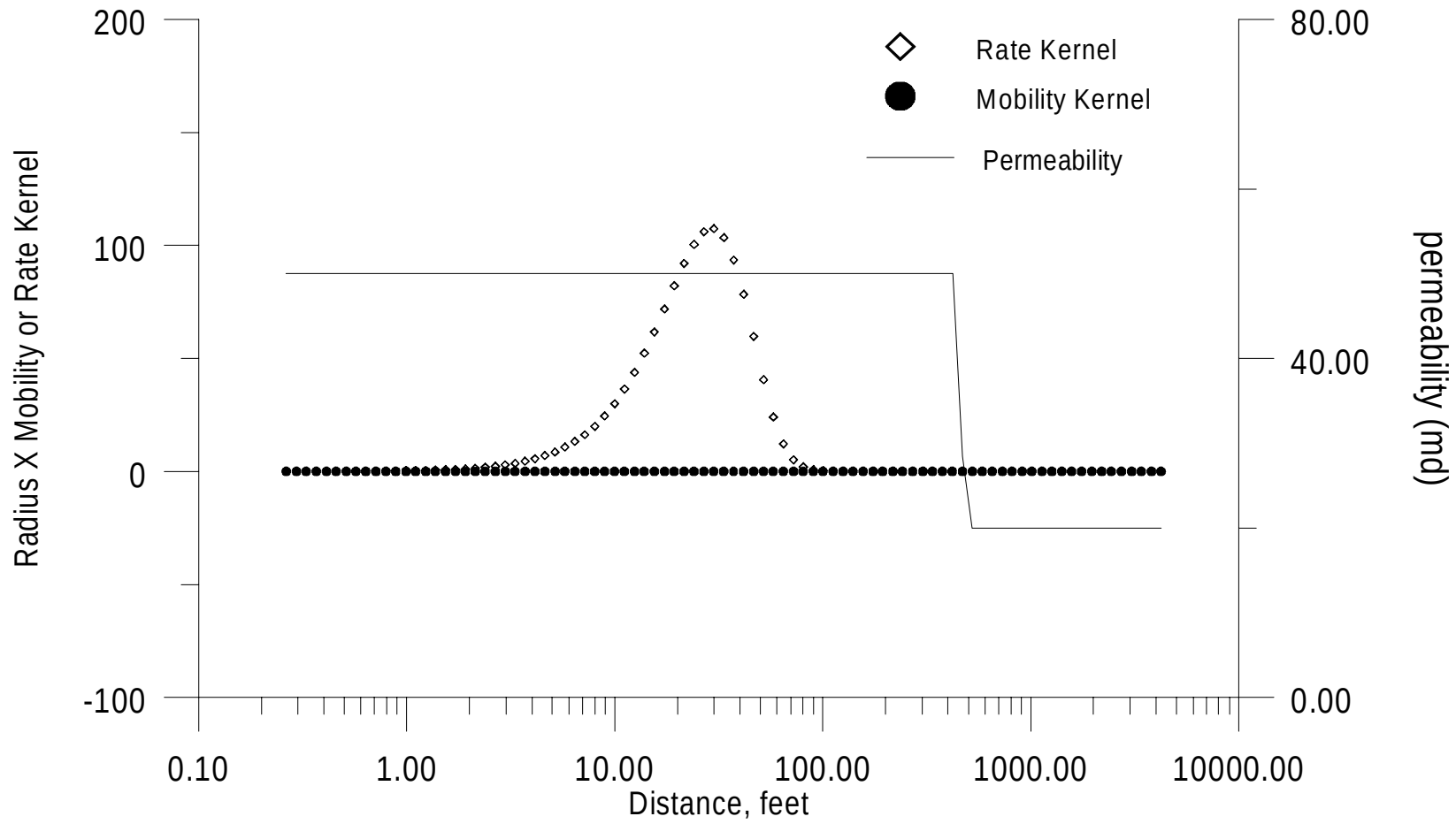

Figure 2.4.1: Mobility and Rate Kernel at 1 e-2 ds - (Case VIII)

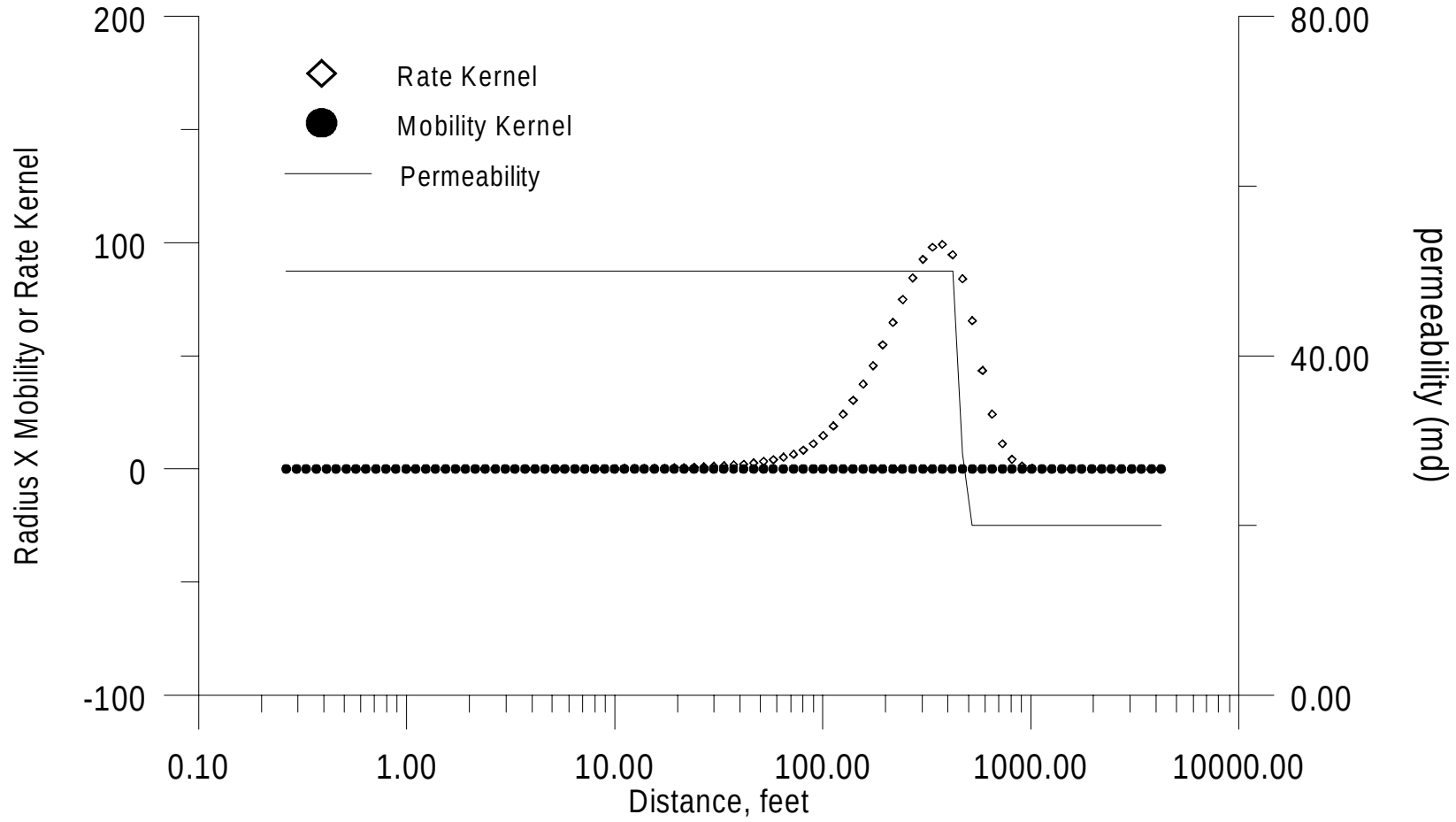

Figure 2.4.2: Mobility and Rate Kernel at 1 day (Case VIII)

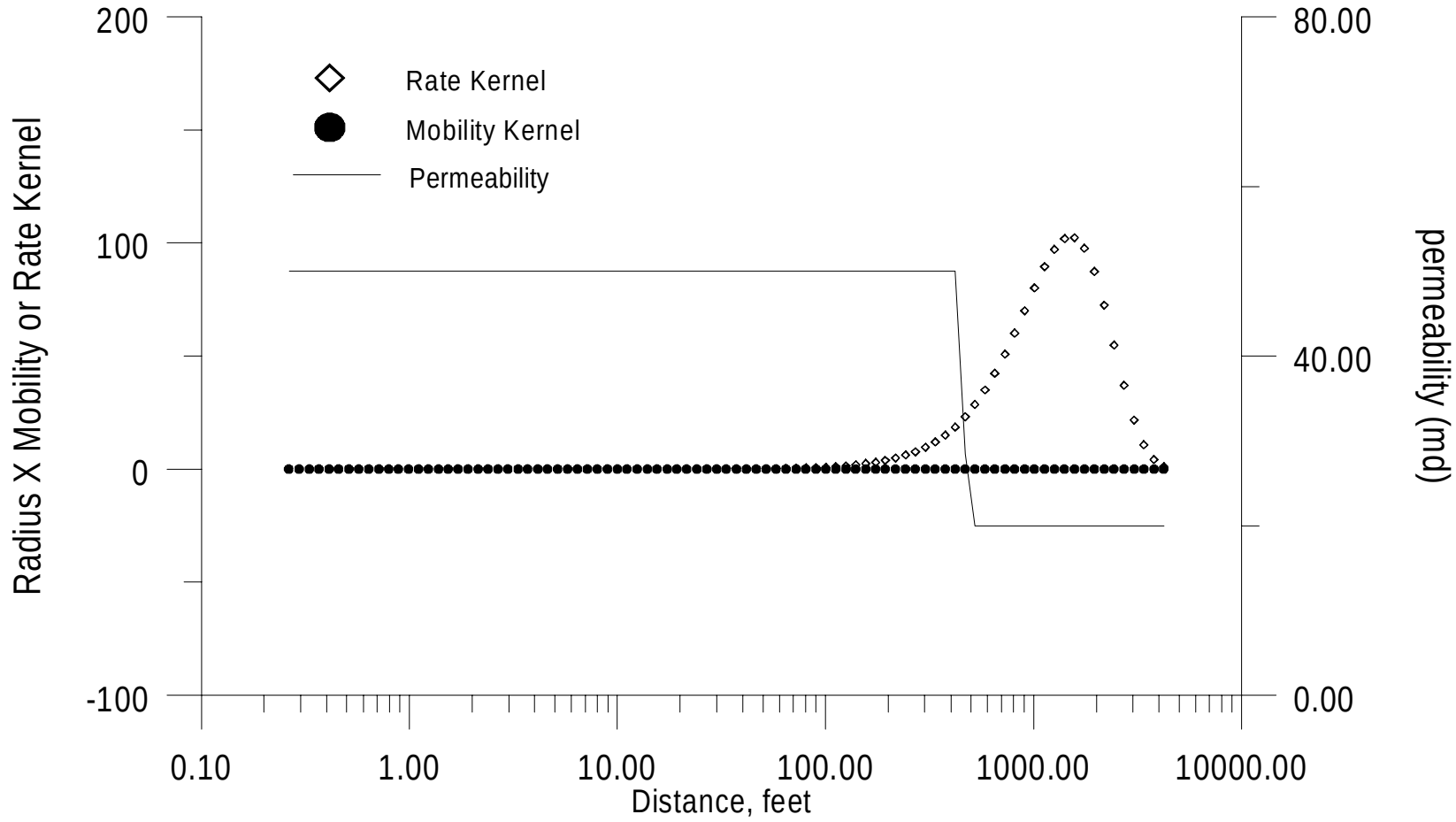

Figure 2.4.2: Mobility and Rate Kernel at 2 days (Case VIII)

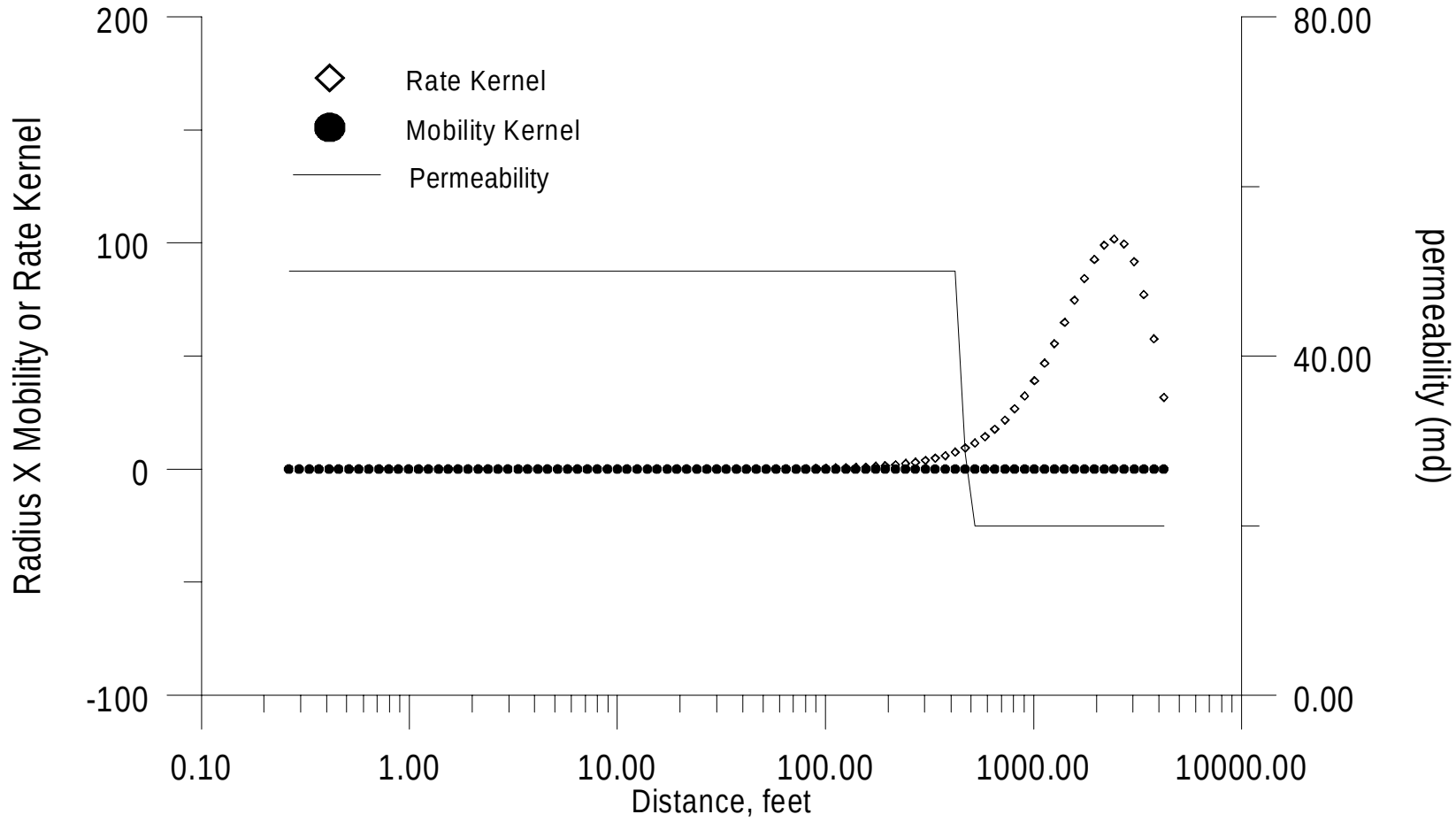

Figure 2.4.4: Mobility and Rate Kernel at 10 days (Case VIII)

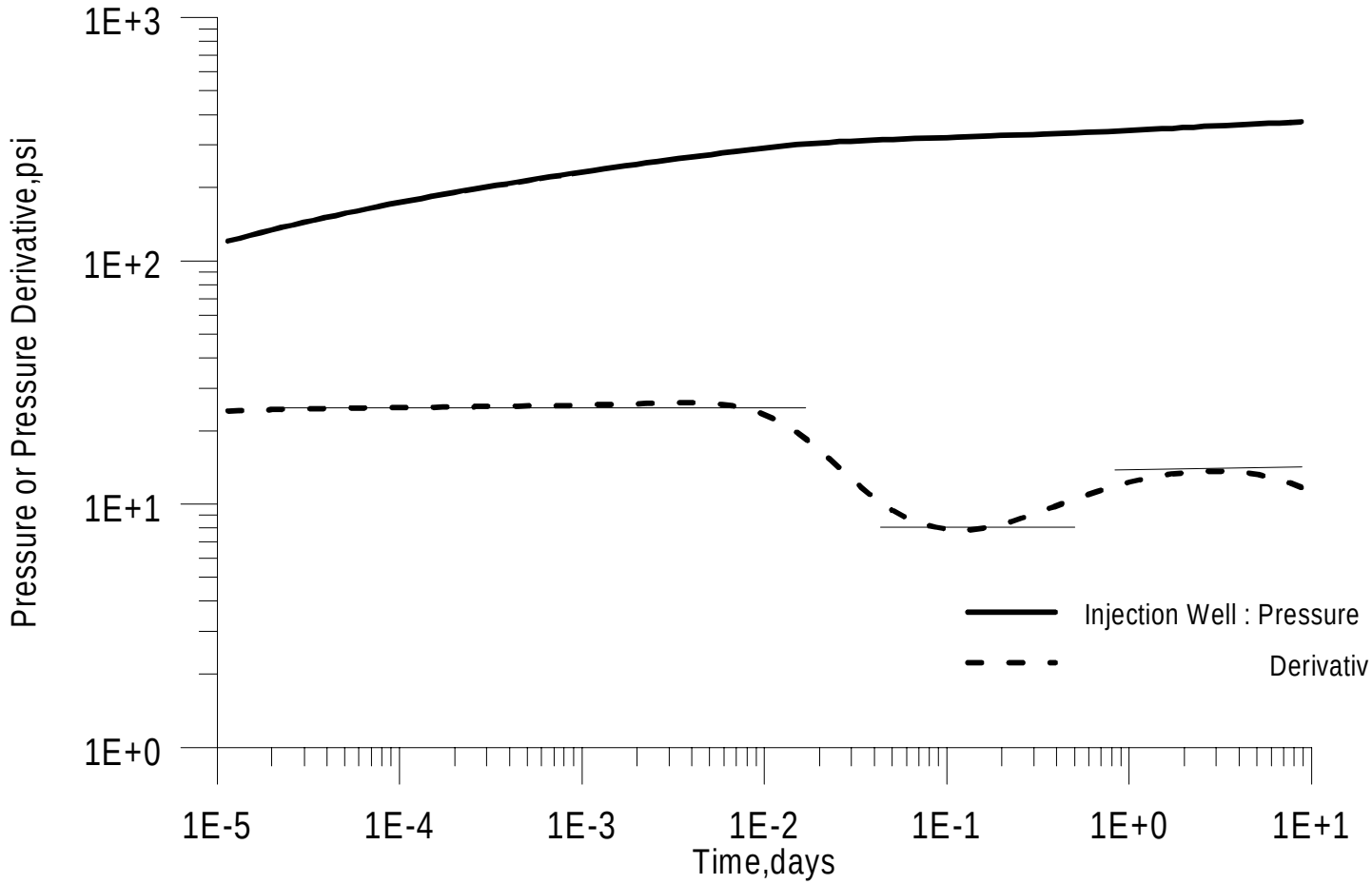

Figure 3.4.5 : Pressure/Pressure Derivative Response at Injection Well

of the injection period in Fig. 3.4.6. Clearly the ISA result shows the same trend as latter. We used Eq. 3.1.6 to calculate the position of the flood front at the end of the injection period at 30 days. We obtained a value of 77 ft which roughly corresponds with the first slope change in the ISA plot. Thus the mobility-permeability change is due to change in relative permeability and fluid viscosity at the flood front. Obviously, the second change in slope is due to change in permeability. Reconsidering Fig. 3.4.5, we selected the first straight line as the derivative data for $t < 10^{-3}$ days. We calculated the permeability using Eq. 3.1.5 and assuming mobility of the flooded zone as the water mobility. We obtained a value of 49.70 which compares very well with the input value of 50 md. Next, we assumed a second straight line region for $0.07 < t < .15$ day and the fluid mobility and viscosity to be that of oil. We obtained the permeability to be 45.86 md as compared to the input value of 50 md. The reason for this small discrepancy is easy to see from Fig. 3.4.2. At 0.1 day the rate kernel is non zero beyond 500 ft. Thus the effect of the low permeability zone beyond 500 ft influences the pressure derivative data. Finally, we considered a third straight line at the range $2 < t < 5$ days. Assuming the fluid mobility and viscosity to be that of oil we calculated a permeability of 26.50 md. This differs slightly from the input value of 20 md because, in this case too, the rate kernel spans a little of the first zone.

Also as seen in Fig. 3.4.5 there is a fall in pressure derivative beyond 5 days which results in high calculated mobility towards the end of the reservoir (Fig. 3.4.6). This is attributed to the rate kernel has reaching the outer boundary of the reservoir (Figs. 3.4.3 - 3.4.4).

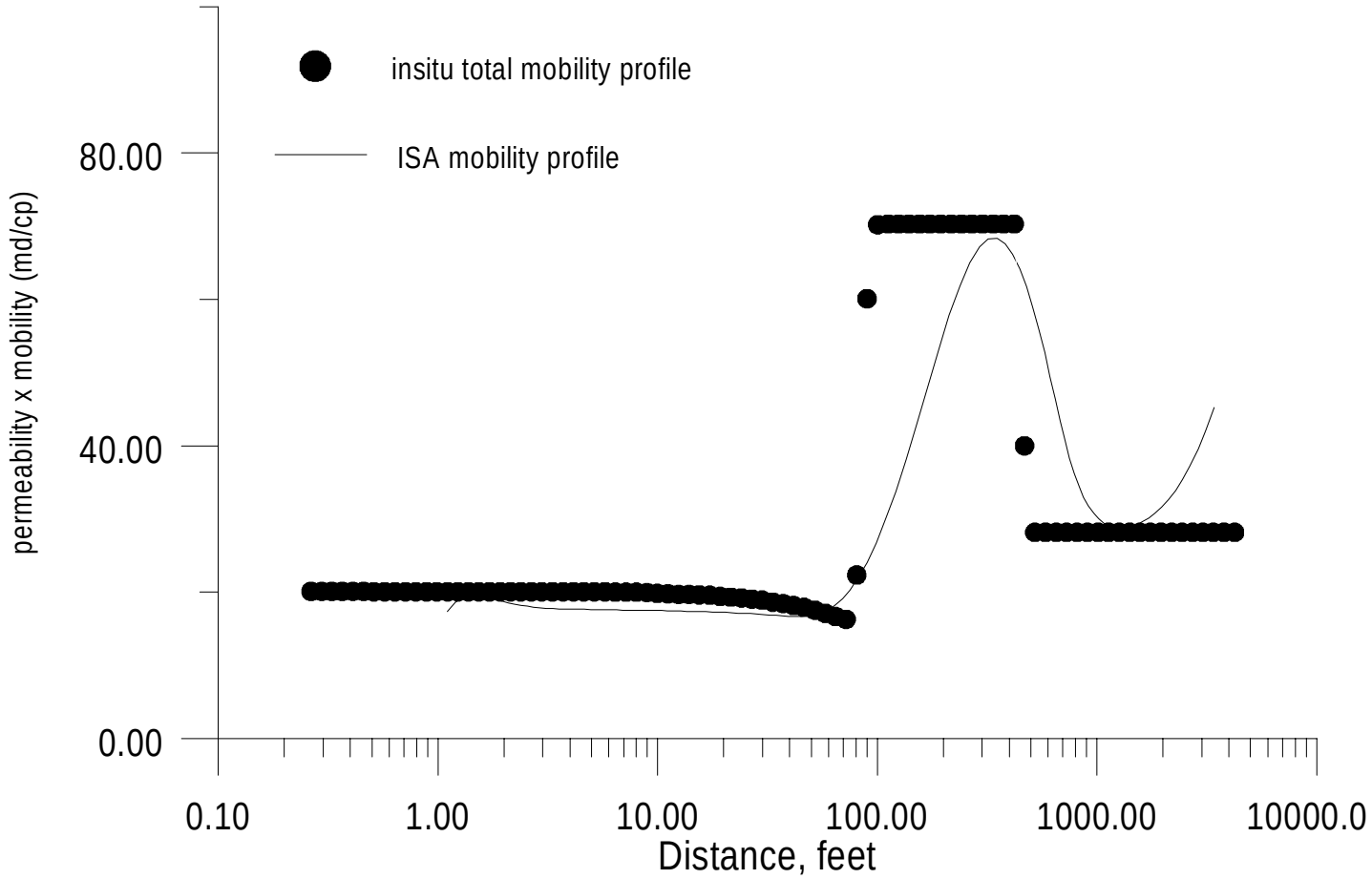

Figure 3.4.6 : ISA and Simulated Mobility-Permeability Product

- CASE IX

In order to test the validity of our theory on determination of skin in a falloff test, we used the same model except that in this case we considered a falloff of 3 days for a homogeneous reservoir having a permeability of 30 md. We used the same relative permeability curves (Fig. 2.4.1) and other reservoir and fluid properties (Table 2.4.1) of the cases discussed in the previously. In this case, however, we assumed a skin of 10. In order to incorporate this skin in our simulator we assumed a damaged zone radius of 0.51 ft and arrived at a damaged zone permeability of 2.0 md using Eq. 2.3.2. Thus, effectively we had a composite system with k = 2 md for $0.25 < r \leq 0.51$ ft and k = 30 md for $0.51 < r \leq 5000$ ft. Figure 3.4.7 presents a semi-log plot of pressure versus injection time. We calculated skin factor using the conventional equation, viz., Eq. 3.2.1 and the first constant slope line and obtained a value of 10.15 compared to the input value of 10.0. Using the second constant slope line and Eq. 3.2.1 we obtained a value of 57.93 which we denoted as s_{app}. This value in Eq. 3.2.3 yielded the value of skin as 12.38 which again is close to the input value.

We repeated the run for negative skin with s = -2. In order to incorporate this skin in our simulator, we assumed a modified zone radius of 5.75 ft and arrived at a modified zone permeability of 82.76 md using Eq. 2.3.2. Figure 3.4.8 presents a semi-log plot of pressure versus injection time. We calculated skin factor using Eq. 3.2.1 and the first constant slope line and obtained a value of -1.8 compared to the input value of -2. Using the second constant slope line and Eq. 3.2.1 we obtained a value of 9.37. Considering this

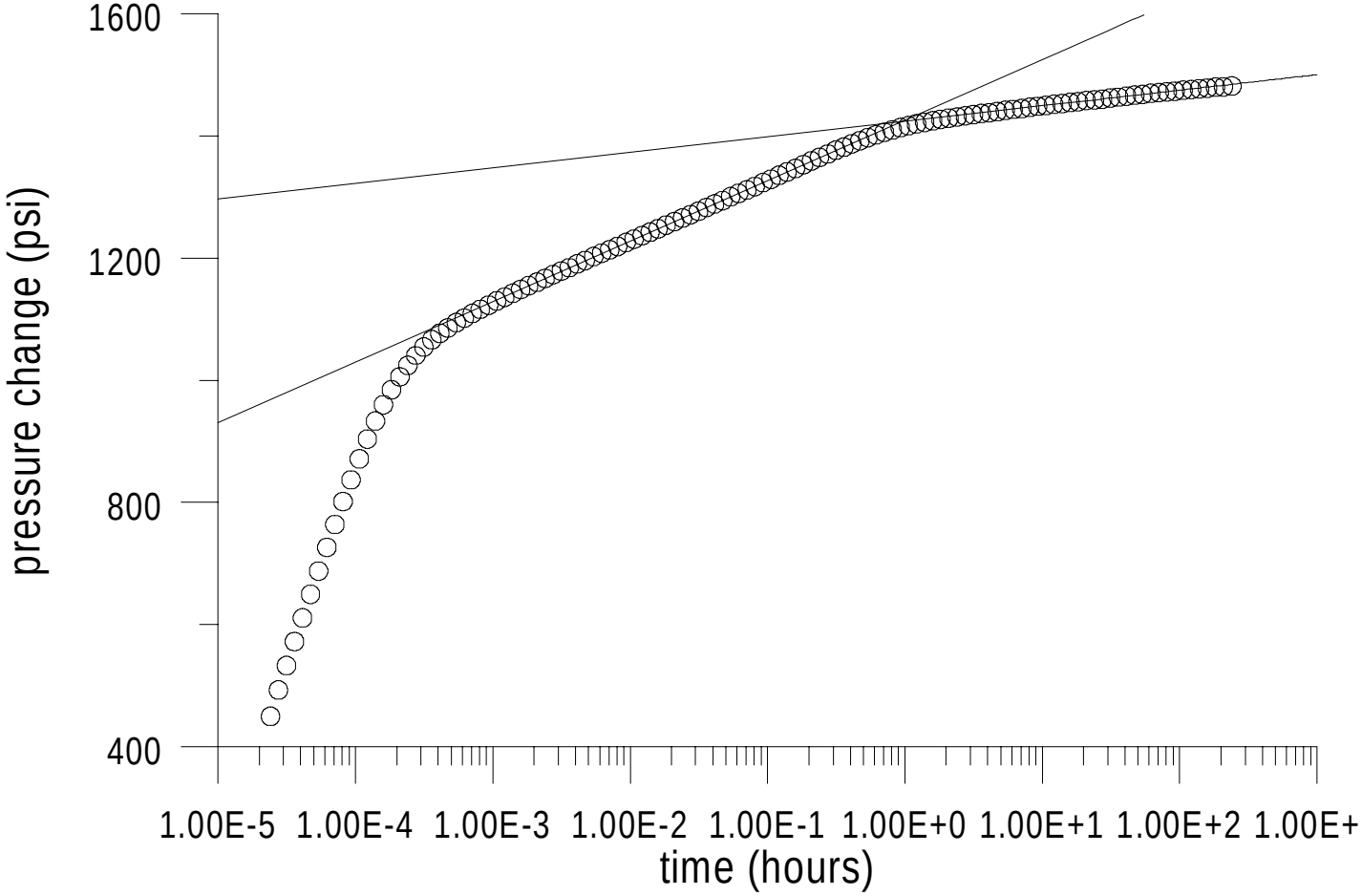
1600
1200
800
400
pressure change (psi)
1.00E-5
1.00E-4
1.00E-3
1.00E-2
1.00E-1
1.00E+0
1.00E+1
1.00E+2
1.00E+
time (hours)

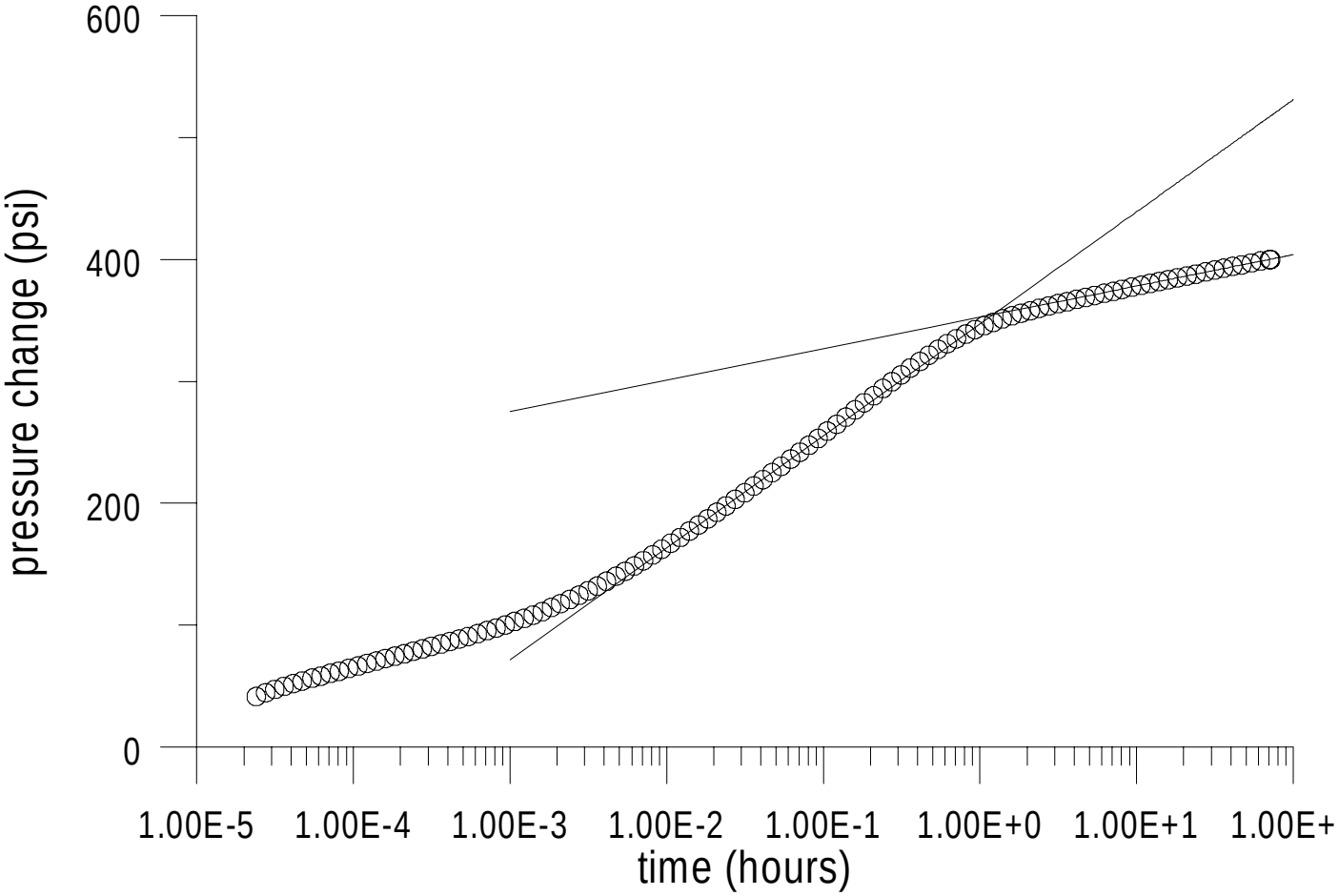
600
400
200
0
pressure change (psi)
1.00E-5
1.00E-4
1.00E-3
1.00E-2
1.00E-1
1.00E+0
1.00E+1
1.00E+
time (hours)

value as s_{app} in Eq. 3.2.3 yielded the value of skin as -1.44 which again is close to the input value.

- CASE X

In this exercise, we investigated the effect of lowering the injection rate instead of completely shutting off the injection. At the end of 30 days of injection at 250 barrels/day, we lowered the injection rate to 150 barrels/day and observed the simulated pressure response for 10 days. Figure 3.4.9 - 3.4.12 gives the rate and mobility kernel plots. Observing Figs. 3.4.9 - 3.4.10 it appears that the mobility kernel is not present at early times. However, if we zoom into these figures we see the presence of the mobility and the first rate kernel caused due to the first injection period (see Figs. 3.4.13 - 3.4.14). Clearly, the rate kernel initiated by the rate change has masked the earlier kernels. While we think that there could be numerical errors in calculating the size of the mobility kernel as it involves working with slowing changing mobility at small time intervals, the fact remains that we have a large rate kernel attenuated by small radial distance. Therefore, at early times, the pressure derivative is primarily affected by this second rate kernel. However, after some time when the rate kernel crosses the mobility kernel, the mobility kernel once again begins to influence the pressure derivative data (see Figs. 3.4.11 - 3.4.12). During the time when the mobility kernel has no influence, classical single phase analysis can be applied. Thereafter, the derivative departs from single phase behavior.

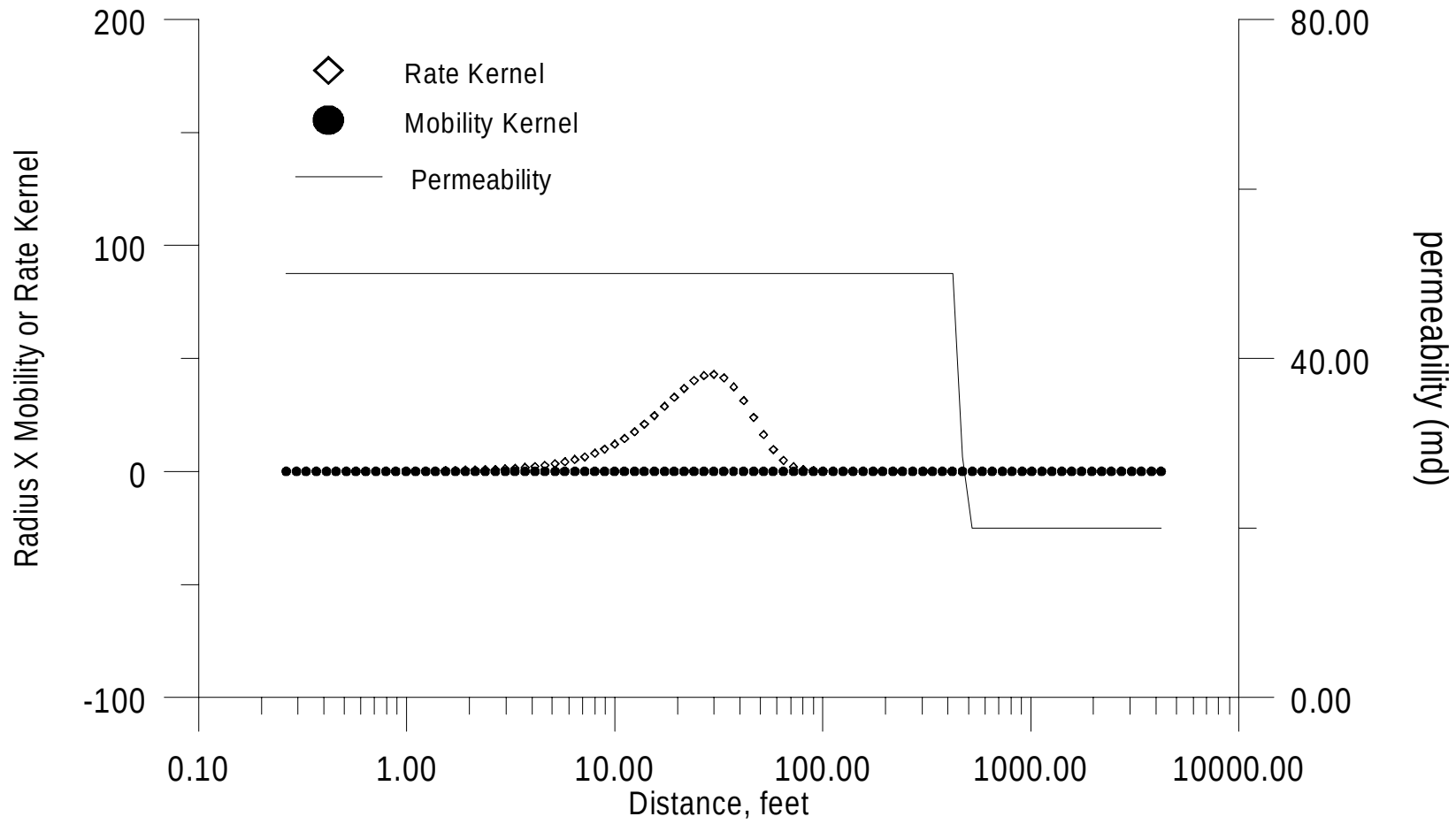

Figure 3.4.9: Mobility and Rate Kernel at 1.e-3 day

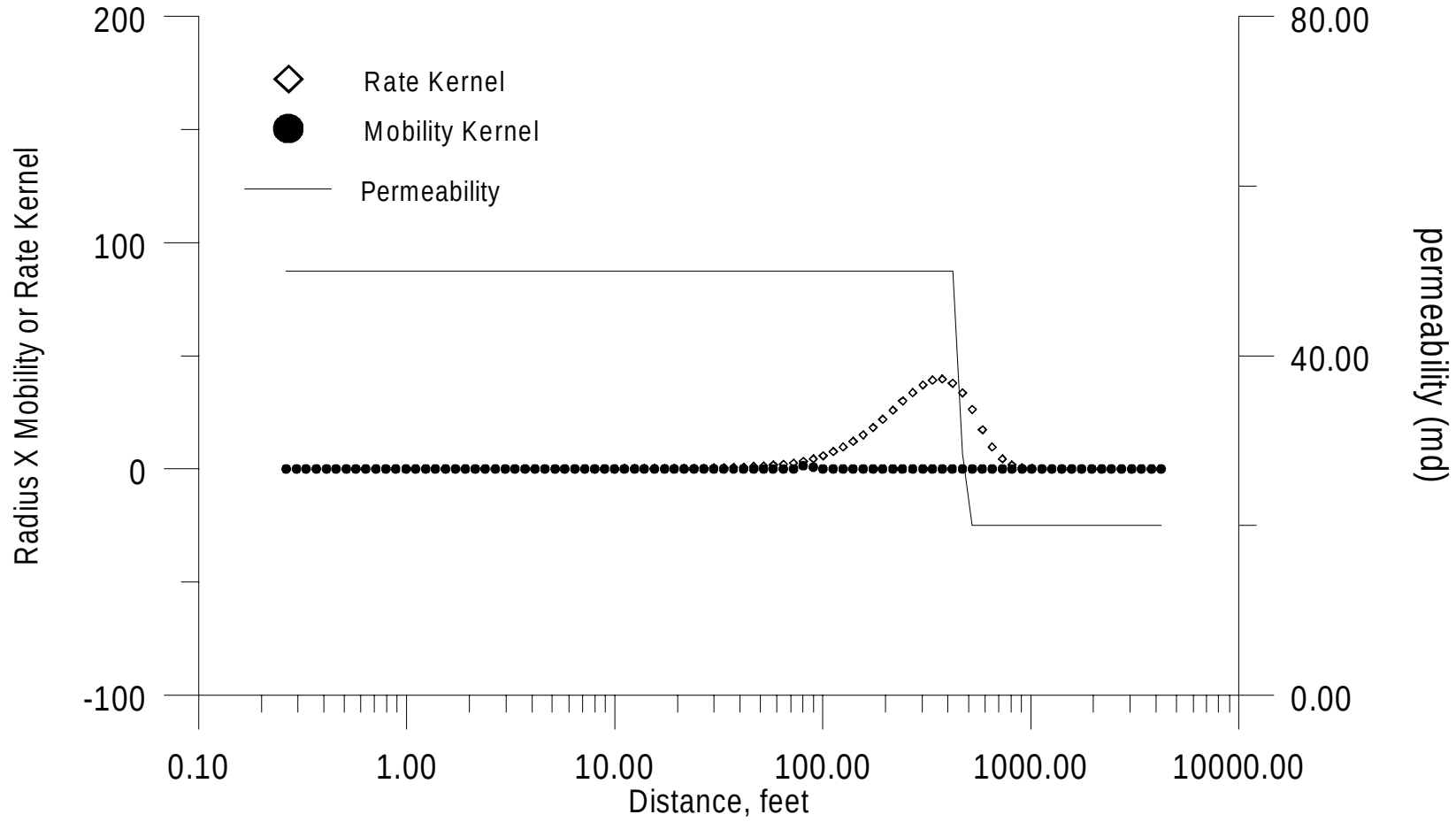

Figure 2.4.10: Mobility and Rate Kernel at 1 day (Case X)

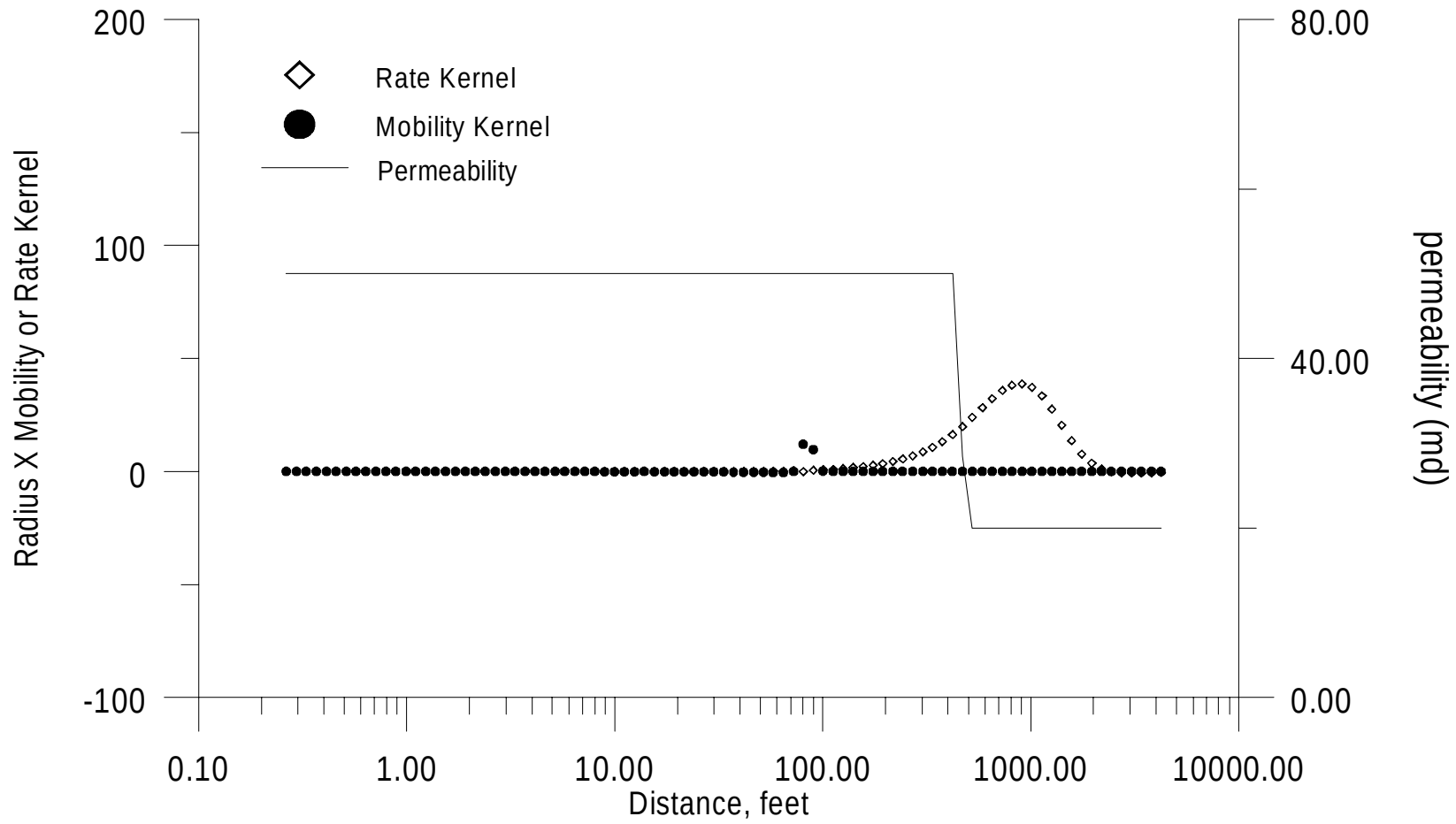

Figure 2.4.11: Mobility and Rate Kernel at 1 day (Case X)

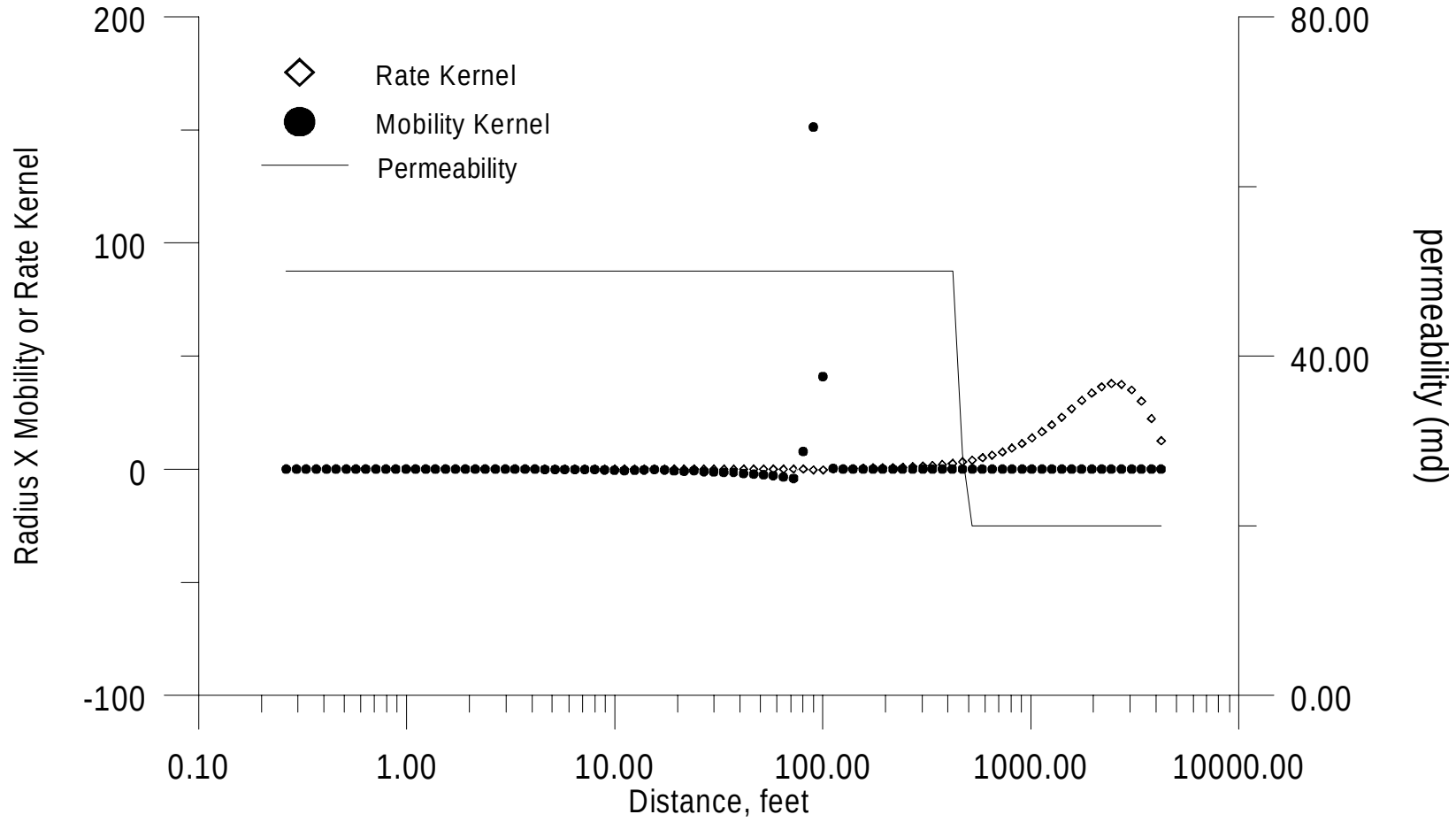

Figure 3.4.13: Mobility and Rate Kernel at 10 days (Case X)

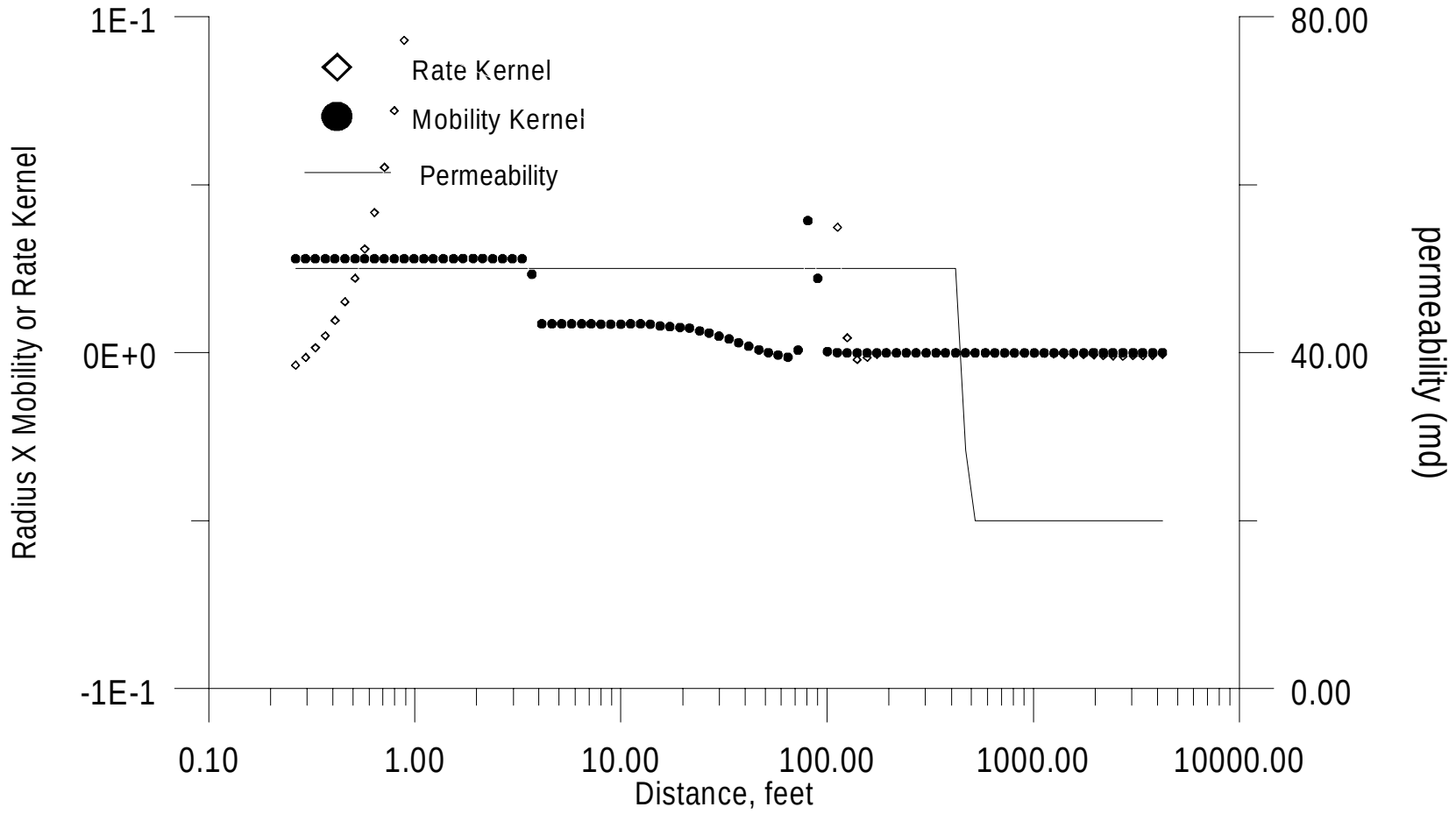

Figure 3.4.13: Mobility and Rate Kernel at 1.e-3 day - Zoomed
(Case X)

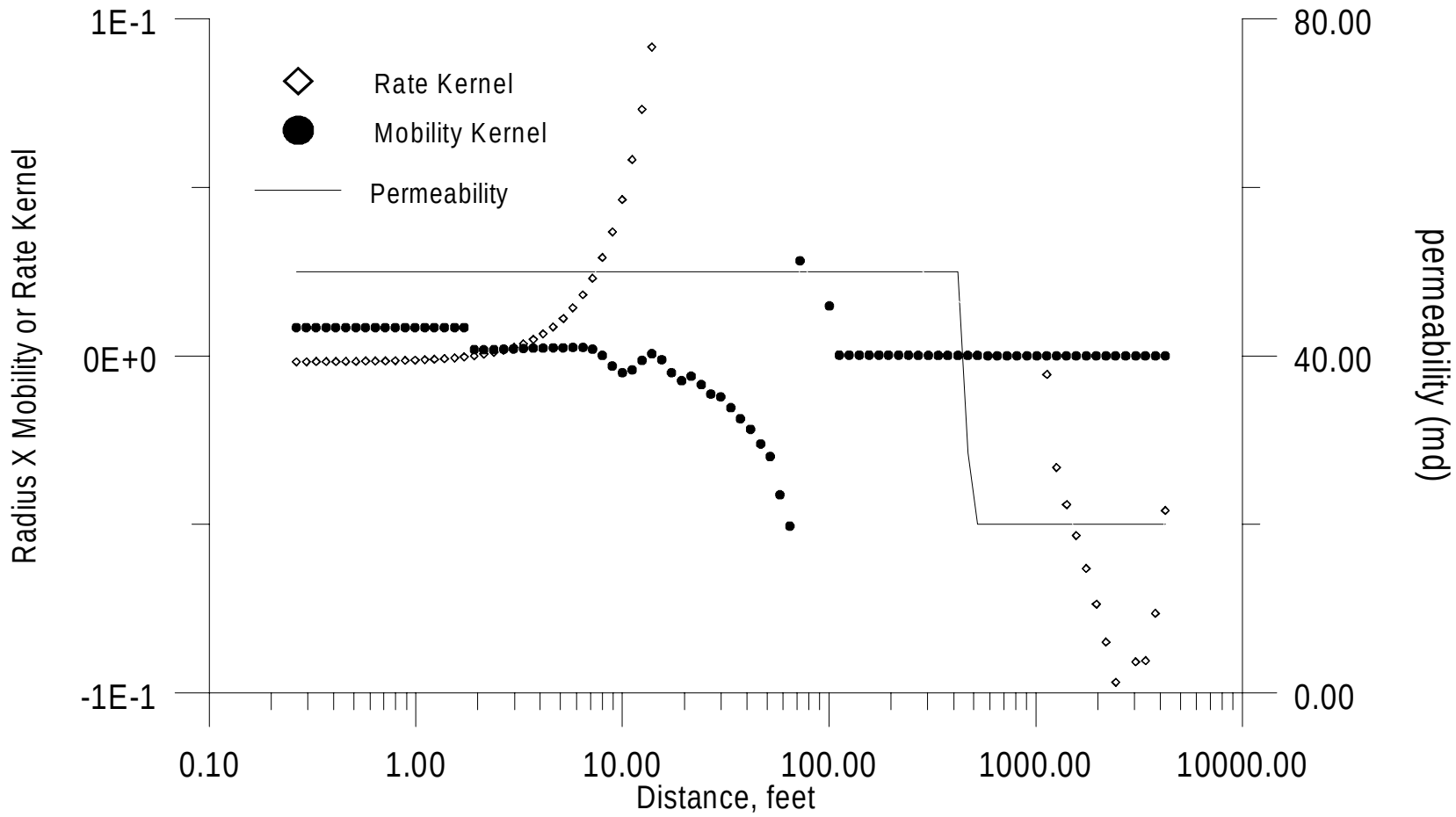

Figure 3.4.14: Mobility and Rate Kernel at .1 day - Zoomed
(Case X)

Let us define:

$$\Delta p = p_{wf}\Big|_{\Delta t=0} - p_{wf}\Big|_{\Delta t=t'}. \qquad (3.4.1)$$

As discussed in Sections 3.1 and 3.3, the pressure derivative equation when the rate kernel is within a zone of constant permeability-mobility product can be written as

$$\frac{d\Delta p}{d\ln\Delta t} = \frac{70.6\Delta q_{inj} B_w}{k\lambda_t h}, \qquad (3.4.2)$$

where Δq_{inj} represents the change in injection rate, and Δt is the elapsed time after the rate change.

Figure 3.4.15 gives a log-log plot of pressure and pressure derivative versus elapsed time. It follows the same trend as the falloff data. Figure 3.4.16 gives a comparative plot of ISA and simulator generated mobility-permeability product; we see that similar behavior as the falloff case is observed. Considering the first, second and third straight lines to be corresponding to the time ranges $t < 10^{-2}$ day (first zone before the flood front), $0.07 < t < .15$ day (first zone beyond the flood front) and $2 < t < 5$ days (second zone) respectively we calculated the permeability values to be 50.81, 46.91, 33.35. As before, the two zones had input permeability values of 50 and 20 md. Note that the deviation in the second zone permeability is more than that of the falloff test case and cannot be explained solely by presence of a part of the rate kernel in the first zone. From

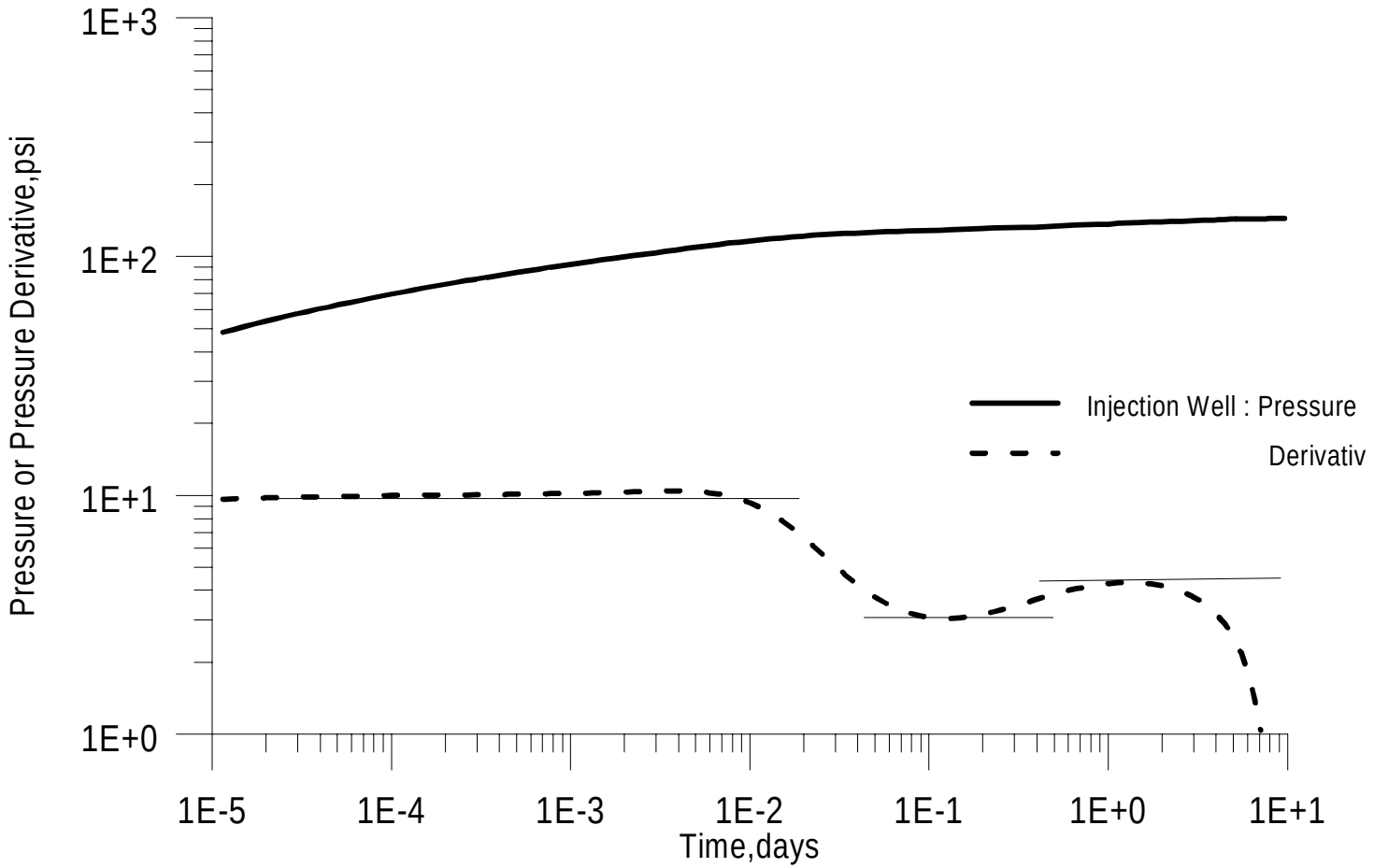

Figure 3.4.15: Pressure/Pressure Derivative Response at Injection Well

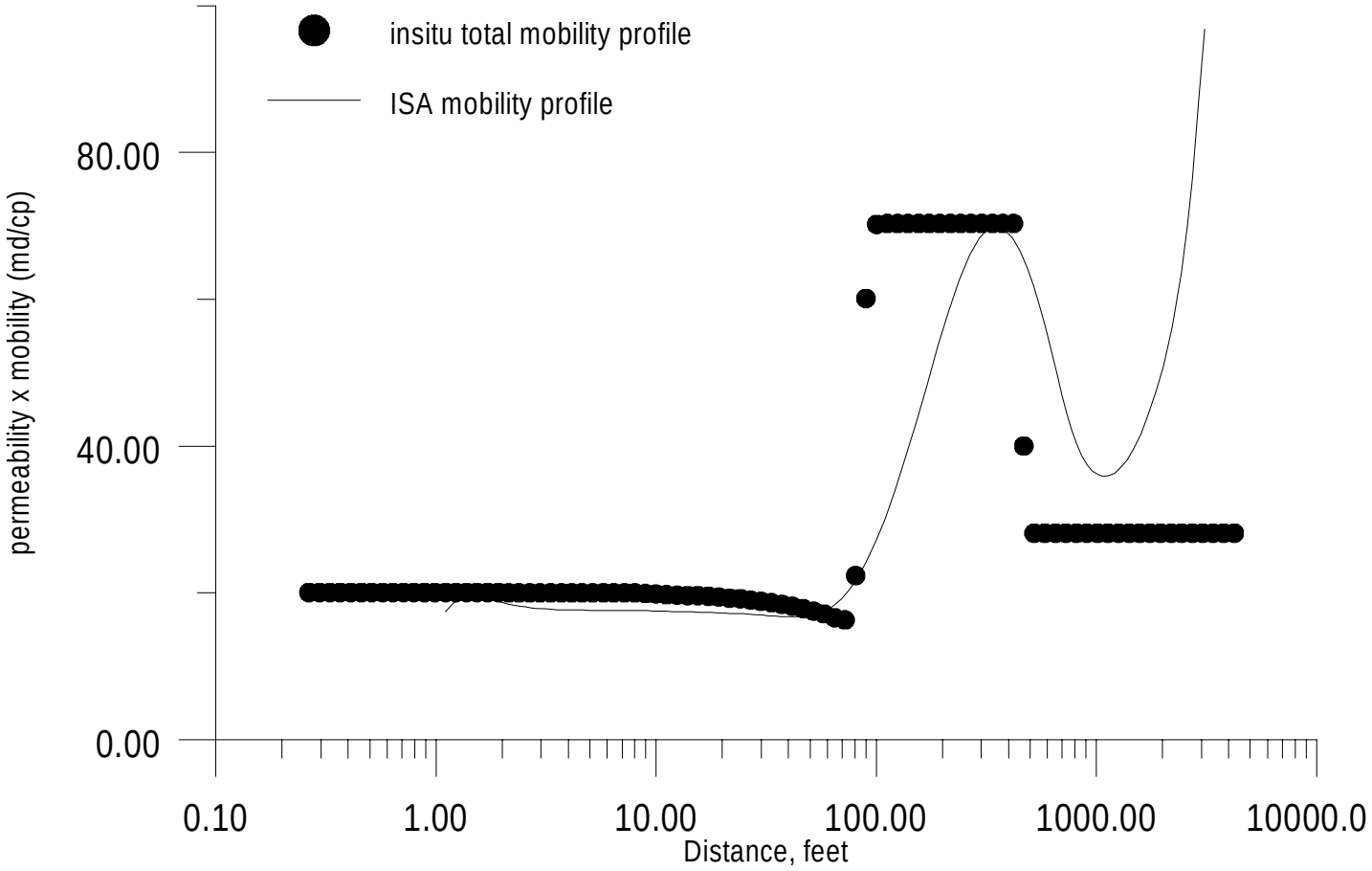

Figure 2.4.16: ISA and Simulated Mobility-Permeability Product (Case X)

Fig. 3.4.11 we see that the mobility kernel becomes significant at the time period corresponding to the time interval assumed for the "third straight line". Since the flood front is in the first zone, its effect on the derivative plot becomes apparent.

The sharp drop in the derivative at late time is due to the combine effect of the rate kernel the reaching the boundary and the mobility kernel becoming dominant (see Fig. 3.4.12)

- Case XI

In another muti-rate test case, the same system as before was considered. However, in this case we simulated injection at 150 barrels/day for 30 days and the increased the rate to 250 barrels/day. Plots of rate and mobility kernels at various times are given in Figs. 3.4.17 - 3.4.20. As in the previous case the mobility kernel is not evident at small elapsed times after the rate change; (i.e., the rate kernel to due rate change masks the other kernels). A log-log plot of pressure change and pressure derivative is presented in Fig. 3.4.21. Here we define pressure change as

$$\Delta p = p_{wf}\Big|_{\Delta t=t'} - p_{wf}\Big|_{\Delta t=0}. \qquad (3.4.3)$$

While the observation regarding multi-rate tests as described in the earlier case is still valid in general and we did get the first zone permeability from the horizontal pressure derivative corresponding to both flooded and unflooded regions in the first permeability zone, the second zone permeability could not be obtained using single phase

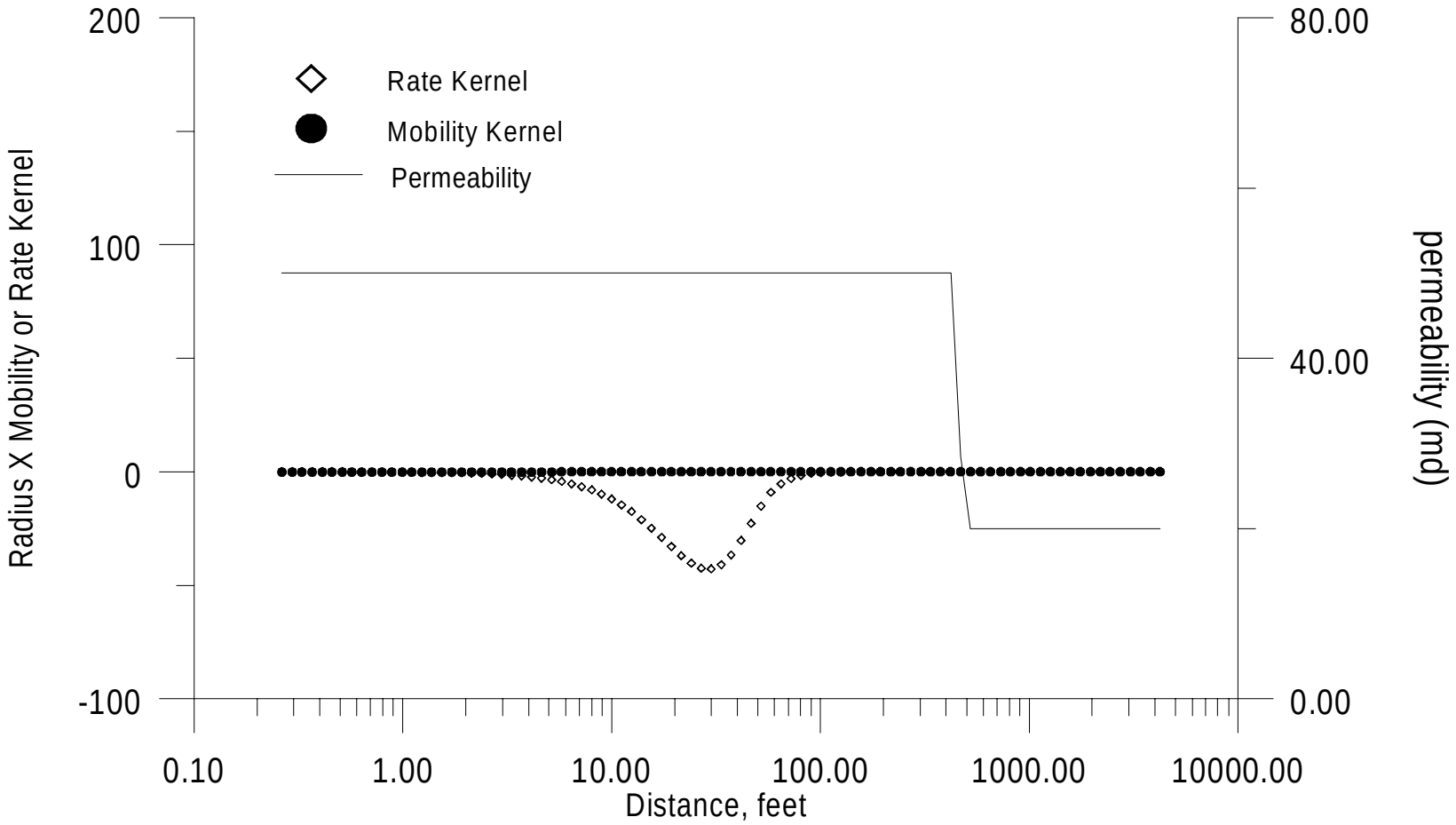
200
100
0
-100
80.00
40.00
0.00
Rate Kernel
Mobility Kernel
Permeability
Radius X Mobility or Rate Kernel
permeability (md)
0.10
1.00
10.00
100.00
1000.00
10000.00
Distance, feet

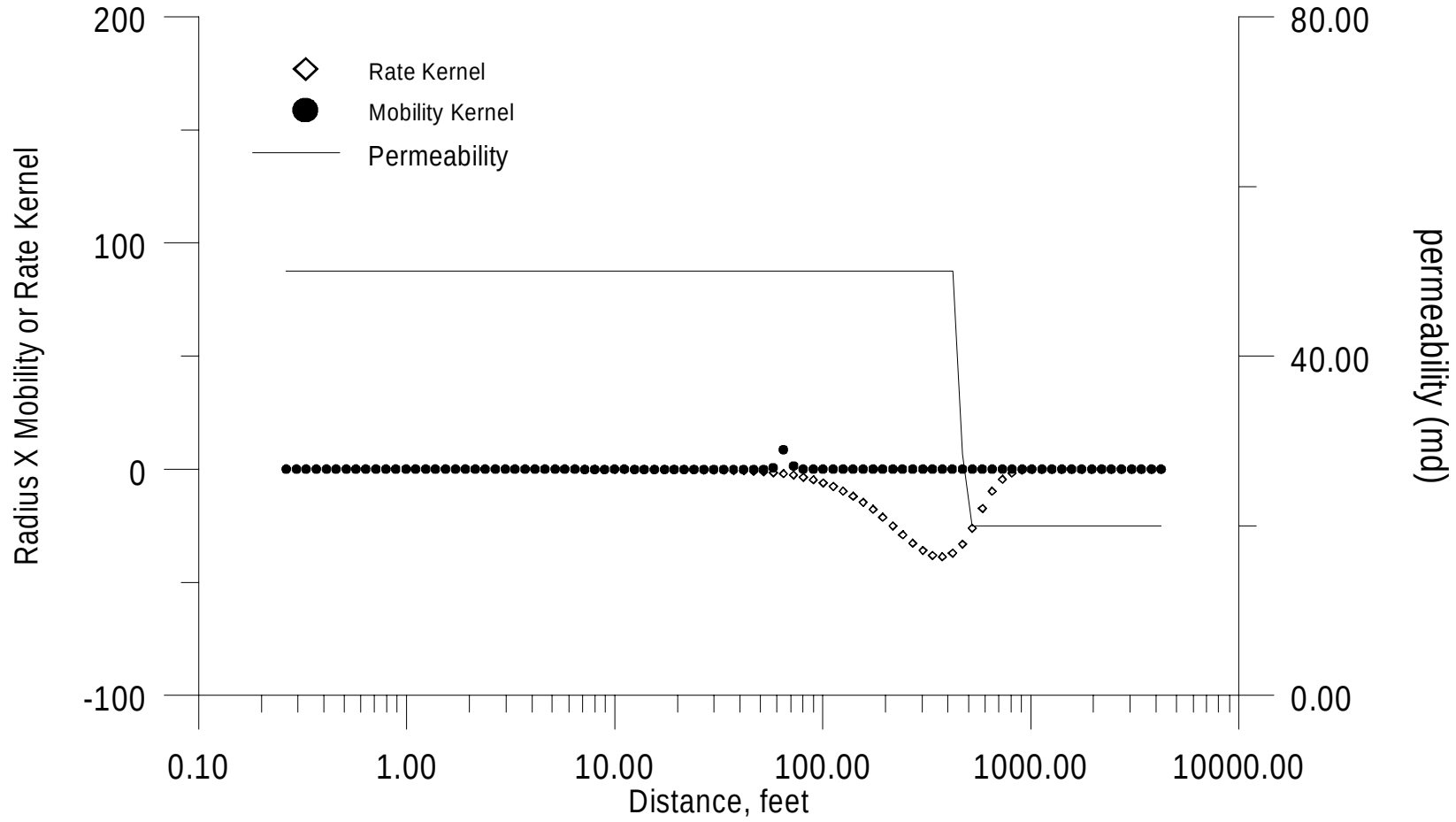

Figure 3.4.19: Mobility and Rate Kernel at 1 day (Case XI)

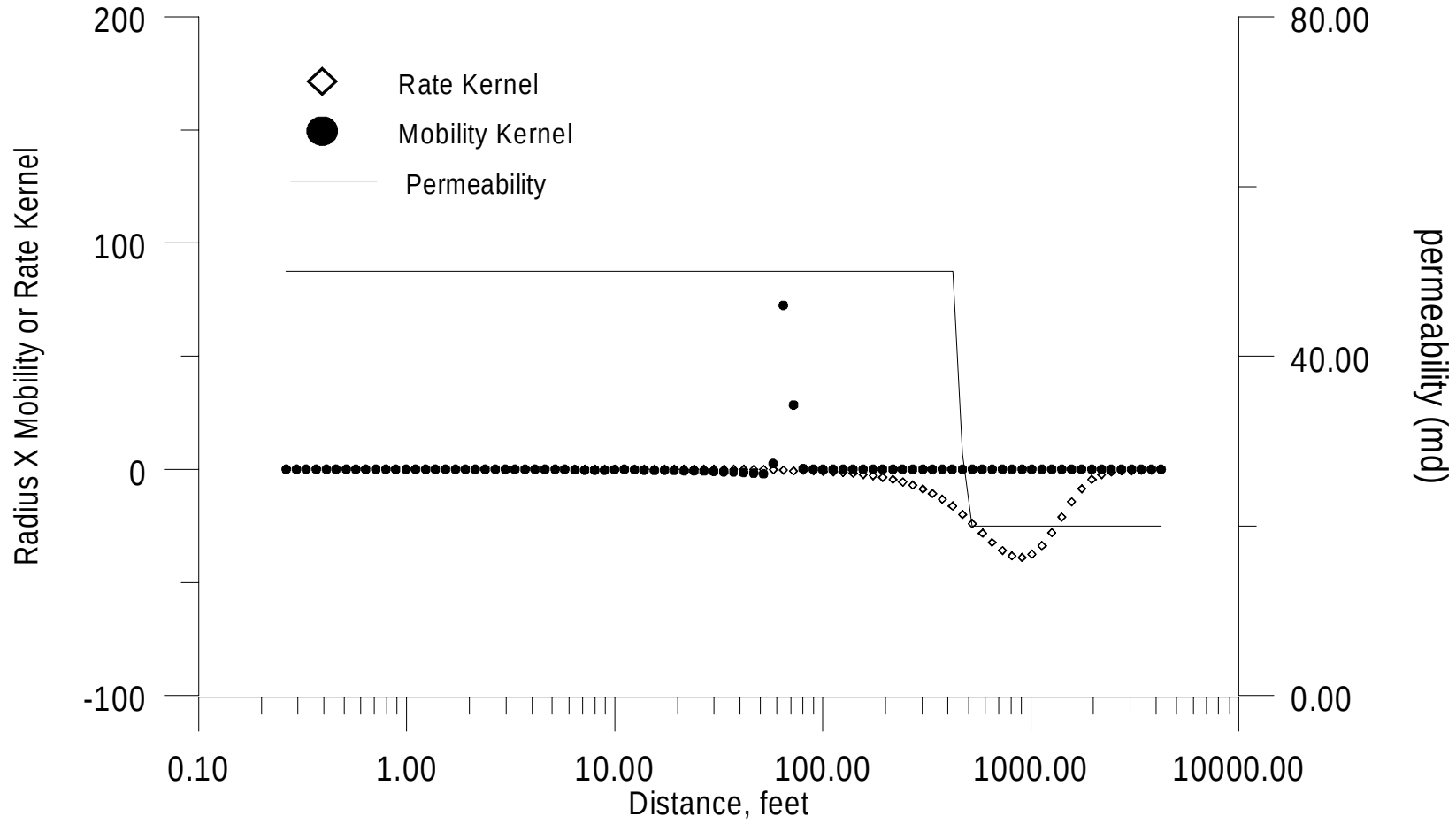

Figure 2.4-19: Mobility and Rate Kernel at 1 day (Case XI)

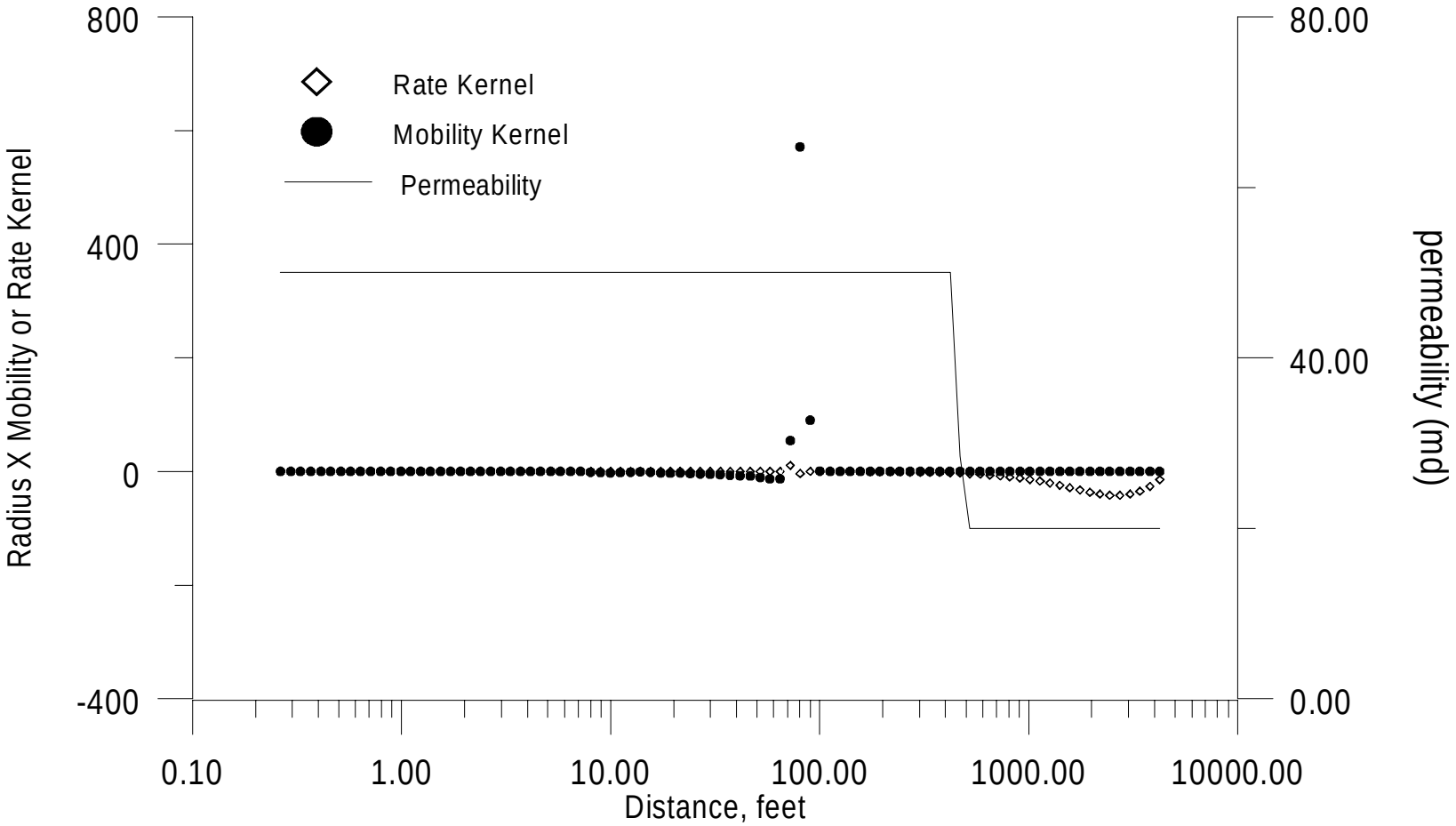

Figure 2.4.30: Mobility and Rate Kernel at 1 day (Case XI)

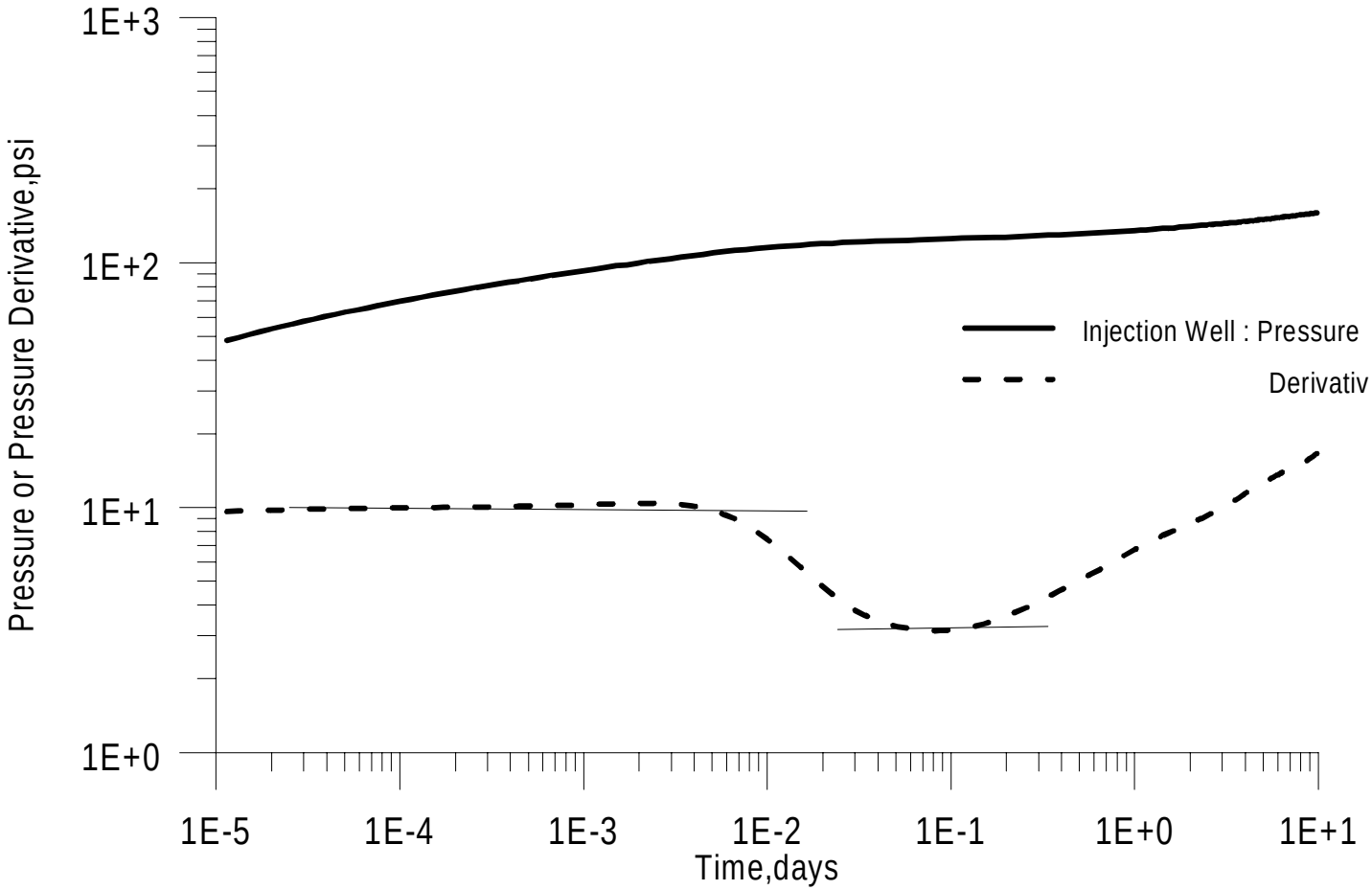

Figure 3.4.21 : Pressure/Pressure Derivative Response at Injection Well

methods as before. This is because the the mobility kernel started to affect the pressure derivative data earlier than the preceding case. Furthermore, we could not apply the multi-phase technique of Chapter II due to absence to any clear horizontal line towards the end. Also note that the rate kernel is affected by the boundary towards the end of the test.

We do not pursue this case further as in practice injection is carried out at the optimum rate which often coincides with the maximum permissible rate. Thus any increase in rate could cause operational problems including fracturing the formation.

On the other hand, multi-rate tests done by decreasing the injection rate may appear practically feasible. We have the possibility of obtaining all the information that can be obtained from a falloff test without having to shut off injection. However, one should note that in practice it is difficult to implement constant step production or to measure variable production accurately. Another problem in implementing multi-rate test would be to accurately determine the time periods when the mobility kernel has significant effect on the pressure derivative. Simulation studies indicate that, at a minimum, this time depends on injection rates and distance to the flood front.

CHAPTER IV

CONCLUSIONS

This chapter summarizes the work we have presented in the previous chapters, and enumerates the contributions and conclusions of this study.

The objective of this work was to provide a theory to explain the pressure transient behavior of injection/falloff tests. Based on the theory developed, we suggested possible methods of data analysis.

In Chapter II, we summarized the general mutiphase flow well test theory of Thompson and Reynolds which served as a basis for our understanding and analyzing injection/falloff tests. We then derived an analytical solution for water injection in radially heterogeneous reservoirs. We also investigated the relationship between the apparent skin factor obtained by classical analysis of injection test pressure data and the true mechanical skin factor. Finally, we validated our theory by analyzing synthetic well test data generated using a two-phase simulator. The conclusions of this part of the work are as follows:

(i) We found that in an injection test the pressure derivative data reflects permeability both at the flood front and in the unflooded region. Therefore, for a heterogeneous system, it is possible to detect permeability changes ahead of the flood front.

(ii) We derived a generalized equation as follows,

$$\frac{d\Delta p_{wf}}{d\ln t} = \frac{70.6 q_{inj} B_w}{h}\left[\frac{1}{k_{l+1}\lambda_f} - \frac{1}{\lambda_o}\left[\frac{1}{k_{l+1}} - \frac{1}{k_{N+1}}\right]\right], \qquad (4.1)$$

which shows that it is possible to compute the permeability at the flood front and the permeability in the uninvaded zones.

(iii) We explained why Eq. 4.1 would not be valid when the flood front crossed a zone interface. In absence of other evidence, this fact could be used to determine the position of a zone interface.

(iv) We presented an equation for the calculation of mechanical skin factor and showed that this skin factor is different from the skin factor calculated by conventional analysis, the difference being due to the difference in mobilities of oil and water.

(v) In the case studies where we applied our method to analyze synthetic data, we demonstrated by plotting mobility and rate kernels that the pressure derivative data reflect permeability of regions where mobility and in-situ rate changes most rapidly. We also showed that while rapid mobility changes occur at the flood front, rapid in-situ rate changes occur ahead in the oil zone.

In Chapter III, we focused on pressure falloff testing. We showed that, since the flood front remains static in these tests and there is no change in mobility, pressure derivative reflects permeability of that region where in-situ rate changes rapidly. We also explained the intricacies involved in calculation of skin. Next we investigated the behavior of multirate tests. Finally, we validated our findings using synthetic data. The results presented in this chapter lead to the following conclusions.

(i) Conventional single phase techniques can be used to analyze falloff tests by considering permeability-mobility product in place of permeability. More specifically, the Inverse Solution Algorithm (ISA) may be used to obtain the permeability-mobility profile.

(ii) The skin factor obtained by performing classical analysis considering the constant slope line corresponding to the flooded zone represents the true mechanical skin factor. We also presented an equation for calculation of mechanical skin factor using the constant slope line corresponding to the uninvaded zone.

(iii) We found that in case of a multirate test, when a rate change is made a second rate kernel propagates into the reservoir which overshadows the first mobility and rate kernel. Thus, the pressure derivative reflects permeability of only that region where the second in-situ rate change takes place most rapidly. Thus, single phase techniques may be applied to analyze data corresponding to times before the mobility kernel again becomes dominant.

NOMENCLATURE

B_o	Oil formation volume factor, res.bbl/STB.
B_w	Water formation volume factor, res.bbl/STB.
C_1	constant - see Eq. 2.1.3.
c_o	oil compressibility, psi^{-1}
c_t	total system compressibility, psi^{-1} .
c_{to}	total system compressibility of uninvaded zone, psi^{-1}.
c_w	water compressibility, psi^{-1}
h	formation thickness, ft.
k	absolute reservoir permeability, md.
k_{ro}	oil relative permeability.
k_{rw}	water relative permeability.
p	pressure, psia.
p_i	initial reservoir pressure, psia.
p_{wf}	flowing bottom hole pressure, psia.
p_{ws}	shut-in bottom hole pressure
q_t	total rate, res.bbl/day.
r	radius, ft.
r_w	wellbore radius, ft.

S_o oil saturation.

S_{or} residual oil saturation.

S_w water saturation.

S_{wc} connate water saturation.

t time, days.

Δt shut-in time, days.

ϕ porosity, fraction.

λ_f mobility at flood front.

λ_o oil mobility.

λ_t total mobility.

μ viscosity, cp.

μ_o oil viscosity, cp.

μ_w water viscosity, cp.

π constant ≈ 3.142

REFERENCES

1. Hazebroek, P. , Rainbow, H . and Matthews, C . S . : “Pressure Fall-Off in Water Injection Wells,” paper T.P. 8034, presented at 32nd Annual Fall Meeting of the Society of Petroleum Engineers, Dallas, Texas, Oct. 6-9, 1957.
2. Kazemi, H ., Merrill, L . S . and Jargon, J . R . : “Problems in Interpretation of Pressure Fall-Off Tests in Reservoirs With And Without Fluid Banks,” Journal of Petroleum Technology, Sept., 1972, 1147-1156.
3. Merrill, L . S . , Kazemi, H . and Gogarty, W . B . : “Pressure Falloff Analysis in Reservoirs With Fluid Banks,” Journal of Petroleum Technology, July., 1974, 809-818.
4. Weinstein, H . G . : “Cold Waterflooding a Warm Reservoir,” paper SPE 5083 presented at the 49th Annual Meeting of the Society of Petroleum Engineers, Houston, Oct. 6-9, 1974.
5. Sosa, A . , Raghavan, R . and Limon, T . J . : “Effect of Relative Permeability and Mobility Ratio on Pressure Falloff Behavior,” Journal of Petroleum Technology, Jun. , 1981, 1125-1135.
6. Abbaszadeh, M . and Kamal, M . : “ Pressure-Transient Testing of Water-Injection Wells,” SPE Reservoir Engineering, Feb., 1989, 115-124.

7. Yeh, N . S . and Agarwal, R . G . : “Pressure Transient Analysis of Injection Wells in Reservoirs With Multiple Fluid Banks,” paper SPE 19775 presented at 64th Annual Technical Conference and Exhibition of the Society of Petroleum Engineers, San Antonio, Texas, Oct. 6-11, 1989.
8. Ramakrishnan, T . S . and Kuchuk F . J . : “Pressure Transients During Injection: Constant Rate and Convolution Solutions,” Transport in Porous Media, Vol. 10, 1993, 103-136.
9. Ramakrishnan, T . S . and Kuchuk F . J . : “Testing and Interpretation of Injection Wells Using Rate and Pressure Data,” paper SPE 20536 presented at the 65th Annual Technical Conference and Exhibition of the Society of Petroleum Engineers, New Orleans, LA, Sept. 23-26, 1990.
10. Oliver, D . S . : “The Averaging Process in Permeability Estimation From Well-Test Data,” SPE Formation Evaluation, Sept., 1990, 319-324.
11. Feitosa, G . S ., Chu, L . , Thompson, L . G . and Reynolds, A . C . : “Determination of Reservoir Permeability Distributions From Pressure Buildup Data,” paper SPE 26457 presented at the 68th Annual Technical Conference and Exhibition of the Society of Petroleum Engineers, Houston, Texas, Oct. 3-6, 1993.
12. Feitosa, G . S ., Chu, L . , Thompson, L . G . and Reynolds, A . C . : “Determination of Reservoir Permeability Distributions From Well-Test Pressure Data,” paper SPE 26047 presented at the 1993 SPE Western Regional Meeting, Anchorage, May. 26-28, 1993.
13. Thompson, L . G . and Reynolds, A . C . : “Well Testing for Heterogeneous Reservoirs Under Single and Multiphase Flow Conditions,” paper SPE 30577

presented at the SPE Annual Technical Conference and Exhibition, Dallas, Texas, Oct. 22-25, 1995.

14. Thompson, L . G . and Reynolds, A . C . : “Well Testing for Heterogeneous Gas Condensate Reservoirs and Other Multiphase Flow Systems”, TUPREP Research Report 12, May,1995
15. Dake, L. P. : “Fundamentals of Reservoir Engineering,” Elsevier,
16. Hawkins, M. F. : “A Note on Skin Effect”, Trans. AIME 207, 1956, pp 356-357.
17. Earlougher, R. C. : “Advances in Well Test Analysis”, Society of Petroleum Engineers Monograph, 1977
18. Thompson, L . G . and Reynolds, A . C . : “Pressure Transient Analysis for Gas Condensate Reservoirs”, to be published.
19. Letkeman, J. P. and Riding, R. L. : “A Numerical Coning Model”, SPEJ, 1970

APPENDIX 1

TWO-PHASE ONE DIMENSIONAL RADIAL RESERVOIR SIMULATOR

In order to generate synthetic data for verification of our water injection and falloff test theory we developed a two-phase one dimensional radial simulator. An overview of the simulator is given in this section for reference.

The simulator developed was specifically designed to generate pressure response for both constant and variable rate water injection in the center of a single layer cylindrical reservoir with a closed outer boundary. However, the simulator can be readily adapted for other uses as well. The model uses a logarithmic gridding system with the grid size increasing with distance from the wellbore. In order to ensure stability we have used Letkeman and Riding's[19] method. While we found that our model did not have step-size limitation for stability, in-situ rate calculation was not very accurate for large saturation changes in the grid blocks. In particular at the flood front where the saturation changes most rapidly, the in-situ rate shows an anomaly as presented in Fig A1.1. Figure A.1.2 shows that the anomaly disappears when we cut down the time step so that the maximum saturation change is less than 1.0 percent.

For all the examples we considered in our study the outer radius of the reservoir was considered to be 5000 ft. For accuracy 90 grids blocks were considered sufficient.

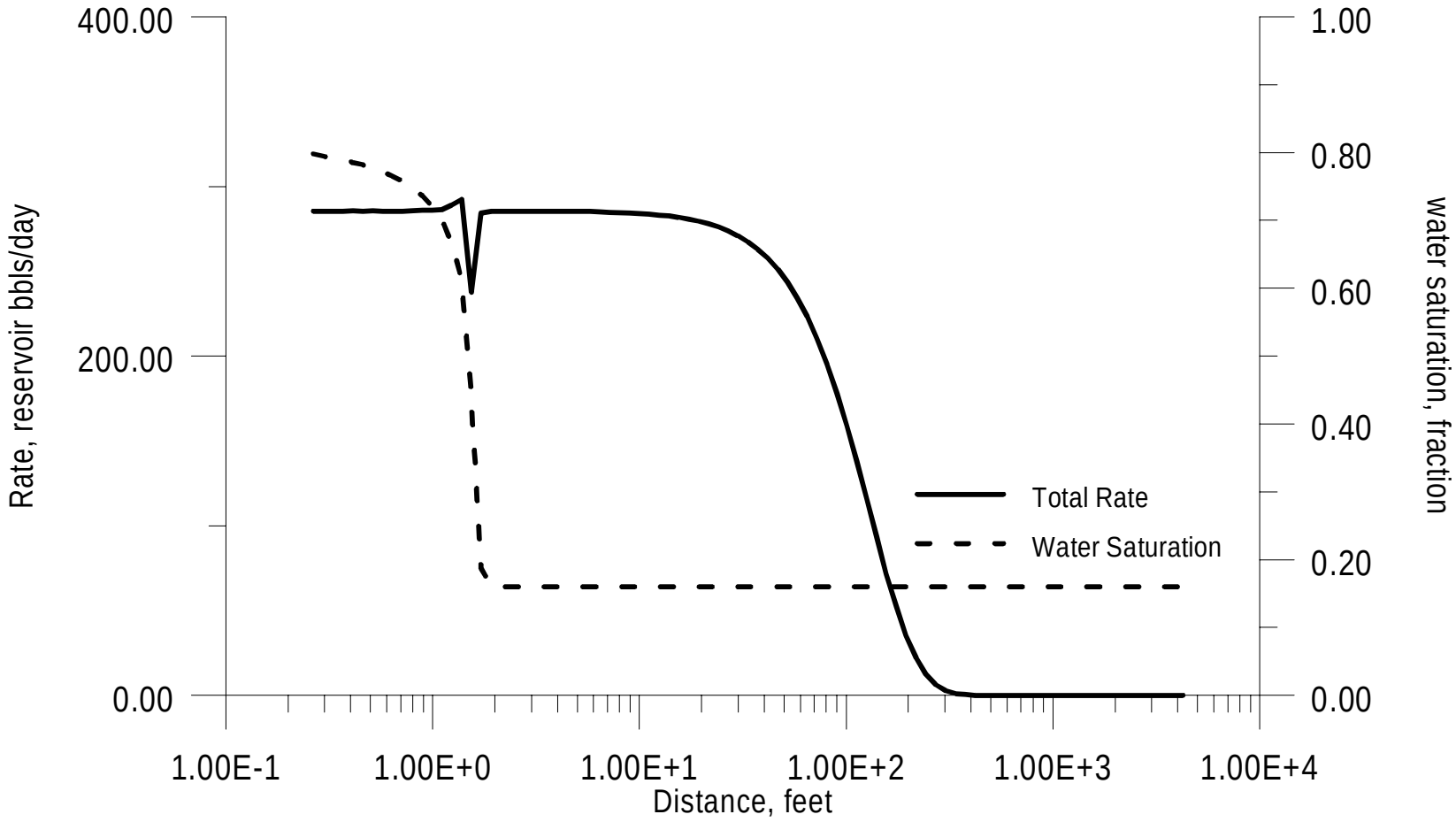

Figure A1.1: Rate and Saturation Profiles as a function of Radius at 0.01 day
(Unrestricted Saturation Change)

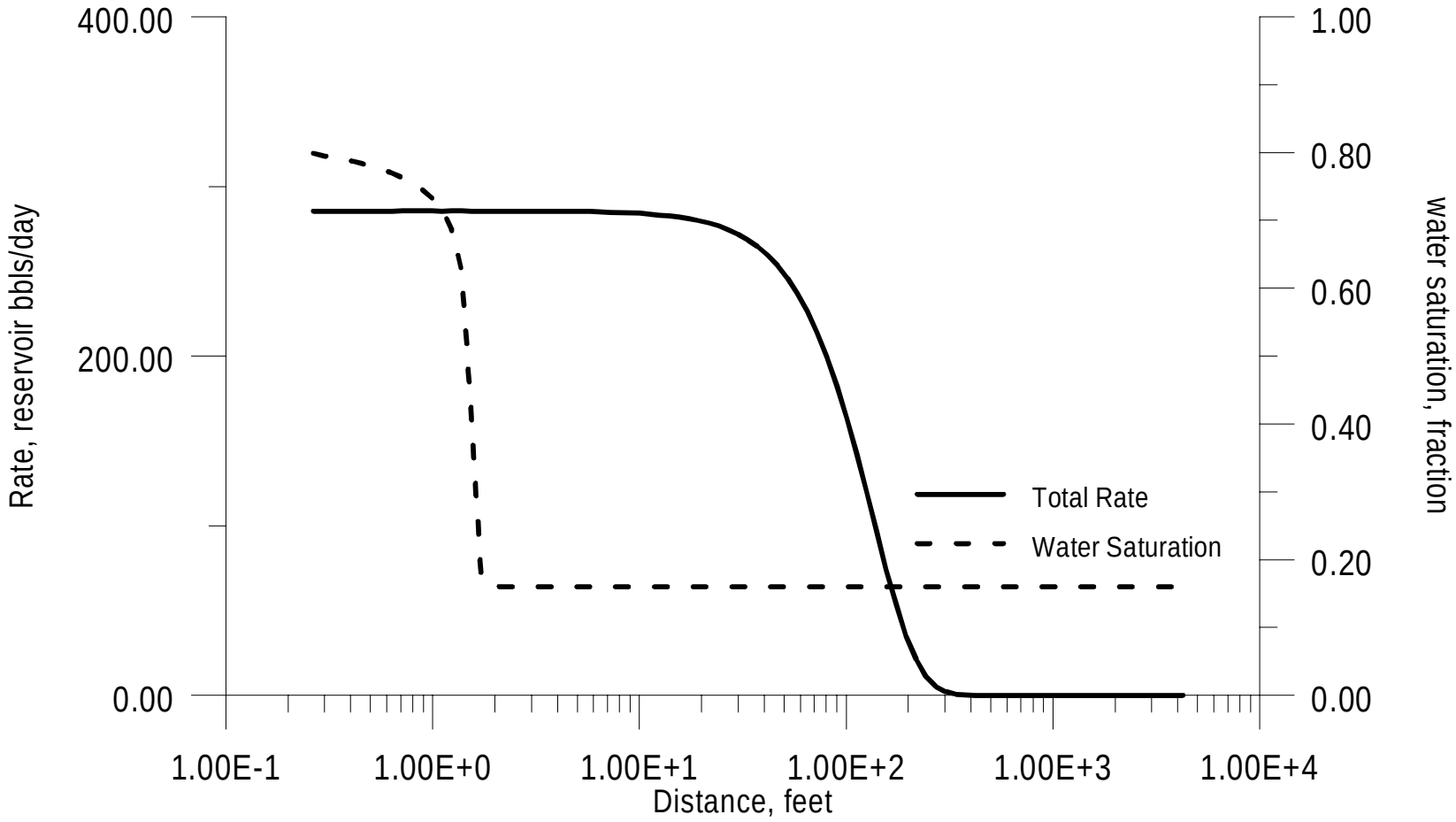

Figure A1.2: Rate and Saturation Profiles as a function of Radius at 0.01 day
(Maximum Saturation Change 1 percent)

The maximum saturation change in each grid block was restricted to 1.0 percent, i.e., if the saturation in any grid block exceeded 1.0 percent the simulator reduced the time step size by 50 percent and repeated the calculation for that time step. Note that even though our model had an outer closed boundary, it was irrelevant as we were only interested in the behavior of the transient part of the data